UNIVERSIDADE DE LISBOA

FACULDADE DE MEDICINA

Organotypic Hippocampal Slice Culture Model of Epileptogenesis: Electrophysiological and Molecular Features

Noémia Marisa Félix Pereira

Mestrado em Neurociências

Lisboa, 2014

UNIVERSIDADE DE LISBOA

FACULDADE DE MEDICINA

Organotypic Hippocampal Slice Culture Model of Epileptogenesis: Electrophysiological and Molecular Features

Noémia Marisa Félix Pereira

Orientadora: Doutora Cláudia Valente de Castro, Instituto de Farmacologia e Neurociências, Faculdade de Medicina de Lisboa e Unidade de Neurociências, Instituto de Medicina Molecular, Universidade de Lisboa.

Mestrado em Neurociências

Lisboa, 2014

Todas as afirmações contidas neste trabalho são da exclusiva responsabilidade do candidato, não cabendo à Faculdade de Medicina da Universidade de Lisboa qualquer responsabilidade.

Esta dissertação foi aprovada pelo Conselho Científico da Faculdade de Medicina da Universidade de Lisboa em reunião de 22 de Julho de 2014.

ACKNOWLEDGEMENTS

À Doutora Cláudia Valente, pela orientação, paciência e amizade. O seu apoio e dedicação constante, bem como os valiosos conhecimentos transmitidos permitiram-me fazer desta experiência uma aprendizagem proveitosa e extremamente valiosa.

Ao Professor Joaquim Alexandre Ribeiro e à Professora Ana Maria Sebastião por me terem concedido a oportunidade de desenvolver o meu projeto de tese na Unidade de Neurociências. A eles agradeço o apoio.

A todos os colegas de laboratório, pelo carinho com que me receberam, pelo espírito de entreajuda que sempre demonstraram e pelas amizades daí resultantes.
Em especial agradeço à Rita Aroeira por toda a ajuda e disponibilidade demonstrada desde o primeiro dia. À Vânia Batalha pela prontidão com que sempre teve em me ajudar e por toda a riqueza de conhecimentos que me transmitiu, os quais foram cruciais para o desenvolvimento deste trabalho. Ao Diogo Rombo e Daniela Magalhães pela preciosa ajuda e colaboração na obtenção dos resultados.

Agradeço à minha família pela oportunidade que me proporcionaram em desenvolver este projeto e percurso, e por toda a confiança que me concederam.

Por fim, deixo um agradecimento muito especial ao Rui pelo apoio e confiança incondicionais e por ter estado sempre presente, nos bons e maus momentos.

INDEX

ABBREVIATIONS

Ab – Antibody

Abs – Antibodies

ADK – Adenosine kinase

AED – Antiepileptic drug

AIF-1 – Allograft inflammatory factor 1

ANOVA – One-way analysis of variance

AP – Alkaline phosphatase

BSA – Bovine serum albumin

CA – Cornus Ammonis

cDNA – Complementary DNA

CNS – Central Nervous System

CP – Crossing point

Ct – Threshold cycle

DEPC – Diethylpyrocarbonate

DG – Dentate gyrus

DIV – Days *in vitro*

DNA – Deoxyribonucleic acid

dNTP – Deoxyribonucleotide thriphosphate

dsDNA – Double-stranded DNA

E – Efficiency

EC – Entorhinal cortex

EDTA – Ethylenediaminetetraacetic acid

EEG – Electroencephalography

EPSP – Excitatory postsynaptic potential

EtBr – Ethidium bromide

fEPSP – Field excitatory postsynaptic potential

GABA – Gamma-aminobutyric acid

GABA-T – GABA transaminase

GABAR – GABA receptor

GAD – Glutamic acid decarboxylase

GAPDH – Glyceraldehyde-3-phosphate dehydrogenase

GAT – GABA transporter

GBSS – Gey's balanced salt solution

GCS – Glycine cleavage system

GFAP – Glial fibrillary acidic protein

GlyR – Glycine receptor

GlyT – Glycine transporter

GS – Glutamine synthetase

HBSS – Hanks' balanced salt solution

HRP – Horseradish peroxidase

HS – Horse Serum

I/O – Input-output

Iba1 – Ionized calcium-binding adapter molecule 1

IF – Immunofluorescence

IgG – Immunoglobulin G

IHC – Immunohistochemistry

IL-1β – Interleukin-1β

ILAE – International League Against Epilepsy

IPSC – Inhibitory postsynaptic current

KCC2 – Potassium chloride cotransporter

mRNA – Messenger RNA

MTLE – Mesial temporal lobe epilepsy

NeuN – Neuronal Nuclei

NKCC1 – Sodium, potassium, chloride cotransporter

NMDA – *N*-methyl-D-aspartate

NO – Nitric oxide

OHSC – Organotypic hippocampal slice culture

P – Postnatal

PBS – Phosphate buffered saline

PBST – PBS 0.1 % Tween-20

PCR – Polymerase chain reaction

PFA – Paraformaldehyde

PI – Propidium iodide

pSpike – Population spike

PVDF – Polyvinylidene difluoride

RNA – Ribonucleic acid

rRNA – Ribosomal RNA

RT – Room temperature

RT-PCR – Reverse transcriptase PCR

SC – Serum-containing

SDS-PAGE – Sodium dodecyl sulfate-polyacrylamide gel electrophoresis

SF – Serum-free

SHMT – Serine hydroxymethyltransferase

sIPSC – Slow inhibitory postsynaptic current

SSA – Succinic semialdehyde

TBS – Tris-buffered saline

TBST – TBS with 0.1% Tween 20

TLE – Temporal Lobe Epilepsy

TM – Transmembrane segment

TNF-α – Tumor necrosis factor-α

Tris – Tris-hydroxymethyl-aminomethane

VIAAT – Vesicular inhibitory amino acid transporter

Vm – Membrane potential

RESUMO

***Introdução*:** As culturas organotípicas podem ser mantidas por longos períodos de incubação através do uso de dois meios de cultura: o meio Optimem, com soro de cavalo, e o meio Neurobasal, suplementado com B27. O soro contém substâncias indefinidas e em quantidades desconhecidas. O meio de cultura Neurobasal, por seu turno, é totalmente definido, o que permite um controlo preciso do ambiente extracelular das culturas. Porém, as propriedades funcionais das células mantidas em meio Neurobasal não são totalmente conhecidas. Além disso, neste meio as fatias desenvolvem atividade epileptiforme espontânea, que se assemelha com a epilepsia *in vivo*.

Objectivo: O objectivo deste estudo é explorar as propriedades celulares e moleculares correlacionadas com a epileptogénese em culturas organotípicas de hipocampo.

Metodologia: De forma a explorar os efeitos da remoção do soro nas culturas organotípicas, utilizaram-se duas condições: **1)** fatias mantidas num meio com soro, **2)** fatias mantidas num meio isento de soro. Avaliou-se a integridade das fatias, a morte celular, e as propriedades funcionais das células. Por fim, de modo a explorar as características correlacionadas com a epilepsia, em fatias mantidas num meio sem soro, avaliou-se a atividade epileptiforme, a ativação dos astrócitos e da microglia, bem como a transcrição das subunidades dos receptores do $GABA_A$ e da glicina.

Resultados: Observou-se um aumento da excitabilidade das células piramidais de CA1 nas fatias mantidas num meio isento de soro, bem como uma diminuição da eficiência sináptica, sem afectar a integridade das fatias e a morte celular. Estes efeitos, ao longo do período de incubação, aumentam a vulnerabilidade e incidência da atividade epileptiform espontânea, tendo sido observado um progressivo aumento da prevalência da atividade ictal que acompanhou a ativação dos astrócitos e da microglia, bem como a alteração na expressão das subunidades dos receptores $GABA_A$ e da glicina.

Conclusão: As culturas organotípicas de hipocampo são um modelo útil no estudo da epileptogénese, uma vez que desenvolvem características semelhantes às observadas na epilepsia *in vivo*.

Palavras-chave: Culturas organotípicas de hipocampo; Epileptogénese; Meio de cultura; Gliose; Neurotransmissão inibitória.

ABSTRACT

Introduction: Organotypic hippocampal slice cultures can be maintained for long periods of time *in vitro* using an Optimem horse serum-based medium, which contains unknown quantities of undefined substances, or using a chemically defined Neurobasal medium supplemented with B27. Neurobasal B27-supplemented allows precise control of extracellular environment and avoids the effects of unknown growth factors. However, the functional properties of these cells maintained in this serum-free medium were not yet fully known. Moreover, organotypic slices maintained Neurobasal medium develop spontaneous epileptiform activity that resembles *in vivo* epilepsy.

Aim: The aim of this study is to explore the cellular and molecular correlates of epileptogenesis in organotypic hippocampal slice cultures.

Methodology: In order to explore the effects of serum removal, slices were maintained in two different conditions: **1)** serum-contain growth medium, **2)** serum-free growth medium. Slice integrity, cell death, and functional properties were evaluated. Finally, using serum-free organotypic slice cultures as a model of epileptogenesis, epileptiform activity, astrogliosis and microglia activation, as well as $GABA_A$ and glycine receptor transcripts were assessed.

Results: Serum removal increased cells excitability and decreased the synaptic efficiency of CA1 hippocampal pyramidal cells, without changing the slice integrity and cell death. These effects, throughout incubation period, lead to increased vulnerability and incidence of spontaneous epileptiform activity. Ictal-like activity becomes progressively more prevalent and overlaps the astrocyte and microglia activation, as well as the changes in $GABA_AR$ e GlyR subunits expression.

Conclusion: Organotypic hippocampal slice cultures comprise a useful model of epileptogenesis. They develop many features correlated with epilepsy, and can be kept as "*in vivo*-like" using a defined culture medium.

Key-words: Organotypic hippocampal slice cultures; Epileptogenesis; Growth medium; Gliosis; Inhibitory neurotransmission.

LIST OF FIGURES

LIST OF TABLES

1 BACKGROUND

1.1 Epilepsy

Epilepsy is among the most common neurological diseases affecting around 50 million people worldwide. There is an estimated prevalence in Europe of 4.3-7.8 per 1000 people, and as high as 16-20 per 1000 in Africa (according with data of World Health Organization).

Clinically, epilepsy is characterized by spontaneous, recurrent epileptic seizures, which are defined as "a transient occurrence of sign and/or symptoms due to abnormal excessive or synchronous neuronal activity in the brain" [1]. Epilepsy is not a singular disease entity but a variety of disorders reflecting underlying brain dysfunction that may result from many different causes. It may arise due to a disruption of mechanisms that normally create a balance between excitation and inhibition. Such provoking factors include head trauma, stroke intracranial, infections, acute metabolic disruption (e.g., hypoglycemia, anoxia), acute drug or toxin poisoning, and neurological diseases (e.g., Alzheimer's disease). The diagnosis of the epileptic syndrome is usually based upon several characteristics, such as symptoms, seizure types and electroencephalographic (EEG) patterns [2,3].

Antiepileptic drugs (AEDs) are the main treatment of epilepsy. The mechanisms of action of the currently AEDs involve alterations in the balance between neuronal excitation and inhibition, with a range of mechanisms of action such as modulation of voltage-gated ion channels (e.g., phenytoin, carbamazepine and lamotrigine); enhancement of synaptic inhibitory neurotransmission (e.g., barbiturates and benzodiazepines); and attenuation of brain excitation (e.g., topiramate). Nevertheless, most of the AEDs share common mechanisms of action [4].

Most of the patients with epilepsy respond to AEDs, but still fail to control seizures in approximately 30% of them. Not all forms of epilepsy have the same rate of drug-refractoriness, being particularly frequent (70%) in adult patients diagnosed with mesial

temporal lobe epilepsy (MTLE). Drug-refractoriness in epilepsy is responsible for increased morbidity, and risk of premature mortality [5].

When AED therapy fails to control seizures, patients with surgically remediable syndromes could be assessed for epilepsy surgery. However, both treatments are associated with adverse effects. The patients that suffer from refractory epilepsy take at least two AEDs, which increase the risk of cognitive complications, such as memory decline. Likewise, surgical therapy may produce seizure freedom, but anatomically disrupts neural networks necessary for cognitive processing [6]. Even those patients who undergo surgery, are not completely free of seizure remission [7].

Because only a minority of patients with epilepsy benefit from epilepsy surgery, there is a huge need of more research into the mechanisms that lead to pharmacoresistance, and development of novel antiepileptic drugs.

1.1.1 Temporal Lobe Epilepsy

Temporal lobe epilepsy (TLE) is a chronic disease that is manifested by recurrent unprovoked partial seizures with or without secondary generalization. MTLE, one of the most common types of TLE, is characterized by seizure generation from the mesial temporal lobe structures including the amygdala and hippocampal formation [8].

MTLE has a typical clinical presentation. Patients often have a history of complicated febrile seizures or other initial precipitating injuries, such as head trauma or intracerebral infections, within the first four or five years of life. There is also an increased prevalence of a family history of epilepsy. After a 5- to 10-year latency period, seizures start to occur and initially respond to appropriate AED treatment. During adolescence, or later, seizures habitually recur, and are mostly insensitive to current AEDs [9,10].

Histopathologically, MTLE can be subclassified as paradoxical temporal lobe epilepsy or hippocampal sclerosis. No lesions are observed in paradoxical temporal lobe epilepsy, whereas 70% of MTLE patients with hippocampal sclerosis (Ammon's horn sclerosis) lesions show severe unilateral atrophy of the hippocampal formation. It is also shown, **1)** a stereotypical pattern of cell loss in Cornus Ammonis (CA) 1 and hilus (CA4), whereas CA2 and dentate granule cells seem to be spared, and **2)** loss of GABAergic interneurons in the dentate hilus. Additionally, most hippocampal sclerosis patients

display cell loss in other mesial temporal areas such as the entorhinal cortex (EC), reactive gliosis, and aberrant sprouting of dentate granule cell axons, or mossy fibers, which project back into the region of their proximal dendrites. Mossy fiber sprouting produces a monosynaptic excitatory feedback circuit that may also synapse with inhibitory interneurons, enhancing inhibition [8,9,11]. Moreover, some studies identified laminar dispersion of the dentate granule cell layer in human hippocampal sclerosis. This may indicate a preexisting migration disturbance of the hippocampus itself which could predispose to the typical cell loss and neuronal reorganization, as well as synaptic reorganization [10,12].

Other changes can be associated with this epileptogenic process, including alterations in receptors and channels on key hippocampal cell populations as well as changes in the relative rates of neurogenesis. For example, after seizures, the number of ectopic granule cells located in the hilus seems to increase dramatically [13]. Nevertheless, it is not fully understood whether these structural abnormalities are the cause of the epileptic condition or the consequence of repeated seizures. In addition, the sequence of events leading to the development of hippocampal sclerosis and chronic epilepsy cannot be systematically studied because the human hippocampal tissue is often obtained at a late stage of chronic MTLE, and the presently used animal models display significant disparities comparing to the features of the human disorder [11,14].

1.1.2 Glial Cells and Gliosis

Glial cells are involved in maintaining, regulating, signaling and altering neuronal synaptic junctions. Glial cell types include: microglia, astrocytes and radial glial cells [15]. In the mature central nervous system (CNS), microglia and astrocytes are distributed in large non-overlapping regions throughout the brain, in which astrocytes represent the major cell type while microglia cells comprise up to 20% of the total glial cells population [16].

Astrocytes are no longer regarded as simple supportive cells for neurons, being considered as the third element of a structure known as “tripartite synapse” [17,18]. Astrocytes play a pivotal role in brain homeostasis through several cooperative metabolic processes that they establish with neurons, such as energy supply,

neurotransmitter recycling functions and regulation of ionic environment and interstitial volume [19]. At the synapse, astrocytes can be stimulated by released neurotransmitters, which cause intracellular calcium (Ca^{2+}) elevations and trigger gliotransmitter release (such as ATP, D-serine and glutamate), that in turn regulate synaptic transmission and plasticity [20]. Furthermore, astrocytes are also interconnected with blood vessels, as component of the neurovascular unit that controls blood-brain barrier permeability, and other astrocytes by a highly ramified structure of thin processes [21]. Microglia are considered resident immune cells of the CNS and serve as sensors and executors of innate immunity within the CNS. They are in a surveying state, with random filopodia-like protrusions. However, upon an insult or stress, astrocytes and microglia become reactive (activated) leading to release of pro-inflammatory mediators, following by release of anti-inflammatory molecules and growth factors that help to orchestrate and resolve the inflammatory tissue response [22].

Reactive glial changes are frequently encountered in the hippocampus in association with MTLE in humans [23], as well as in epilepsy animal models [24,25]. Moreover, recent evidence strongly suggests that glia-mediated inflammation plays a role in the pathogenesis of seizures and epilepsy [26] (**Figure 1**).

During the activation process, microglia changes from a ramified structure to a hyperramified and finally to an amoeboid morphology. The amoeboid morphology facilitates the microglial cell migration through the parenchyma toward lesion sites [22]. Furthermore, microglial cells can increase in number since they are capable of proliferating [27].

Reactive astrogliosis is characterized by cellular, molecular, morphological and functional changes in astrocytes and can be classified in three main categories: **1)** reversible alterations in gene expression, **2)** cell hypertrophy with preservation of cellular domains, and tissue structure and **3)** newly proliferated astrocytes, with rearrangement of tissue structure and deposition of dense collagenous extracellular matrix [15]. When normal feedback mechanisms fail to limit and extinguish inflammation, this glia-mediated response can result in harmful consequences to the surrounding cells [15]. For example, chemokine-activated microglia cooperate with astrocytes in releasing tumor necrosis

factor-α (TNF-α), and other cytokines, which in turn promotes glutamate release from astrocytes [23]. The increased synaptic glutamate causes paroxysmal depolarization shifts in neurons, contributing to neuronal synchronization and cell loss [15]. Moreover, environmental toxins and products released upon neuronal death or damage induce overactivation of glia cells. The overactivated astrocytes and microglia can then release several cytotoxic substances including nitric oxide (NO) or superoxide and the pro-inflammatory factors interleukin-1β (IL-1β) and TNFα [22]. Chronically activated astrocytes, can also leads to formation of a glial scar, considered to have both beneficial and detrimental effects [28]. In this environment axon regeneration fails and remyelination may also be unsuccessful. However, glial scars can also protect neurons from oxidative stress, and restrict the spread of inflammatory cells [23].

Another mechanism by which glial cells can contribute to epileptogenesis is through functional and molecular changes of astrocytes. Altered astrocytic transporters, including reduced expression of potassium channels and dislocation of water channels favor an altered water influx and impaired potassium buffering [15]. Consequently, the impairment of the osmotic balance increases the susceptibility to seizure. In addition, gliotransmission impairment by reactive astrogliosis has been described. For example, downregulation of glutamine synthetase (GS) expression leads to rapid depletion of synaptic Gamma-AminoButyric Acid (GABA). On the other hand, adenosine kinase (ADK) deregulation may be central to epileptic synchronization, since ADK is a predominantly astrocytic enzyme that regulates brain extracellular adenosine levels, which is a powerful inhibitory substance during seizures [23].

Together with dendritic sprouting and new synapse formation, loss of astrocytic domain organization may contribute to the structural bases of recurrent excitation in epilepsy.

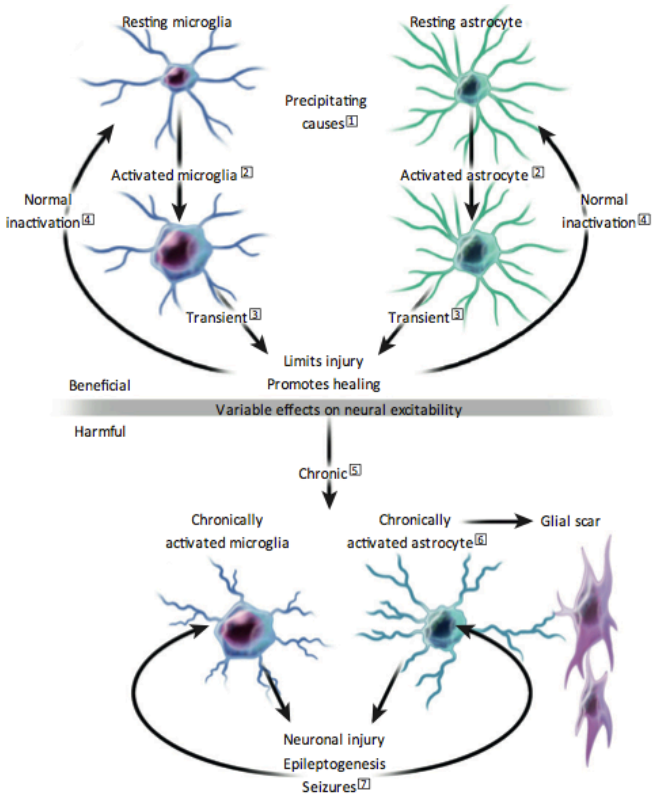

Figure 1| Intersecting roles of astrocytes and microglia in epilepsy. (1) A precipitating injury such as trauma, or seizures causes astrocytic and microglial activation. **(2)** Inflammatory proteins are released by activated glia. **(3)** Activated astrocytes exhibit homeostatic functions such as increased glutamate uptake (a function also displayed by microglia), glutathione release to decrease oxidative stress, adenosine release to control neuronal excitability, regulation of fluid/ion homeostasis, and release of anti-inflammatory mediators to control innate immunity activation. **(4)** Normal inactivation of activated microglia is partly mediated by astrocytes through inhibit microglial phagocytosis and lower microglial production of anti-inflammatory molecules. **(5)** Chronic uncontrolled astrocytic and microglial activation is associated with excessive release of pro-inflammatory molecules, ionic imbalance, and decreased glial glutamate reuptake and GABA synthesis in neurons. This set of phenomena has numerous detrimental effects, including neuronal injury and seizures induction. **(6)** Chronically activated astrocytes can form a glial scar. The effects of such a scar can decrease axonal regeneration, protect neurons from oxidative stress, and restrict the spread of inflammatory cells. **(7)** Epileptogenesis, seizures, and neuronal injury can arise from chronic pathological glial activation and cause pro-inflammatory changes that maintain chronic, pathological activation of astrocytes and microglia (adapted from Devinsky et al., 2013 [23]).

1.1.3 GABAergic Inhibitory System

GABAergic system plays an important role in the central regulation of somatic and mental functions, as it serves as the main fast inhibitory neurotransmitter in the brain. It is a target for several AEDs, being an important mechanism for controlling excessive excitatory activation, as occur in epilepsy [29].

1.1.3.1 GABAergic synapses

GABA is localized primarily in short-axon interneurons that synapse on cell bodies and proximal axons (**Figure 2**). GABA is formed by transamination of α-ketoglutarate to glutamic acid, followed by decarboxylated by glutamic acid decarboxylase (GAD). Synaptic release can occur *via* vesicular or nonvesicular processes. Vesicular GABA release is Ca^{2+}-dependent and triggered by high potassium (K^+) concentration. This process is regulated by negative feedback control through presynaptic autoreceptors (e.g., kainate receptors, adrenoreceptors and $GABA_B$ receptors). Nonvesicular GABA release is Ca^{2+}-independent and occurs secondary to depolarization of the cell membrane and sodium (Na^+) influx. Synaptically released GABA can either activate GABA receptors (GABARs), or be transported into nerve terminals and astrocytes through GABA transporters (GATs), GAT-1 and GAT-3, respectively. Reuptake into axon terminals allows immediate recycling by vesicular uptake. Astrocytes reuptake, in turn, leads to GABA metabolism. GABA is metabolized into succinic semialdehyde (SSA) by 2-oxoglutarate aminotransferase (GABA-T), and SSA is then converted to succinic acid, by succinic acid semialdehyde dehydrogenase, entering in the Kerbs cycle [29–31].

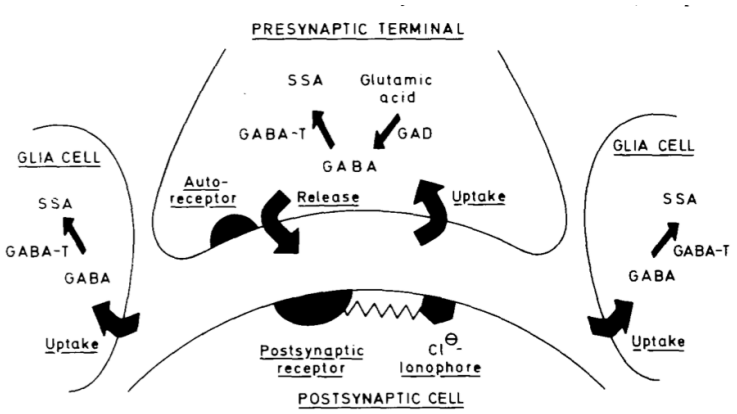

Figure 2| GABAergic axo-dendritic synapse. The synthesis of GABA from glutamic acid in nerve terminals is catalyzed by L-glutamate-1-carboxylase (GAD), and the degradation of GABA into succinic semialdehyde (SSA) in nerve terminals and glial cells is catalyzed by 2-oxoglutarate aminotransferase (GABA-T). The GABA release system is regulated by presynaptic autoreceptors. GABA acts on postsynaptic receptors, $GABA_AR$ and $GABA_BR$ (Adapted from Krogsgaard-Larsen, 1980 [30]).

Postsynaptically, GABA acts on two types of GABARs: $GABA_A$Rs, which mediate the fast, and transient inhibitory postsynaptic currents (IPSCs), and $GABA_B$Rs, which mediate the slow inhibitory postsynaptic currents (sIPSC). $GABA_A$Rs controls chloride (Cl^-) entry into the cell, whereas $GABA_B$Rs increases K^+ conductance, decrease Ca^{2+} entry, and inhibits the presynaptic release of other transmitters [32].

The effect of GABA transmission on the excitability of a network depends on the Cl^- reversal potential of the postsynaptic cell, which is determined by two Cl^- transporters NKCC1 (i.e., sodium, potassium, chloride cotransporter) and KCC2 (i.e., potassium chloride cotransporter). In particular, NKCC1 activity increases intracellular Cl^-, whereas KCC2 decreases it. The developmental GABA switch from excitatory to inhibitory neurotransmitter is caused by a differential expression of these two transporters. In immature neurons NKCC1 is highly expressed, while in mature neurons NKCC1 expression decreases and KCC2 expression increase. This transition is crucial for seizure susceptibility, since it affects the differentiation and migration of neurons [33,34].

1.1.3.2 $GABA_A$ receptor

$GABA_A$Rs are pentameric in structure, with the five subunits arranged around a central Cl^- selective pore, as shown in **Figure 3**. There are 19 subunits ($\alpha 1-6$, $\beta 1-3$, $\gamma 1-3$, δ, ε, θ, π, $\rho 1-3$) encoded by 19 distinct genes. Receptors containing two α subunits in combination with two β subunits and one γ subunit are the most common in the brain [35]. The subunit composition determines both the biophysical properties of the receptor-channel complex and its pharmacology, and so the sensitivity to modulators (e.g., barbiturates, benzodiazepines and neurosteroids). For instance, a typical benzodiazepine-sensitive $GABA_A$R consists of two α subunit subtypes ($\alpha 1$, $\alpha 2$, $\alpha 3$, or $\alpha 5$), and two β ($\beta 2$ or $\beta 3$) subunits (or one each), and a $\gamma 2$ subunit [36].

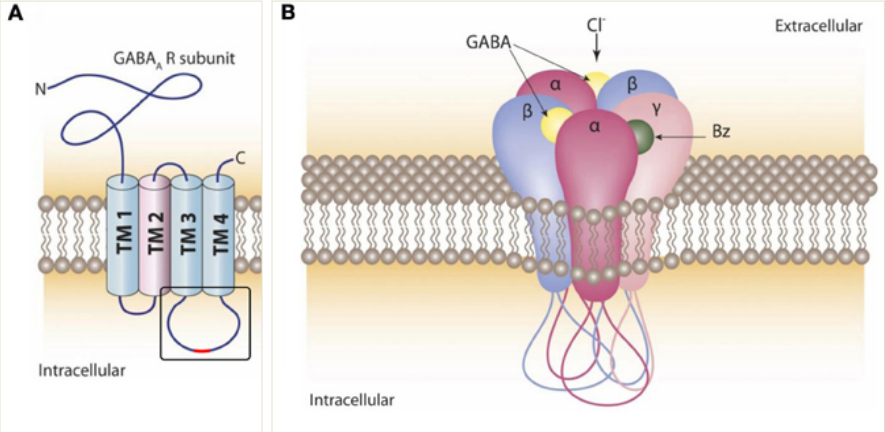

Figure 3| Schematic representation of GABAAR structure. A – Extracellular N- and C- terminus, as well as the transmembrane domains TM1 to TM4. **B –** Most common assembly of $GABA_AR$ subunits: two $\boldsymbol{\alpha}$ subunits, two $\boldsymbol{\beta}$ subunits, and one $\boldsymbol{\gamma}$ subunit; two recognition sites for GABA and the benzodiazepine recognition site. (Adapted from Tretter et al., 2012 [37]).

Classically, $GABA_A$ receptors have been recognized as mediating phasic inhibition in postsynaptic neurons. However, $GABA_A$ receptors can also contribute to tonic inhibition [38]. Both phasic and tonic inhibitions are associated with different subunit compositions of $GABA_ARs$, GABA affinities, and rates of desensitization. Nonsynaptic receptors characteristically contain the δ subunit, rather than the γ subunit, and $\alpha 4$, $\alpha 5$, or $\alpha 6$ subunits. Interestingly, these subunit receptor compositions are not potentiated by benzodiazepine receptor agonists [31,39].

1.1.3.3 $GABA_ARs$ function in epilepsy

Impairment of GABAergic system in epilepsy has been already described from several lines of evidence from genetic epilepsies and animal models [40]. Alterations could occur both pre- and post-synaptically. Presynaptic alterations include a decrease in GABA availability at synaptic cleft, a decrease in GABAergic neuron firing, or a decrease in the number of GABAergic nerve terminals. Postsynaptic alterations comprise a decrease in the number or types of $GABA_ARs$ activated, or a change in the structural or physical properties of these postsynaptic $GABA_ARs$ [35]. Also, altered function of $GABA_BRs$ has been described in epilepsy [41–43]. However, this is still controversial since both $GABA_BR$ agonists and antagonists showed anticonvulsant as well as pro-convulsant effects [44–46].

In TLE with hippocampal sclerosis, postsynaptic $GABA_A$Rs alterations seem to occur from pathologic modifications during epilepsy, interfering directly with both number and subunit composition [47–51], as well as with its function [52]. However, there are some limitations when considering the results due to the diversity of epilepsy models and to the different quantification methods used [35]. There are also differences between rodent brain and human brain concerning the $GABA_A$ receptor subtypes distribution [47]. Despite these differences, the studies were convergent in demonstrating a global increase in $\alpha 1, \alpha 2$, β1-3, and $\gamma 2$ subunits expression, particularly in the dentate granule cell layer. This was accompanied by loss of pyramidal cells in the CA1 and CA3 layers as well as loss of certain interneurons in the hilus of the dentate gyrus (DG). This pattern of cell loss decreases innervation of the DG which can explain the compensatory increase in subunit expression [35,51,53].

Similarly, several genetic studies in humans have revealed a range of idiopathic generalized epilepsy syndromes linked to mutations in the $GABA_A$R, and studies in genetically modified mice have helped establishing the role played by subunit composition $GABA_A$Rs in epilepsy [54]. Together, these data suggest that changes which occur over the course of seizures activity may lead to changes in GABARs function and pharmacology, making more difficult to treat and stop the excessive excitation [35].

1.1.4 Glycinergic Inhibitory System

Since Aprison & Werman [55] have reported glycine as a neurotransmitter in spinal cord, it is now clear that glycine and glycine receptors (GlyRs) are present in several other areas of the CNS [56,57].

In the hippocampus, the study of GlyRs has been largely ignored due to the apparent absence of glycinergic synaptic transmission. However, recent studies have revealed the expression of functional GlyRs in CA1 pyramidal cells and GABAergic interneurons, as well as granule cells and hilar interneurons in the DG [58,59].

Moreover, glycine has been shown to have a dual role on synaptic transmission, as an agonist of GlyRs, and as a co-agonist of the excitatory *N*-methyl-D-aspartate (NMDA) receptors [57,60], thereby providing a potential mechanism underlying balanced regulation between excitation and inhibition in hippocampal networks.

1.1.4.1 Glycinergic synapse

Glycine in CNS can be reached both from *de novo* synthesis from glucose through serine in nerve terminals, or from serine *via* the glycine cleavage system (GCS) in astroglial cells (**Figure 4**). At nerve terminals, serine is converted into glycine by the enzyme serine hydroxymethyltransferase (SHMT), a pyridoxal-5-phosphate-dependent enzyme. This enzyme presents two isoforms, one mitochondrial and the other cytosolic, which suggest that glycine synthesis from serine occurs in the mitochondria, whereas the conversation of glycine to serine is a cytosolic process [61].

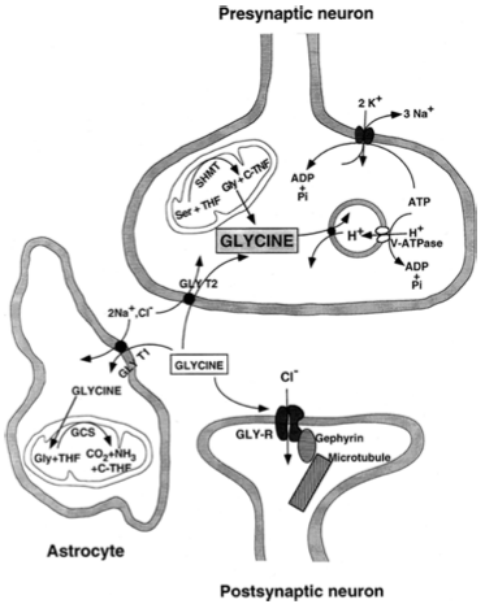

Figure 4| Glycinergic axo-dendritic synapse. Glycine is synthesized in the mitochondria of presynaptic terminals by the enzyme SHMT, and accumulated in synaptic vesicles. Glycine is released to the synaptic cleft on depolarization. Their synaptic action is terminated by transporters in presynaptic plasma membrane (GlyT2) and in the glial plasma membrane (GlyT1). Glycine is degraded in astrocytes mitochondria by glycine cleavage system (GCS) (adapted from Zafra et al., 1997 [61])

Glycine is packaged into synaptic vesicles by the H^+-dependent vesicular inhibitory amino acid transporter (VIAAT or vGAT), which is also involved in the vesicular uptake of GABA. The ability of VIAAT to transport GABA and glycine may depend on the relative extravesicular concentration of the two amino acids. Glycine inhibits GABA uptake and vice versa [62–64]. Glycine is released to the synaptic cleft in a Ca^{2+} -dependent manner. After acting on postsynaptic receptors, glycine is inactivated by a rapid

reuptake mechanism, which is mainly mediated via specific Na^+/Cl^- -dependent glycine transporters (GlyT). Until now two GlyT have been identified, GlyT1 and GlyT2, sharing about 50% of amino acid sequence homology but displaying different pharmacology [61]. GlyT1 is widely expressed in astrocytic glial cells as well as glutamatergic neurons, and is thought to control extracellular glycine concentration and regulate excitatory neurotransmission mediated by glycine binding to NMDARs. GlyT2, in turn, is largely localized to the presynaptic terminals of glycinergic neurons in the brain stem and spinal cord, and is thought to provide the principal glycine uptake mechanism at glycinergic synapses [65,66]. In addition, recent findings have shown that GlyT2, and not only GlyT1, is expressed and functionally active in brain astrocytes, although with a lower affinity for glycine than GlyT1 [67]. These data support the idea that glycine is mainly accumulated in astrocytes and hence these cells play an important role in the regulation of the extracellular levels of glycine [60,61,68].

1.1.4.2 Glycine receptor

GlyRs channels are pentameric assemblies of α and β subunits, arranged around a central pore, as represented in **Figure 5**. Each GlyR subunit comprises a large N-terminal extracellular domain, four transmembrane segments (TM1-TM4), a long intracellular loop, which connects TM3 and TM4, and a short extracellular C-terminus. TM2 forms the channel pore permeable to Cl^- ions, which contributes to inhibition of neuron firing. To date, four α subunits (α_1-α_4) and one β subunit of GlyRs have been identified [57]. The α subunit is the obligatory subunit, which is capable of forming functional homomeric channels, while the β subunit modulates ligand binding upon co-assembly with α subunit, and is responsible for the GlyR synaptic anchoring to the postsynaptic scaffolding protein gephyrin. GlyR-gephyrin interaction is reversible and highly dynamic, regulating the number of receptors at synapses [65,69].

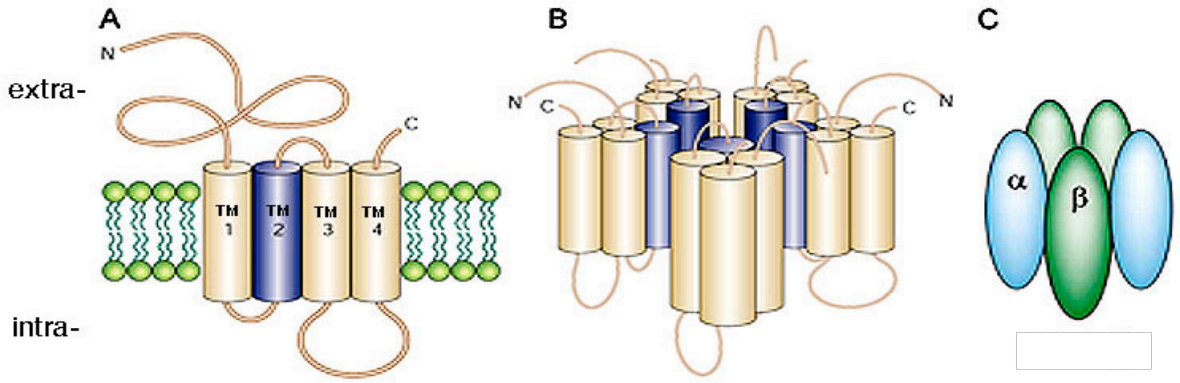

Figure 5| Schematic representation of GlyR structure. A - Extracelular N- and C- terminus, as well as the transmembrane domains TM1 to TM4. **B -** GlyR structure outlining the ion pore. **C –** GlyR subtypes (adapted from Moss & Smart, 2001 [70]).

The subunit composition and distribution of GlyRs differ in different brain areas and developmental stages. The expression of $\alpha 1$ and $\alpha 3$ subunits progressively increases during the first postnatal (P) week, whereas the expression of $\alpha 2$ subunit declines with development [56]. Thus, it is assumed that in immature caudal CNS neurons, extrasynaptic $\alpha 2$ homomeric GlyRs are progressively replaced by $\alpha 2\beta$ heteromeric GlyRs and then by $\alpha 1\beta$ and $\alpha 3\beta$ heterometric GlyRs [71]. In the mature hippocampus the expression of extrasynaptic GlyR α_2/α_3 predominate, in contrast with a few synaptic GlyR $\alpha_1\beta$, which seems to provide a tonic inhibition in the hippocampus [72,73]. It also indicates a potential role of GlyR in early brain development [65]. Indeed, there is a temporal correlation between the developmental switch in GlyR function, from excitatory to inhibitory, and the changes in receptor subunit composition [72]. The expression of KCC2, which determines the Cl^- transmembrane gradient, becomes higher in the second postnatal week, thereby GlyR currents become hyperpolarizing [74].

1.1.4.3 GlyRs function in epilepsy

Regarding the function of glycinergic transmission on hippocampal excitability and synaptic circuits, previous work *in vivo* has reported that exogenous glycine application can depress seizure activity in an animal model of epilepsy [75], and can potentiate the antiepileptic action of inhibitors of GABA-T though synergistic interaction of the two inhibitory neuronal systems [76]. Moreover, another studies recording glycine currents in hippocampal slices under hyperexcitable conditions, or recording epileptiform

discharges induced by magnesium (Mg^{2+}) removal, have demonstrated that GlyR activation depresses bursting activity, even when $GABA_A$ receptor inhibition is compromised [77–79]. Recently, it was shown that antagonists of the glycine transporter (GlyT1) significantly depressed the excitatory postsynaptic potential (EPSP)-spike induced, reflecting a decrease in the ability of the EPSP to generate a spike [60]. Taken together, these findings are consistent with a possible role of GlyRs in the control of network activity in the hippocampus. Hence, it is speculated that the activation of GlyRs alone or in combination with $GABA_A$ receptors may provide an alternative therapeutic approach for the treatment of epilepsy.

The predominantly extrasynaptic location of GlyRs in the hippocampus also predicts a tonic inhibitory role in hippocampal neuronal excitability [65]. Regarding this issue, Eichler and co-workers [80] have observed, in TLE hippocampi obtained from patients with a severe course of disease, an up-regulation of α2 and α3 RNA-edited high-affinity GlyRs expression and a down-regulation of KCC2. This was related to increased glycinergic signaling at GABAergic synapses, providing elevated Glutamate/GABA ratios of synaptic input, reduced dendrite length and elevated susceptibility of hippocampal neurons to excitotoxicity. Moreover, the analysis of GlyRα3 splicing in human hippocampus showed that GlyR α3L is the predominant splice variant in the brain. Hippocampi obtained from patients with intractable TLE, showed an up-regulation of GlyRs α3K splice variant at the expense of the long splice variant GlyRs α3L [81]. Together, these results predict a functional interaction between GlyRs and GABAergic transmission in the hippocampus of TLE, and also suggest a role in the regulation of glutamatergic transmission. It also adds a new sight into the pathophysiology of TLE in terms of increased glycinergic signalling at GABAergic synapses, provided that the Cl^- equilibrium potential is high enough.

1.2 Animal Models of Epilepsy

Animal models constitute essential tools to investigate fundamental neuronal mechanisms of epileptogenesis [82]. In experimental epilepsy models, both control and epileptic groups are available for electrophysiological, neuropathological and molecular biological experiments [11].

Several animal models have been created, involving pharmacologic (e.g., pilocarpine, kainate), electrical (e.g., kindling), genetic (e.g., knock-out mice), and other injurious (e.g., trauma, hypoxia, stroke) methods or stimuli, in order to mimic many types and causes of epilepsy in humans [83]. The most commonly used animal models of MTLE are kainic acid- (a glutamate analogue), pilocarpin- (a cholinergic agonist) and kindling-induced chronic seizures. The neuropathologic alterations overlap with the ones observed in human hippocampal sclerosis, although the CA1 sector cell loss is less dramatically affected in animals compared to humans. On the other hand, subconvulsive electrical kindling of the amygdala results in sustained hippocampal seizure activity, which usually does not produce gross histopathological alterations [8,11,84]. However, these *in vivo* models present several disadvantages including: high mortality, the need for large number of animals, and the relative slow data collection due to the fairly long latent initial insult in relation to seizures onset [84,85].

Given the complexity of epilepsy, there is increasing interest in simplified *in vitro* models of epilepsy that allow more detailed, well-controlled, research of cellular and molecular mechanisms of epileptogenesis while still preserving the critical network phenotypic features of epilepsy, particularly the development of spontaneous seizures [86].

In vitro models can be acute [87], including slices and dissociated cells, or long-term preparations such as tissue culture [88]. Acute brain slices maintain much of the needed circuitry to generate electrographic seizures. However, these preparations are only viable for some hours and thus are not useful for studying chronic epileptogenesis. Tissue cultures, conversely, can be maintained up to 1-2 months while retaining many aspects of the *in vivo* context (e.g., functional local synaptic circuitry, preservation of brain architecture). Therefore the effects of seizure activity including cell death, changes in neuronal interactions, and morphologic rearrangement of networks can be followed for extended periods of time [89–91].

1.2.1 Organotypic Hippocampal Slice Cultures (OHSC)

Over the past two decades, organotypic hippocampal slice cultures (OHSCs) derived from perinatal rats have been developed, optimized and implemented for a variety of studies including both normal and disease models. There are currently two techniques used for culturing brain slices: the roller tube and the membrane interface techniques. The roller tube technique was pioneered by Hogue and later popularized and refined by Gahwiler (1981) [92]. In 1991 Stoppini and co-workers [93] introduced the interface method, which was later modified by others [94]. In the roller-tube cultures, slices flatten to a greater extent, typically into a quasi-monolayer, whereas slices in the interface method stay thicker and retain a semi-three-dimensional structure. The interface method allows hippocampal slices to survive for up to several months in culture and are suitable for electrophysiological recordings and for biochemical studies that require more tissue [92].

To maintain cells *in vitro* for longer periods of time and to evaluate proliferation, migration and differentiation, media that contain components like nutrients and pH buffering substances are used. Horse Serum (HS) is the most commonly used in OHSCs, and includes a complex mixture of growth factors, proteins, vitamins, trace elements, hormones, etc. It also contains several unknown factors and batch-to-batch variations, which have been described as the cause of phenotypical differences among slices, resulting in high variability among results [95]. Moreover, glial cells continue to proliferate, which usually required the addition of cytotoxic inhibitors [96]. It demanded the establishment of a chemically defined medium that would provide long-term growth and healthy metabolic activity of OHSCs [97]. Thus, the OptiMEM-based culture medium supplemented with 25% HS was replaced by a defined serum-free Neurobasal based medium with B27 supplement [98].

Neurobasal medium B27-supplemented enables long-term culture without astrocyte overgrowth. However, agreement has not been established between scientists and manufacturers about the quality of cultures using Neurobasal medium B27-supplemented [99]. Indeed, very few studies have explored the different effects of serum withdrawal from OHSCs [100–102].

1.2.1.1 OHSC as a model of epileptogenesis

OHSC can be prepared from postnatal rats, P0-P7 up to P30. Organotypic slices cultured from P6-P7 periods are ideally suited for epileptogenesis studies. At these age, the hippocampal cytoarchitecture is already established, whereas dentate granule cells are still proliferating, and pyramidal cells as well as interneurons are at postmitotic stages [103]. Additionally, GABA and Glycine receptors act as excitatory [34]. After two weeks of incubation period of maturation, at age of 14 days *in vitro* (DIV), the different cell types, synaptic contacts, and receptor expression resembles that seen *in situ* [92,104,105]. Nevertheless, the deafferentation and deeferentation that occurs during tissue slicing leads to reorganizational processes. These reorganizational processes include: mossy fiber sprouting; reorganization in area CA1 with extended interconnectivity between CA1 hippocampal pyramidal cells; and interconnections between CA1, subiculum and DG [106–108]. Because some of this abnormal connectivity mimics aberrant connectivity in epileptic brain, OHSCs provide a model of chronically epileptic tissue. OHSCs allow exploring molecular and functional alterations at various stages, e.g., acute seizure syndrome, occurrence of neurodegeneration, and development of a chronic epileptic state [90,109].

Despite the abnormal connectivity that is developed in OHSC, spontaneous epileptiform activity in the absence of pharmacological manipulation has rarely been described [110]. Recently, Dyhrfjeld-Johnsen and co-workers [111] provide a detailed functional characterization of the spontaneous development and evolution of epileptiform activity within OHSC. A high incidence of spontaneous epileptiform activity was recorded by field-potential recordings from area CA3 during perfusion with the slices' growth medium of OHSCs from 7 to 30 DIV. A higher incidence of spontaneous epileptiform activity developed later than 7 DIV with primarily interictal-like spikes and bursts at 14-17 DIV followed by ictal-like discharges after 21 DIV. Seizure frequency and rate of epileptogenesis in this model were higher than *in vivo* models, but the epileptiform activity presented similar characteristics, such as the latent period until onset of interictal spikes, progressive transition to ictal events and sensitivity to anticonvulsants [86,111]. Later on, further studies explored the progression of epileptogenesis and ongoing neuronal death in this *in vitro* model. An initial peak of cell death modeled by dissection

in organotypic cultures, and a later secondary peak after 7 DIV, which coincided with the peak of seizure-like activity, was described [112].

Both ictal activity and cell death were prevented by treatment with kynurenic acid (glutamatergic transmission blocker), phenytoin (anticonvulsant), and inhibitors of PI3K-Akt-mTOR pathway (important in apoptosis), while rapamycin led to reduced sprouting, however without inhibiting epileptogenesis [112,113].

Taken together, these results outline that OHSC provide a straightforward model to study the cellular and molecular mechanisms involved in epileptogenesis. It retains several features of clinical epileptogenesis, including gradual onset, axonal sprouting, spontaneous epileptiform activity, activity-dependent cell death, response to anticonvulsants, and emergence of anticonvulsant resistance.

2 AIMS

The focus of this study is to explore the cellular and molecular correlates of epileptogenesis in organotypic hippocampal slice cultures (OHSCs).

In order to accomplish this main goal, the following tasks were pursued:

I – Investigation of the effect of **serum removal** from the OHSC growth medium, through:

- Evaluation of slice integrity;
- Assessment of cell death;
- Spontaneous activity recordings;
- Functional properties.

II – Characterization of the progression of **epileptogenesis** in OHSC growing in a serum-free medium, in terms of:

- Epileptiform activity;
- Astrogliosis and microglia activation;
- $GABA_AR$ and GlyR transcripts expression.

3 MATERIALS AND METHODS

3.1 Animals

Sprague-Dawley rats used for experimental procedures were obtained from Harlan Interfauna Iberia (Barcelona, Spain). The procedures were performed according to the European Community guidelines (2010/63/EU) and Portuguese law concerning the protection of animals for scientific purposes. All efforts were made to minimize animal suffering and to use the minimum number of animals.

3.2 Organotypic Hippocampal Slice Cultures

In this work, OHSC were prepared from 6- to 7- days-old Sprague-Dawley rats, according to the interface culture method presented by Stoppini and co-workers [93]. Rats were decapited, the brains were removed and placed in cold Gey's balanced salt solution (GBSS) with 25 mM glucose, under aseptic conditions. Combined EC-hippocampi were rapidly dissected out and sliced transversely at 350 µm using a McIlwain tissue chopper. Five slices were placed onto porous (0.4 μm) insert membranes (PICM 03050, Millipore, Bedford, MA), which were transferred to six-well culture trays (Corning Costar, Corning, NY) (**Figure 6**). Each well contained 1 mL of culture medium composed of 50% OPTI-MEM, 25% Hanks' balanced salt solution (HBSS), 25% heat-inactivated horse serum (HS), 25 mM glucose, 100 units/mL of penicillin and 100 µg/mL of streptomycin. Culture were maintained in an incubator with 5% CO_2 and 95% atmospheric air at 37ºC. This interface method allows oxygen to diffuse into the slice at a sufficiently high concentration to maintain tissue viability [93].

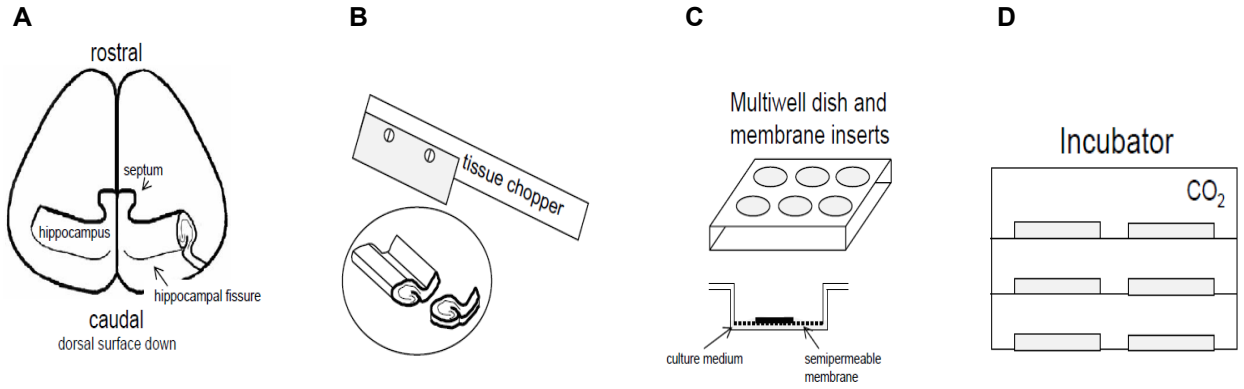

Figure 6| Preparation of OHSCs. (A) The hippocampus and part of the entorhinal cortex are first dissected from the brain. **(B)** Thin sections are cut under aseptic conditions using a tissue chopper. **(C)** Five slices are placed onto a single culture insert in a multiwell dish. **(D)** They are maintained in a CO_2 incubator (Adapted from Heinemann et al., 2006 [90]).

In order to perform the first task, slices were maintained in two different conditions: **1)** in **serum-containing (SC)** growth medium and **2)** in **serum-free (SF)** growth medium. SC medium is the Opti-MEM based medium defined above, while SF medium is a Neurobasal A-based medium. For condition 1, medium was renewed twice a week up to 14 DIV. For condition 2, slices were kept in Opti-MEM based medium until 3 days. Starting at 3 DIV, slices were kept in 1 mL of chemically defined serum-free medium: Neurobasal A, 2% B27, 1 mM L-glutamine, 100 units/mL of penicillin and 100 µg/mL of streptomycin, and decreasing horse-serum concentrations (as depicted in **Figure 7**) until a serum-free condition was reached at 9 DIV.

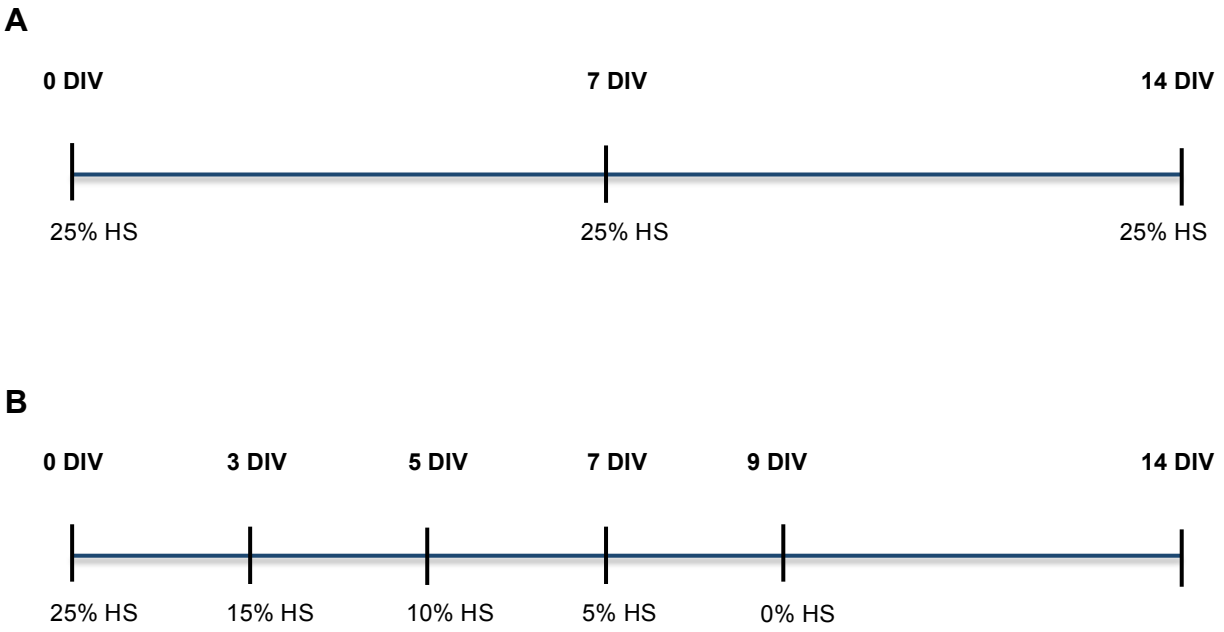

Figure 7| Schematic representation of the experimental procedure. A – Slices growing in a serum-based medium (50% Opti-MEM; 25% HBSS; 25% HS; glucose; antibiotics). The medium was changed twice a week 14 days *in vitro* (DIV). **B –** Slices growing in a serum-free medium (Neurobasal A; B27; L-glutamine; antibiotics). At 3 DIV the medium was changed to supplemented Neurobasal A in the presence of decreasing concentrations of HS (15%, 10% and 5%) until complete serum-free medium that was reached at 9 DIV, in order to ensure a condition of 0% HS at 14 DIV, the time of the functional and molecular analysis.

3.3 Functional Analysis

3.3.1 Extracellular Field Potentials

Electrophysiology techniques enable the study of electrical properties of neurons by measuring voltage change or electric current from single ion channel proteins (intracellular recordings) to the electrical activity of neurons (extracellular recordings).

The hippocampal slice is the principal preparation for studying functional properties of the neurons. This is due to its orderly anatomical arrangement of the neurons and the highly laminated pattern of inputs and outputs (**Figure 8**), which facilitates experimentation. The hippocampal slice has also proved to be a particularly useful *in vitro* preparation for analyzing epileptiform activity [114].

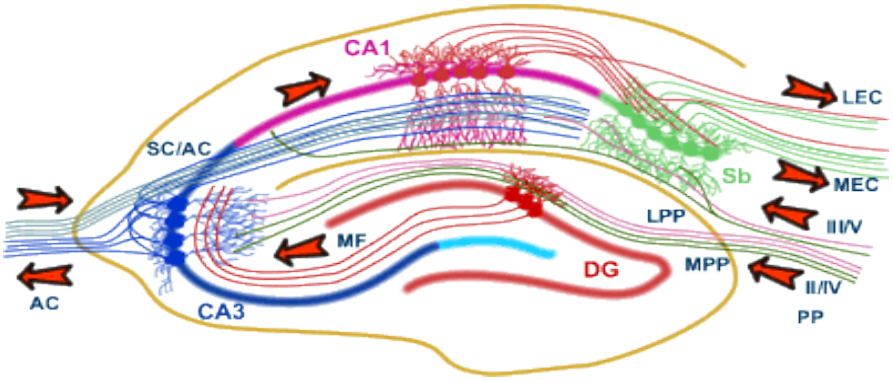

Figure 8| The hippocampal Network. CA – Cornu Ammonis; **DG –** Dentate Gyrus; **Sb –** subiculum; **AC -** associational commissural; **MF -** mossy fibres; **SC -** Schaffer collaterals; **LEC -** lateral entorhinal cortex; **MEC -** medial entorhinal cortex; **PP -** perforant path; **LPP -** lateral perforant path; **MPP -** Medial perforant path [115].

The measurement of action potentials through extracellular field recordings is produced by a current flow from a group of neurons through the extracellular space. Usually those recordings take place in the dendritic regions of CA1 area, and are utilized to monitor synaptic transmission at Schaffer-collateral synapses. A bipolar stimulating electrode is placed on the *stratum radiatum* subfield of area CA1 (**Figure 9**). Stimuli delivered in this fashion stimulate the output axons of CA3 neurons that pass nearby, causing action potentials to propagate down these axons. Responses are typically recorded through an amplifier coupled to a computer, using a data acquisition software [116].

There are three main components in the evoked potentials recorded extracellulary from CA1 area: the pre-synaptic volley, the field synaptic potential and the population spike.
The **pre-synaptic volley** is a biphasic deflection that results from the sum of the action potentials of the afferent fibers stimulated. It is an indicator of the pre-synaptic action potential arriving at the recording site (**Figure 9A, a**).
The **field synaptic potential** is a negative wave if recorded at the *stratum radiatum* level. It reflects the activity of field excitatory postsynaptic potentials (**fEPSPs**), which correspond to a manifestation of synaptic activation (depolarization) in the CA1 pyramidal neurons. For measuring fEPSPs, the parameter typically measured is the initial slope of the EPSP waveform (**Figure 9A, b**). The changes in the excitatory synaptic activity are reflected in the initial slope, while the changes in the inhibitory are mostly reflected in the late phase, i.e., ascendant slope. If there is recording from the

cell body layer, so called *stratum pyramidale*, the EPSP is an upward deflection, and if the cells fire action potentials, the EPSP has superimposed upon it a downward deflecting spike (**Figure 9B**), **the population spike** [117].

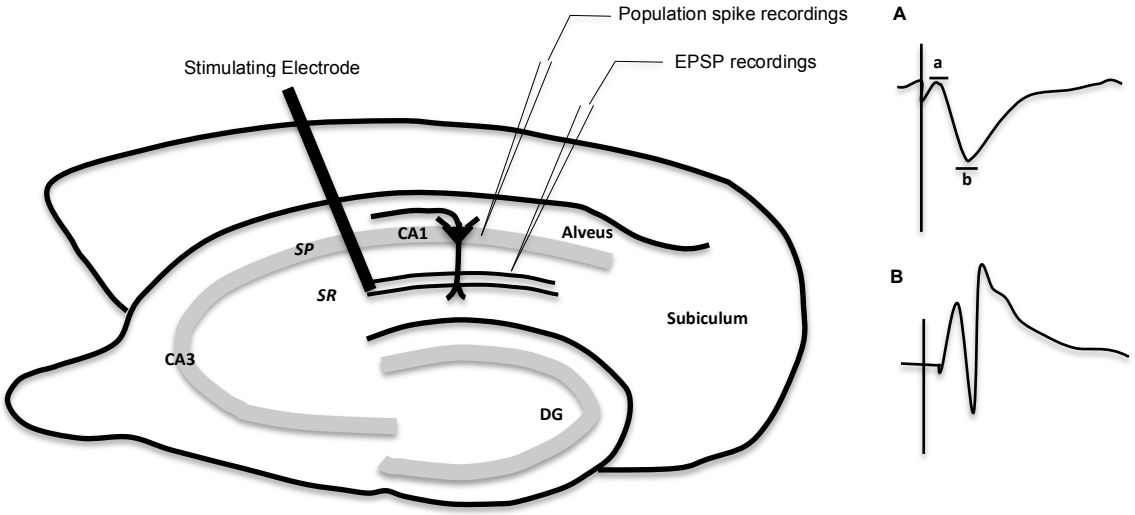

Figure 9| Drawing of the slice preparation showing electrode placements population responses. SR – *Stratum radiatum*; **SP –** *Stratum pyramidale*; **A –** Population EPSP recording, **(a) –** Pre-synaptic volley, **(b) –** EPSP waveform; **B –** Population spike recording.

Information about synaptic transmission can be obtained by constructing input-output (**I/O**) curves. The plots are obtained from the measurement of fEPSP slope versus stimulus intensity. The shape of the curve reflects the number of fibers activated at the different stimulus intensities and the fEPSPs that result from these activated fibers. Therefore, changes in the excitability or threshold of the postsynaptic neurons could be measured so that for a given EPSP a neuron is more likely to fire [118].

Since field potentials reflect activity of a population of neurons, they can be used to monitor epileptiform activity. It is due to the capacity of some populations of neurons to generate high-frequency synchronous discharges underlining the development of epileptogenesis [119].

3.3.1.1 Input-Output (IO) curves

I/O curves in slices, maintained in the two different growth medium (**section 3.2**), were performed in order to evaluate serum effects on basal synaptic transmission.

Individual slices were cut off from the insert and transferred to the submersion recording chamber (1 mL capacity). Slices were continuously superfused at a constant flow (3 mL/min) with prewarmed (34ºC ± 0.2 ºC) and oxygenated (5% CO_2/95% O_2) Krebs solution of the following composition (mM): NaCl 124, KCl 3, $NaHCO_3$ 26, Na_2HPO_4 1.25, $MgSO_4$ 1, $CaCl_2$ 2, glucose 10. After 20 minutes immersed in Krebs solution to ensure the energetic and functional recovery of the slices, fEPSPs were recorded through an extracellular microelectrode (4M NaCl, 2-4MΩ resistance) placed in *stratum radiatum* of CA1 area. Stimulation (rectangular 0.1 ms pulses, once every 15 s) was delivered through a concentric electrode placed on the Schaffer collateral/commissural fibers, in *stratum radiatum* near CA3-CA1 border. The intensity of stimulus (60-300 μA) was initially adjusted to obtain a large fEPSP slope, with a minimum population spike contamination, and recording for at least 15 minutes until obtain a stable baseline. Stimuli delivery was then successively increased by steps of 20 μA, with a supra-maximum stimulation amplitude of 300 μA. For each stimulation condition, data from three consecutive average fEPSP (of a mean of eight individual fEPSP) was stored.
The I/O curve was plotted as the relationship of fEPSP slope *vs* stimulus intensity, which provides a measure of synaptic efficiency.
Recordings were obtained with Axoclamp 2B amplifier and digitized (Axon Instruments, Foster City, CA), and monitored on a personal computer with the WinLTP software [120].

3.3.1.2 Epileptiform activity recordings

To monitor the epileptiform activity in OHSCs, a recording system using the interface type chamber as previously described by Dyhrfjeld-Johnsen [111] (**Figure 10**), was established.
Individual slices at 14 to 30 DIV were transferred to the interface recording chamber with a humidified gas (95% O_2/5% CO_2) atmosphere at 36ºC with Neurobasal serum-free medium (**section 3.2)**, continuously superfused and recirculating at a rate of 2 mL/min. After a 20 minutes equilibration period, field-potential recordings were performed with an extracellular microelectrode (4M NaCl, 2-4MΩ resistance) positioned in the CA3/CA1 pyramidal cell layer over 30-40 minutes.

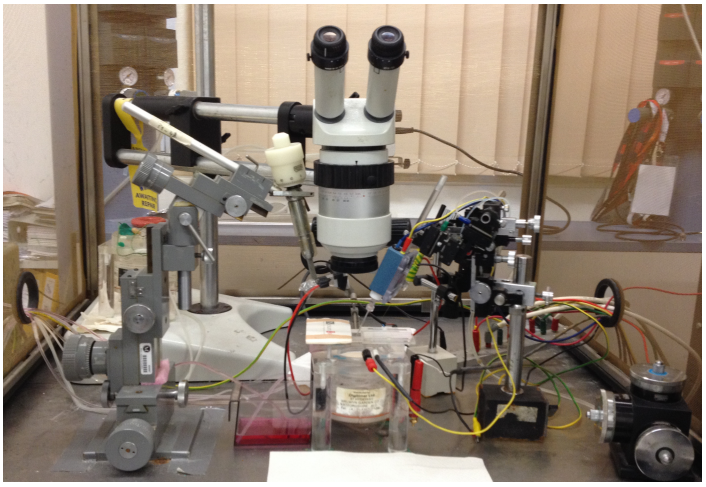

Figure 10| Setup for extracellular recordings

Continuous recordings were obtained with Axoclamp 2B amplifier and digitized (Axon Instruments, Foster City, CA), running on the WinLTP software. Data analysis was carried out by pCLAMP 10 software program (Molecular Device Corporation, CA).

3.3.2 Patch-Clamp Recordings

Whole-cell recordings are from single cells as opposed to a population of cells. In this technique, electrical events in individual neurons are detected even when they are not synchronized across the population. There are two configurations: current-clamp and voltage-clamp. The membrane potential is recorded in current-clamp configuration. Recording currents instead of potentials allows the properties of synapses to be studied without the effects of changing ionic driving forces, which result from changing potential [121].

3.3.2.1 Whole cell recordings

The slices were transferred to a Carl Zeiss Axioskop 2FS upright microscope (Jena, Germany) equipped with infrared video microscopy and difference contrast optics. The recording chamber was continuously superfused by a gravitational superfusion system at 2-3 mL/min with pre-warmed Krebs solution.

Patch pipettes (1.5mm outer diameter, 0.86 inner diameter, Harvard Apparatus) made on a pipette puller (PC-10 Puller, Narishige Group) were filled with an internal solution

containing (mM): K-gluconate 125; KCl 11; $CaCl_2$ 0.1; $MgCl_2$ 2; EGTA 1; HEPES 10; MgATP 2; NaGTP 0.3 and phosphocreatine 10, pH 7.3, adjusted with KOH (1M), 280-290 mOsm.

To optimize success of recording from pyramidal neurons, phase-bright cells were selected based on both size and pyramidal shaped soma.

Whole-cell was recorded in a current clamp plus mode with an EPC-7 amplifier (List Biologic, Campbell, CA). Offset potentials were nulls directly before giga-seal formation. Immediately after establishing whole-cell access, the membrane potential (Vm) of the neurons was measured in current-clamp mode.

Data acquisition was carried out by AxoScope 10 software program (Molecular Device Corporation, CA).

3.4 Molecular Analysis

3.4.1 Quantitative Real-Time PCR (qPCR)

The polymerase chain reaction (PCR) is a simple method used for amplifying DNA sequences *in vitro*, developed in 1983 by Kary Mullis. The standard PCR reaction incorporates three basic steps. Firstly, the double-stranded DNA (dsDNA) is heat denatured (90-95ºC) to separate into two single strands. Secondly, the specifically designed primers are allowed to anneal on a predetermined DNA region by lowering the temperature (40-70ºC). Third, a thermostable DNA polymerase synthesizes the new DNA strand in the presence of four-deoxyribonucleotide thriphosphate (dNTPs) at its optimal temperature (72ºC). Each cycle of replication is repeated a pre-determined number of times, resulting in an exponential amplification of the number of target molecules each cycle. PCR amplification reactions are highly specific, depending on the correct hybridization of primer specific sequences [122].

Reverse transcriptase PCR (RT-PCR) is a variant version of PCR used to detect RNA expression levels in a sample. To this end, reverse transcriptase is added together with a reverse primer and nucleotides to generate a cDNA from mRNA samples. The sample is then subjected to standard PCR procedures. Comparing with other techniques (e.g. Northern blotting, RNase protection assay), the RT-PCR assay is much more sensitive

since it detects very low abundance of mRNA, being ideal for detecting mRNA from small amount of tissue samples. However, it compromises the specificity of the reaction, increasing the likelihood of contamination and of detection of false positives [122,123]. Therefore the monitoring of extracted RNA quality and the use of negative controls are important quality control factors in RT-PCR [124].

The monitoring of extracted RNA quality comprises its purity and its integrity. The extracted RNA purity can be assessed by spectrophotometry based on an absorption ratio of 260/280 nm, where an absorbance ration between 1.9 and 2.0 indicates purified RNA, and a ratio of 2.1 indicates highly purified RNA. Since both DNA and RNA absorb at 260 nm, the absence of genomic DNA is commonly assessed by the use of a negative control. The most common method to assess the integrity of total RNA is to run an aliquot of the RNA sample on a denaturing agarose gel stained with ethidium bromide (EtBr). The ratio 2:1 between rRNA bands (28S:18S) is an indication that the RNA is completely intact. On the other hand, the internal RT-PCR controls allow to be sure that the absence of RT-PCR amplification product is not due to RNA degradation. This can be determined by RT-PCR amplification of mRNA from constitutively expressed "housekeeping" genes from the same sample of extracted RNA, or even within the same RT-PCR mix that is to be used for RT-PCR amplification. Glyceraldehyde-3-phosphate dehydrogenase (GAPDH) is one of the most commonly used housekeeping genes, though others including β-actin and α-tubulin can also be used. The mRNA synthesis of these genes is considered to be stable and secure in various tissues, even under experimental treatments [122,125].

Real-time PCR is the most sensitive and quantitative approach to PCR, which allows quantification of rare transcripts and assessment of small changes in gene expression. Real-time PCR consists in a continuous detection and quantification of fluorescent signal from one DNA fragment over a range of cycles, based on the wavelength light emitted by the dye associated to the DNA. The simplest detection technique uses the SYBR Green I fluorescence dye, which is a highly specific dsDNA binding dye that remains associated with DNA generated during the PCR amplification. The application of fluorescence techniques to real-time PCR combines the PCR amplification, product

detection and quantification of newly synthesized DNA, as well as specificity verification in the melting curve analysis. Melting curves provide an accurate identification of amplified products and distinguishing them from primer dimers and other small amplification artifacts [124]. The advantages of the real-time PCR method are the possibility of being performed in a close-tube system and no requirements for post-PCR manipulation of sample, avoiding potential contaminations. Its high ramping rates, limited annealing and elongation time, the rapid PCR cycle in the LightCycle system offers stringent reaction conditions to all PCR components and leads to a primer sensitive and template specific PCR [126–128].

RT-PCR data analysis can be either absolute or relative. The absolute quantification is adequate for precise determination of total RNA concentration, usually by relating the PCR signal to a standard curve. A relative quantification determines the changes in a steady-state transcription of a gene, always relative to a reference gene.

There are several methods used in relative quantification analysis, which differ in their accuracy and reproducibility [129]. Most of the methods utilize data from the exponential phase of PCR amplification and require setting threshold fluorescence to determine the threshold cycle (Ct) value. The target Ct is directly compared with the control Ct and is recorded as containing either more or less DNA.

In the mathematical model developed by Pfaffl (2001) [130], the relative expression ratio (R_{pfafll}) of a target gene is calculated based on RT-qPCR efficiency (E) and crossing point (CP) deviation of a treated sample *versus* a control sample, and expressed in comparison to a reference gene. The normalization of target gene expression with an internal control gene is useful in order to compensate sample-to-sample and run-to-run variations and to ensure the experimental reliability. The PCR efficiency determination can be assessed by serial dilution of the prepared cDNA. As the diluted cDNA sample accumulates during the early exponential phase of the reaction the crossing threshold on Ct value is taken. From the various Ct values a log graph is prepared from which the PCR efficiency can be deduced [130].

3.4.1.1 RNA preparation

RNA was extracted from OHSCs according to the QIAGEN RNeasy Mini Kit. Firstly, the hippocampus proper was separated from EC using a dissecting microscope (Olympus). Then, the collected tissue was homogenized with QIAzol lysis reagent and with a TissueRuptor homogenizer, previously DEPC-treated. RNA concentration was accurately determined using Nanodrop 1000 (ND-1000 Spectrophotometer, Thermo Scientific). The integrity of total RNA was confirmed by gel electrophoresis.

3.4.1.2 Reverse transcription reaction

In vitro reverse transcription (RT) was performed from 2 μg of total RNA (in 20 μL) and carried out with SuperScript II Reverse Transcriptase (EC 2.7.7.49, Invitrogen, Carlsband, CA, USA) in a thermoclycler (MyCycle – Bio-Rad, Hercules, CA 94547), according to the manufacturer's recommendations (SuperScript First Strand Synthesis Systems for RT-PCR from Invitrogen). For each RNA sample a reverse transcription reaction was carried out in the absence of reverse transcriptase (negative control) to ensure that product amplification did not arise from genomic DNA.

3.4.1.3 Quantification

cDNA amplification was performed in a Rotor-Gene 6000 real-time rotary analyzer thermocycler (Corbett Life Science, Hilden, Germany) in the presence of SYBR Green Master Mix (Applied Biosystems, Foster City, CA, USA) and 0.2 μM of each specific gene primer (**Table 1**). The PCR conditions included an initial denaturation for 2 min at 94ºC, 50 cycles with 30 s at 94ºC, 90 s at 60ºC and 60 s at 72ºC, followed by a melting curve to assess the specificity of the reactions. The Ct and the melting curves were acquired with Rotor-Gene 6000 Software 1.7 (Corbett Life Science). PCR efficiency, needed for the relative quantification by comparative Pfaffl method (**Section 3.4.1**), was determined by calibration curves with 5-fold sequential dilutions of the cDNA for each gene. GAPDH was used as a reference internal standard. For each gene, replica reactions were performed and the mean Ct of the two reactions was used to calculate the corresponding expression level. Two types of negative controls, "no reverse transcription" and "no template" were run with samples.

Table 1| Primers used in qPCR.

Gene	Primer Sequence	PCR Fragment Size (pb)
GAPDH	**Forward:** GTTTGTGATGGGTGTGAACC **Reverse:** TCTTCTGAGTGGCAGTGATG	170
GlyR $\alpha 1$	**Forward:** ACTCTGCGATTCTACCTTTGG **Reverse:** ATATTCATTGTAGGCGAGACGG	300
GlyR $\alpha 2$	**Forward:** CAGAGTTCAGGTTCCAGGG **Reverse:** TCCACAAACTTCTTCTTGATAG	330
GlyR $\alpha 3$	**Forward:** GTGAGACACTTTCGGACATAC **Reverse:** GATGGGTCGAGGTCTAATGAATC	353
GlyR β	**Forward:** CTGTTCATATCAAGCACTTTGC **Reverse:** GGGATGACAGGCTTGGCAG	223
$GABA_AR$ $\alpha 1$	**Forward:** TGTGGCAGAAGATGGGTCAC **Reverse:** AGAACGGTCGTCACTCCAAA	252
$GABA_AR$ $\alpha 2$	**Forward:** ACAACGGGAAAAAGTCAGTGG **Reverse:** ACCGTGTATTCACCTGTGCTT	331
$GABA_AR$ $\alpha 3$	**Forward:** CCAAGGGGAGTCAAGACGAC **Reverse:** AGTCACTGCATCTCCAAGCC	190
$GABA_AR$ $\alpha 4$	**Forward:** GGATTTGGGGGTCCTGTTAC **Reverse:** TGGGACACTCCGCACTTATG	325
$GABA_AR$ $\alpha 5$	**Forward:** TGCAACGTCTCCCTCTCAAC **Reverse:** TATTCACCTGTGCTGGTGCT	388
$GABA_AR$ $\beta 1$	**Forward:** AGCTTGCATGATGGATCTCC **Reverse:** GGATATGCCCCTGTTGTGAAT	216
$GABA_AR$ $\beta 2$	**Forward:** GATTTCGGAGGTCCCCCTGT **Reverse:** GCTTTCGATCTCCAACGTGC	381
$GABA_AR$ $\beta 3$	**Forward:** ATGGAACAGTGCTGTACGGG **Reverse:** AGGCACCTGTGGCGAAGAC	252
$GABA_AR$ $\delta 2$	**Forward:** ATCGCTCTACCCAGGCTTCA **Reverse:** TCCAGTGAGCATCCGCTTTT	395

GlyR – Glycine receptor; **$GABA_AR$** – Gamma-aminobutyric acid A receptor.

3.4.2 Immunohistochemistry (IHC)

Since the first use of an antibody for Immunohistochemistry (IHC) reported in 1941 by A. Coons and colleagues [131], IHC is considered an invaluable tool in the neuroscience field. This technique is based on the interaction process of detecting antigens (e.g., proteins) in tissue sections through specific antibodies (Abs). It has allowed studies of the structure and function of biologically relevant neuronal circuits [132]. IHC is a robust, versatile and sensitive method. It is, however, largely empirical and requires a good understanding of its specific limitations [133].

The interaction antigen-Ab can be detected by either direct or indirect methods. The labels (reported molecules) are enzymes, fluorescent compounds, and metals, attached to the primary, or secondary Ab. **The direct method** is the simplest and involves a one-step process. The Ab against the molecule of interest, called the primary Ab, is reaction chemically conjugated to the reporter molecule. The advantages of this method include shorter sample staining times, and in cases where one has multiple Ab raised in the same species a direct labelling may be necessary. However, it produces a weak signal, generally has high cost, and low flexibility. In **the indirect method**, the Ab specific for the molecule of interest is unlabelled, and a second anti-immunoglobulin (IgG), the secondary Ab, directed toward the constant portion of the first Ab is tagged with the reporter molecule. The indirect method has greater sensitivity and there is greater amplification of the signal. Commercially produced secondary Abs are relatively inexpensive, available in an array of colours, and quality controlled. The disadvantages of this method include the potential for cross-reactivity and the need to find primary Abs that are not raised in the same species or of different isotypes when performing multiple-labeling experiments [134,135].

3.4.2.1 Immunofluorescence microscopy

Immunofluorescence (IF) microscopy uses Abs conjugated to fluorescent reporter molecules, called fluorophores. In order to observe fluorescence through the microscope, the sample is submitted to high intensity light and of specific wavelengths, generally in the region between 300 nm and 700 nm. The fluorophore absorbs light of specific wavelengths (excitation) and simultaneously re-emits part of this energy at longer wavelengths (emission), usually in the visible region of the spectrum. Multicolor fluorescence immunostaining enable to co-localize antigens not only in the same cell but also in the same cellular compartment, comparing with multicolor immunoenzyme staining applicable only for separately located antigens. However, fluorescence decays in time and although anti-quenching agents can be used, the preparations are not permanent. Fluorescent staining can be visualized with standard fluorescent microscopy as well as in confocal microscopes [127,134,136].

Confocal microscope focuses a spot of light onto a single point at a specific depth in the specimen. It requires a very bright source of pinpoint illumination that is usually supplied by a laser whose light has been passed through a pinhole. The fluorescence emitted from the illuminated material is collected and brought to an image at a suitable light detector. Confocal microscopy not only provides information on structures in an individual plane but also can collect multiple sections in the Z direction generating a Z-stack. Computer programs can then reconstruct an optical image of the cell in 3-dimensions. Another advantage of using confocal microscopy is that filtering is used to eliminate out-of-focus signals that otherwise degrades the quality of the image giving significant background. Brighter images are obtained with confocal microscopy in comparison to standard immunofluorescence [137].

Critical limitations of the IHC protocol mainly involve issues of Ab penetration and antigen accessibility. Therefore, the outcome of an immunohistochemical reaction depends on the properties of the Abs used, as well as on several physic-chemical parameters of the tissue to be processed, mainly its fixation [133].
Generally immunostaining is carried out on fixed and permeabilized tissues. Fixed tissues are prepared by agents, including paraformaldehyde and formaldehyde, which maintains structure and make the cell membranes permeable. Further permeabilization of aldehyde-fixed cells is usually accomplished with a detergent, such as Triton X-100. The agents that are used for fixation and permeabilization are strictly cell and antibodies dependent. Other agents, such as methanol can also be used as fixative. After permeabilization, tissue is treated with the primary Ab (mouse, rabbit, chicken, rat, donkey, etc.) followed by incubation with the fluorophore-conjugated secondary Ab directed to the host of the primary one. For multiple immunolabelling, if primary Abs are produced in same species, sequential dual labeling is necessary; if primary Abs derive from different species, both primary Abs can be added simultaneously. This avoids false positive staining. Controls for false negative are also required to assess problems of the specificity of an antibody [127,128,135]. Due to some limitations of the immunohistochemistry, quantitative measurements derived from other methods should also be performed [133].

3.4.2.2 Culture sectioning

Cultured slices (14 and 21 DIV) were fixed with 4% paraformaldehyde in phosphate buffer solution (4% PFA in PBS) for 1 hour at room temperature (RT). Slices were sequentially incubated in increasing concentrations of sucrose in PBS (1h in 10% and 1h in 20%) at RT. Finally cultures were transferred to a 30% sucrose solution and maintained at 4ºC.

Slices were cut off the membranes of the culture plate inserts, embedded in Tissue-Tek (Sakura Finetek Europe, Zoeterwoude, The Netherlands), and gradually frozen in the cryostat (Leica, Germany), where the chamber was maintained below -20ºC. Slices were then sectioned to a thickness of 20 μm. The sections were collected on separate gelatinized slides, 3-4 slices per slide, and stored at -20ºC for further processing.

3.4.2.3 Immunohistochemical staining

One or two slices were surrounded with DAKO pen (Dako, Denmark) to protect staining areas from drying out. After PBS washes, slices were permeabilized with 1% Triton X-100 (Sigma) in PBS for 10 minutes at RT. Washed two times, blocking buffer 6% Bovine Serum Albumin (BSA) in PBS was applied for 1 hour. Slices were incubated with dilute primary Abs (**Table 2**) in blocking solution for 48 hours at 4ºC. After washed with PBST (PBS with 0.1% Tween-20), slices were incubated with the fluorescent-labeled secondary Abs (donkey anti-rabbit Alexa Fluor 488, donkey anti-goat Alexa Fluor 488 or donkey anti-mouse Alexa Fluor 568, 1:400, Invitrogen) for 4-6 hours at RT. Nuclei were stained with Hoechst 33342 (20 mg/mL, Invitrogen) for 15 min at RT. Slices were then washed, mounted, and imaged with a confocal laser scanning microscope (LSM 710, Zeiss, Germany), using either an EC plan-NeoFluar 5x or a Plan-Apochromat 20x objective (Zeiss, Germany), with a frame size of 1024 x 1024 pixels. Negative controls were carried out in absence of primary Abs.

Table 2| Primary antibodies used in immunohistochemistry (IH) assays to target different cell population: astrocytes, microglia cells and neurons.

Protein	Supplier	Host	Dilution
NeuN	Grupo Taper	Mouse monoclonal antibody	1:150
GFAP	Sigma	Rabbit polyclonal antibody	1:750
Iba-1	Abcam	Goat polyclonal antibody	1:1000

NeuN – Neuronal Nuclei; **GFAP** – Glial fibrillary acidic protein; **Iba-1** – Ionized calcium binding adaptor molecule 1.

3.4.2.4 Propidium iodide (PI) uptake assay

In order to evaluate the hippocampal areas most affected by the cell loss propidium iodide (PI) uptake assays was performed. PI can only enter cells with already damaged membranes and bind to nucleic acids rendering the damaged cells brightly fluorescent [138]. PI imaging was carried out in cultured slices at 14 DIV. The slices were incubated with 2μM sterile propidium iodide solution (Sigma, St. Louis, MO, USA) diluted in culture medium for 4 hours before imaging. The photographs of the stained slices were acquired with an EC Plan-NeoFluar 5x objective, on a widefield fluorescence microscope (Axiovert 200, Zeiss, Germany). Fluorescence was quantified using the software ImageJ software 1.44b (NIH).

3.4.3 Western Blot (WB)

Western blotting or immunoblotting is used to identify specific proteins as well as to quantify the protein expression from a complex mixture of proteins extracted from cells or tissues. It is based on protein interaction with a specific Ab and its relative molecular weight. Western blotting comprises three general steps: (**1**) separation by size, (**2**) transfer to a solid support, and (**3**) marking the target protein using a proper primary and secondary Ab to visualize [139].

Protein extraction attempts to collect all the proteins in the cell cytosol. It requires mechanical intervention, such as homogenization, or sonication. This should be done in a cold temperature, in a buffer adequate to maintain pH, ionic strength and stability and in presence of protease inhibitors to prevent denaturing of the proteins. After extracting the protein, its concentration is measured using a spectrophotometer in order to

establish the mass of protein that will be loaded into each well by the relationship between concentration, mass, and volume.

SDS-PAGE (sodium dodecyl sulfate-polyacrylamide gel electrophoresis) is the most widely used method for analyzing proteins. It is quantitative and separates proteins according to their size. Firstly, the protein mixtures are diluted into a loading buffer, which contains SDS, glycerol, and bromophenol blue. Samples are heated at 95ºC for 10 minutes in order to denature the higher order structure, while retaining sulfide bridges. SDS is an anionic detergent that binds to hydrophobic regions, and causes the protein to acquire a net negative charge, enabling the protein to move in an electric field applied during electrophoresis procedure.

Most SDS-PAGE gel is prepared with two types of acrylamide gel, a narrow stacking gel above the primary separating gel. The stacking gel is slightly acidic (pH 6.8) and has a lower acrylamide concentration making it highly porous in order to concentrates the proteins into thin and sharply defined bands. The resolving gel is basic (pH 8.8) and has higher polyacrylamide content, making gel pores narrower. When a voltage is applied, the smaller proteins migrate easily within the pores, and hence rapidly, than larger proteins. This method ensures that all proteins enter the resolving gel at the same time, improving resolution and reproducibility [140].

After separating the protein mixture, proteins can be transferred quantitatively to a membrane by electroblotting. Membranes are typically made of chemically inert substances such as nitrocellulose or polyvinylidene difluoride (PVDF). PVDF membranes are most used since they provide better mechanical support and allow the blot to be reprobed and stored. However, the background is higher in the PVDF membranes. The transferring process is carried on placing the membrane between the gel surface and the positive electrode in a sandwich so that proteins move from gel to membrane (blot). This procedure is carried out in wet conditions in which the membrane is immersed in transfer buffer. Wet conditions are preferred for larger proteins and are usually more reliable [139,140].

Identification of target proteins involves probing the blot with specific Abs. Protein detection encompass two steps: (**1**) membrane blocking, and (**2**) immunodetection and visualization. Membrane blocking is achieved by incubating the membrane in blocking solutions, such as protein-enriched solutions (e.g., BSA or nonfat dried milk) and anionic detergents (e.g., TBST) to prevent non-specific binding of antibody to the membrane itself. The appropriate blocking solution is reliant on compatibility detection labels. For example, BSA blocking solution is preferred with biotin and alkaline phosphatase (AP) antibody labels, and antiphosphoprotein antibodies, since milk contains casein, which is itself a phosphoprotein [139].

After the blocking step, the immunodetection can be targeted either through direct or indirect Ab system, as described in IHC technique (**section 3.4.2**). For indirect labeling the membrane is incubated in the primary Ab solution and after washing, it is treated with a solution of a secondary Ab-enzyme conjugated. Horseradish peroxidase (HRP)-coupled Abs are commonly used. HRP catalyzes the oxidation of luminol in the presence of hydrogen peroxide, and results in light emission capable of impressing an X-ray film. Thus, the image of the blot is visualized by simply exposing the blot to an X-ray film. The signal intensity is proportional to the protein quantity on the blot, allowing relative quantification. The proteins bands are normalized to a housekeeping protein, such as α-tubulin, or β-actin, or GAPDH [140]

3.4.3.1 Whole tissue lysates

Hippocampal tissue derived from 4-5 slices was placed in 200 μL of lysis buffer, containing 50 mM Tris base pH 8, 1 mM EDTA, 150 mM NaCl and 1% NP40 (Fluka Biochemika, Switzerland) and supplemented with protease inhibitors (complete Mini-EDTA free, Roche, Germany). Homogenization took place in a Potter-Elvehjem homogenizer with a Teflon piston. Cell suspension was left shaking for 15 min at 4 ºC and the insolubilized fraction was removed by centrifugation, 11000 g during 10 minutes at 4ºC. The supernatant was collected and protein was quantified using the BioRad DC Protein assay Kit.

3.4.3.2 Western blot quantification

Samples (35μg total protein/well) and protein size marker (Precision Plus Protein Standards, Bio-Rad) were run on a standard 12% SDS-PAGE and transferred to PVDF membranes.

Subsequently, membranes were blocked for 1 hour with 3% BSA in TBST (20 mM Tris base, 137 mM NaCl and 0.1% Tween-20) and probed probed with the primary Abs (**Table 3**), diluted in 3% BSA with 0.02% NaN_3, overnight at 4ºC. Finally, membranes were incubated with goat anti-rabbit or donkey anti-goat horseradish peroxidase (HRP)-conjugated secondary antibodies (1:10000, Santa Cruz Biotechnology).

Development of signal intensity was carried out using the ECL Plus Western Blotting Detection System (Amersham-ECL Western Blotting Detection Reagents from GE Healthcare, Buckinghamshire, UK) and quantifications were attained by densitometric scanning of the films, performed with the Image J software. GAPDH density was used as the loading control.

Table 3| Primary antibodies used in western blot (WB).

Protein	Supplier	Host	Dilution
GFAP	Sigma	Rabbit polyclonal antibody	1:5000
Iba-1	Abcam	Goat polyclonal antibody	1:1000

GFAP – Glial fibrillary acidic protein; **Iba-1** – Ionized calcium binding adaptor molecule 1;

3.5 Statistical Analysis

All statistical analysis was performed using GraphPad Prism software (San Diego, CA, USA). Comparisons between two conditions were made using Student's t-Tests. Multiple comparisons were carried out using one-way analysis of variance (ANOVA) followed by Bonferroni's correction post-test.

4 RESULTS

4.1 Organotypic Hippocampal Slice Cultures

The first step of this work was to evaluate the effects of serum removal from organotypic slice cultures, which concern to slice integrity, degree of cell death and functional synaptic transmission. As described in **section 3.2**, two growth conditions were developed: **1)** cultures maintained in serum-containing media (**SC**), and **2)** cultures progressively changed and maintained in a Neurobasal-based serum-free media (**SF**). Both slice cultures were evaluated at 14 DIV.

4.1.1 Slice Integrity is not Affected by Serum-removal

Cultures of longitudinal slices of combined EC-hippocampus were carried out in this work (**Figure 11).** The EC was maintained since it contributes to the generation of discharges resembling interictal and ictal events [111,141].

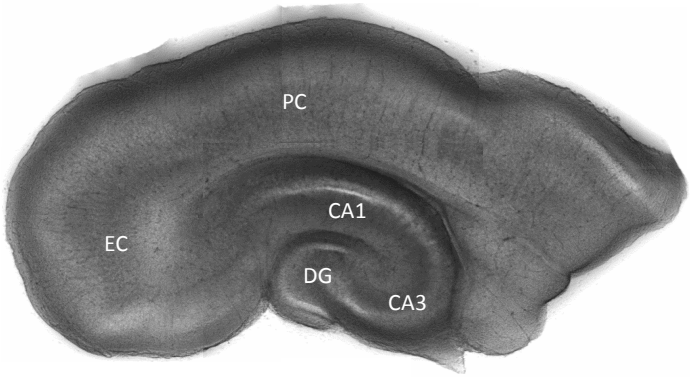

Figure 11| Photograph of combined EC-hippocampal slice immediately after dissection. CA, cornu ammonis**; DG,** dentate gyrus; **EC,** entorhinal cortex; **PC,** perirhinal cortex;

Evaluation of slice integrity was conducted by an immunofluorescence protocol, in which slices were labeled with an Ab against NeuN (a neuron specific nuclear protein) and Hoechst (a nuclear marker).

The gradual removal of serum over a 6-day period starting at 3 DIV (**sections 3.2**), and the maintenance of slices in fully defined culture media (Neurobasal-A plus B27 supplement) did not affect the lamellar organization of the hippocampus **(Figure 12)**. NeuN positive staining, shown in panels **A2** and **B2,** was observed in granular neurons

from DG and pyramidal neurons from CA areas, as well as interneurons present in the dendritic areas. As expected, Hoechst staining, illustrated in panels **A1** and **B1**, was spread within the whole hippocampal structure and observed, not only in NeuN positive nucleus (purple color in panels **A3** and **B3**), but also in other non-neuronal cells (e.g. glial cells). Nevertheless, slices derived from **SF** condition were more difficult to cut in the cryostat. This is presumably caused by larger decrease in cell density of cultures grown under Neurobasal **SF** conditions, compared with cultures maintained in **SC** medium, as previously described [102].

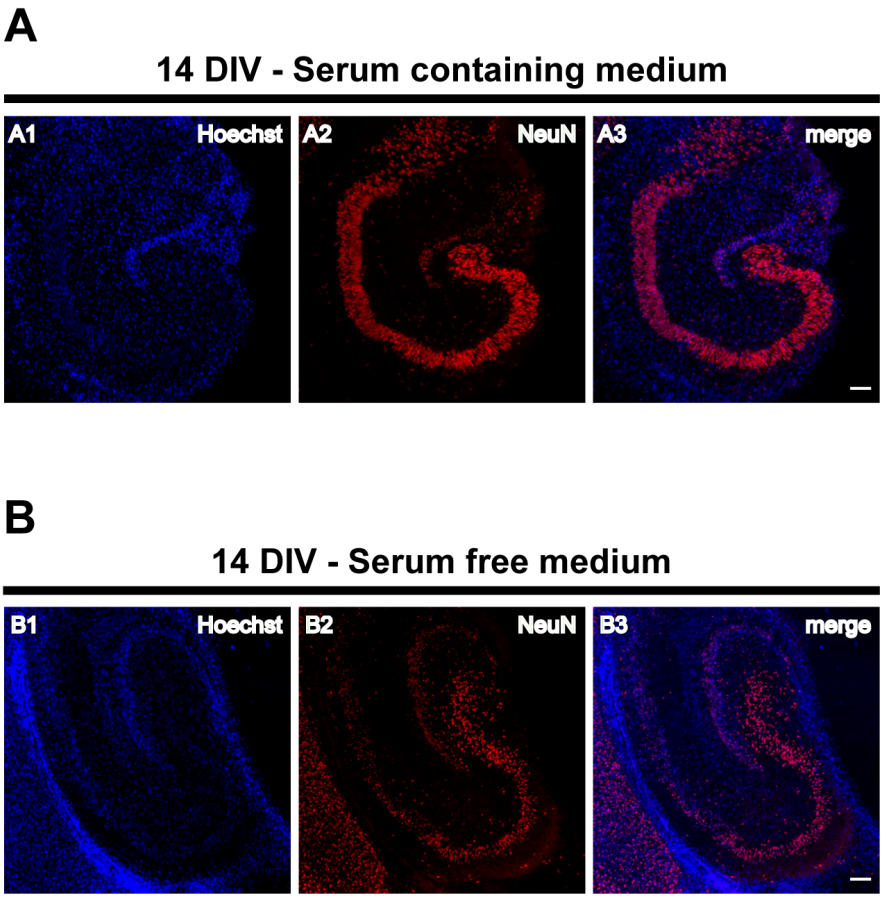

Figure 12| Immunofluorescent characterization of organotypic hippocampal slices obtained from 14 days *in vitro* (DIV) grown in two different conditions. A) Slice grown in serum-containing medium; **B)** Slice grown in serum-free medium. The first two images of each panel represent each labeling alone: blue for nuclear staining with Hoechst **(A1 and B1)** and red for NeuN stained neurons **(A2 and B2).** The merge images **(A3 and B3)** show the preserved hippocampal slice integrity and organization. Confocal images were acquired with a 5x objective. Scale bars, 200 μm.

4.1.2 Cell death is not Serum-dependent

To determine if serum removal plays a role in cell death of the explants, PI staining was analyzed. PI uptake was measured in each slice through the integrated density of fluorescence, normalized to the area and background fluorescence of each image in an independent way.

As shown in **Figure 13A,** both conditions display PI-positive cells. Most of the PI-positive cells were concentrated in DG granule cell layer and CA3 and CA1 pyramidal cell layers, suggesting neuronal cell death. However, no differences were found comparing PI-positive cells from slices growing in **SC** medium and **SF** medium. When comparing between hippocampal cell regions (CA1, CA3 and DG), CA1 region showed significantly higher PI uptake than DG in **SC** slices (152.9 ± 10.45 *vs* 104.4 ± 9.34, n=17, $p<0.05$), as well as in **SF** slices (152.2 ± 48.8 *vs* 105.6 ± 7.83, n=29, ***$p<0.001$). On the other hand, the CA3 region did not show a significant difference in cell death when compared to either CA1 or DG at either growth conditions (**Figure 13B**).

A

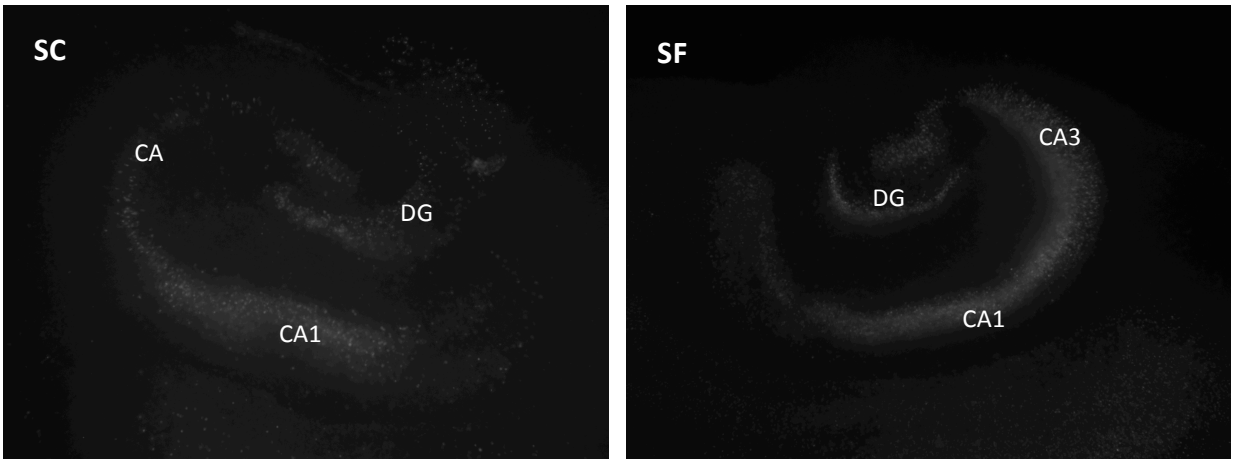

B

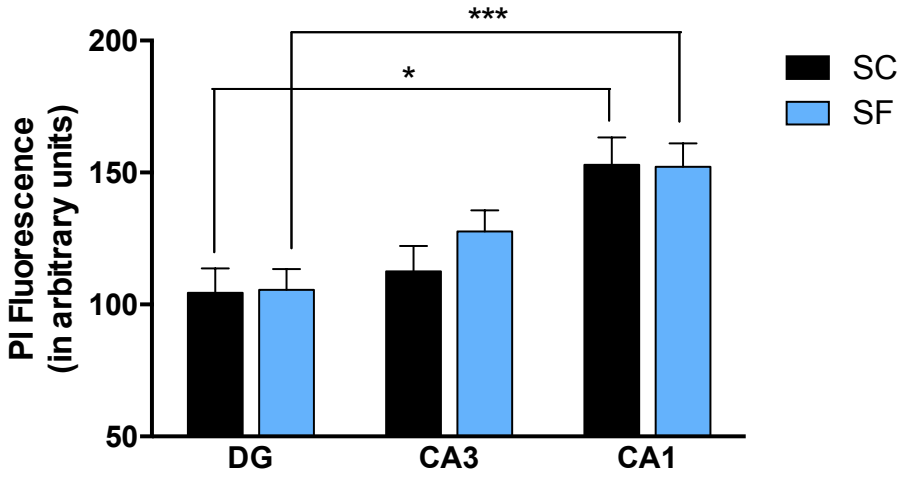

Figure 13| Propidium iodide (PI) uptake in OHSCs at 14 days *in vitro* (DIV). A) Representative PI staining indicating no differences between cell death in slices grown in serum-containing medium (**SC**) and serum-free medium (**SF**). **B)** Quantification of PI uptake by each hippocampal region expressed in arbitrary units of fluorescence intensity. Cell death is significantly higher in the CA1 cell region than it is in the dentate gyrus (DG)**.** All values are mean ± SEM. 17 < slices < 29; p*<0.05, ***p<0.001, one-way ANOVA followed by Bonferroni's Comparison Test.

4.1.3 Serum-free Slices Develop Increased Spontaneous Epileptiform Activity

The culturing of hippocampal slices provides the advantage of long-term use while retaining many aspects of the *in vivo* context (e.g. functional local synaptic circuitry and preservation of brain architecture). However, the mossy fiber pathway develops *in vitro* may be responsible for aberrant synaptic activity, causing organotypic slice cultures to be more excitable than acute slices.

To investigate changes in OHSCs excitability caused by serum removal, field potential recordings from the CA3 region of slices at 14 DIV was performed. Field potential recordings showed spikes and short bursts of population activity, being particularly prominent in slices grown in **SF** medium (**Figure 14**). This suggests that serum-removal increased hyperexcitability of cells in these slices.

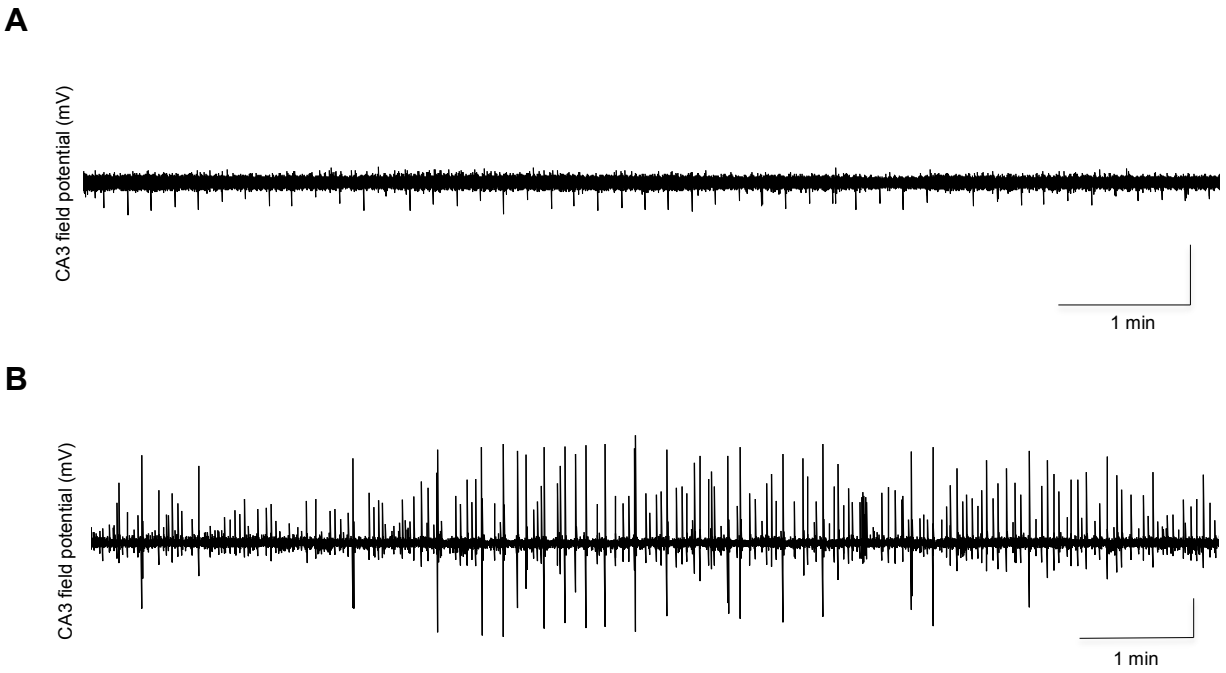

Figure 14| Representative field potential recordings of OHSCs at 14 days *in vitro* (DIV). A) Slice grown in serum-containing (**SC**) medium shows single spikes with short amplitude. **B)** Slice grown in serum-free (**SF**) medium shows short bursts of population activity. All vertical bars = 1 mV (4 < slices < 6).

4.1.4 Serum-removal Induces Alterations in Synaptic Excitability and Efficiency

To further confirm the effects of serum removal on OHSCs functional properties, whole-cell current clamp methods as well as extracellular field recordings were employed. Using the whole-cell patch clamp technique in current-clamp mode (**section 3.3.2**), the resting membrane potential of CA1 pyramidal cells was determined.

Moreover, in order to assess synaptic transmission, an I/O plot (**section 3.3.1.1**) was constructed. Data was presented as the fEPSPs slope *vs* the stimulus intensity.

4.1.4.1 Resting membrane potentials

Whole-cell current clamp recordings were performed at 14 DIV from both conditions. The resting membrane potential of slices grown in **SC** medium (-62.67 ± 1.26 mV, n=9) was significantly higher than the resting membrane potential measured in slices kept in **SF** medium (-55.57 ± 3.09, n=7) (**Figure 15**). These results indicate that the cell's membrane potential of **SF** slices tend to become more positive. Since depolarized cells are more likely to fire an action potential, these results confirm the tendency of slices growing in a **SF** medium towards an increased synaptic excitability.

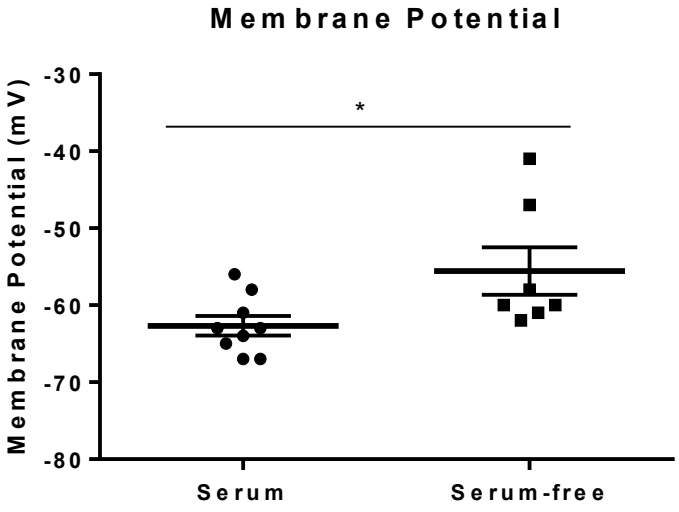

Figure 15| The resting membrane potential of CA1 pyramidal cells of OHSCs at 14 days *in vitro* (DIV), grown in serum-containing (SC) and serum-free medium (SF). 7 < cells < 9, *p<0.05, Unpaired t-Test**.** Experiments performed in collaboration with Diogo Rombo.

4.1.4.2 Input-Output curves

Synaptic field potentials were elicited by stimulation of CA1 pyramidal neurons using graded depolarizing stimulations, as described in **section 3.3.1.1**, in both growth conditions. As shown in **Figure 16**, the fEPSP response to stimulation of Schaffer collaterals in **SC** slices was four times higher than the one obtained from slices growing in a **SF** medium (maximum of 6.829 ± 1.172 mV *vs* 2.431 ± 1.105 mV, respectively). Nevertheless, the sensitivity to electrical stimulation was not affected, with the current required for half-maximal fEPSP amplitude being 180 µA, 1.212 ± 0.221 mV (n=4) in **SF** slices, and 3.657 ± 0.746 mV (n=4) in **SC** slices. These results indicated a reduced size of synaptic responses in **SF** slices, which can be traduced into a reduced synaptic efficiency of **SF** slices compared with **SC** slices. The correlation between fEPSP and the population spike (pSpike) was not possible to perform due to a huge contamination of the recordings with bursts of spikes stimuli-induced.

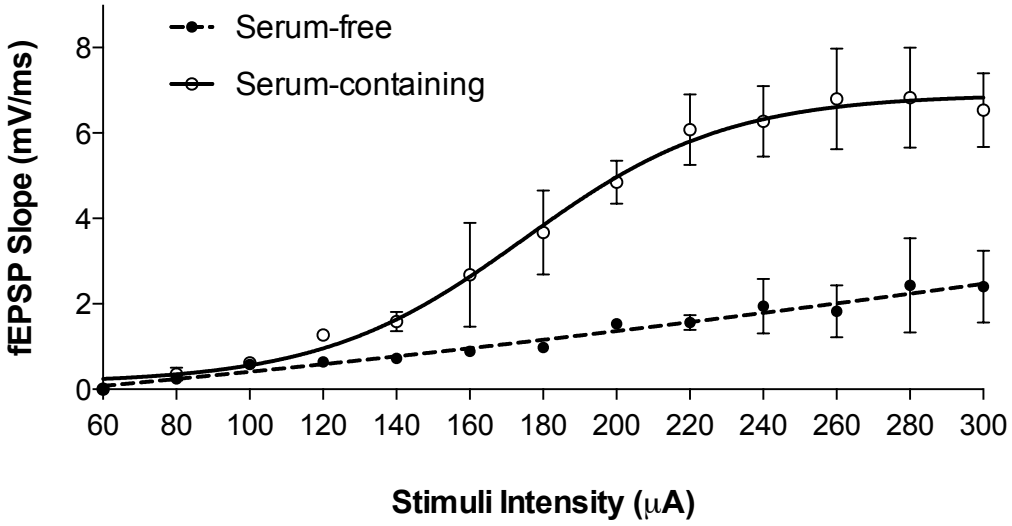

Figure 16| Input-output curves obtained from OHSCs at 14 days *in vitro* (DIV) grown in serum-containing (SC) and serum-free medium (SF). The graph shows fEPSP amplitude (mean ± SEM) as a function of stimulus intensity (60-300 μA) in the CA1 *stratum radiatum*. The curves reflect the number of fibers activated at the different stimulus intensities and the fEPSPs that result from these activated fibers. Sensitivity to electrical stimulus intensity was similar between **SC** and **SF** growth medium condition, while response amplitudes, including the maximal response at 300 μA, were, on average, lower in **SF** growth medium condition. Curves fit to the data were significantly different by global analysis (**p<0.01, 4 slices, Unpaired t-test).

4.2 *In vitro* Model of Epileptiform Activity

OHSCs grown in serum-free medium spontaneously develop epileptiform discharges in the absence of pharmacological manipulation (**section 1.2.1.1**). Thus, in order to identify molecular and cellular hallmarks of epilepsy in OHSCs that are maintained in **SF** medium, as a model of epileptogenesis, epileptiform activity progression was firstly recorded and categorized from slices at 14 to 29 DIV. Then, immunofluorescence, western blot and mRNA expression assays were conducted using slices at two different times in culture – **14 DIV** and **21 DIV**.

4.2.1 Interictal-like Spikes Precede Ictal-like Discharges

To evaluate the progression of spontaneous epileptiform activity over the time in culture, field-potential recordings (30-40 minutes) were made from CA3 area after 14 to 29 days in culture under constant perfusion with 60 mL of recirculated growth medium at 37ºC.
The recorded slices were grouped according to age and the spontaneous activity was classified as: (**a**) No population discharges, (**b**) Interictal-like discharges consisting of

single population spikes and, (**c)** Mixed Interictal- and Ictal-like discharges characterized by repetitive bursts of population spikes that last > 3 minutes including after discharges (**Figure 17**). Band-pass filtered (eight-pole Bessel filter at 60 Hz and Gaussian filter at 600 Hz) field-potential recordings from 14 and 22 DIV OHSC reveals fast ripple-like complexes (data not shown).

A – 14 DIV Interictal-like

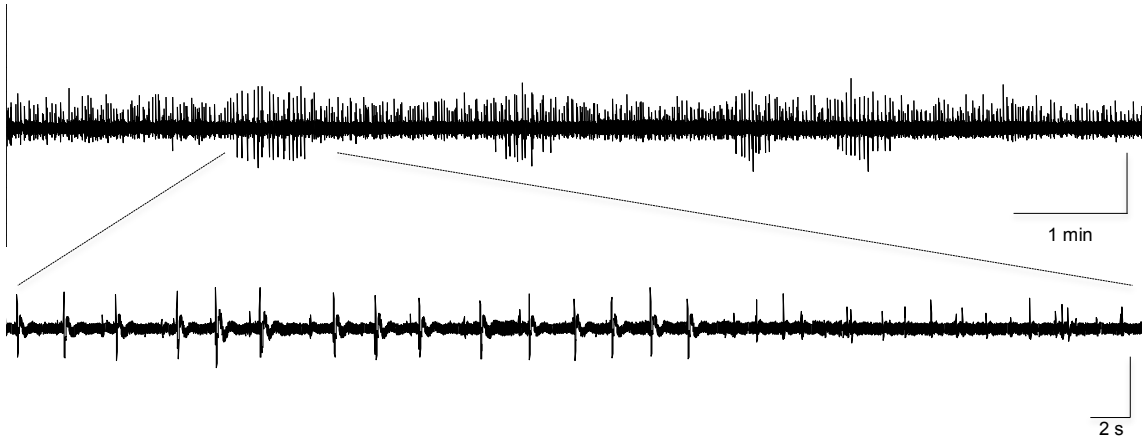

B – 21 DIV Ictal-like

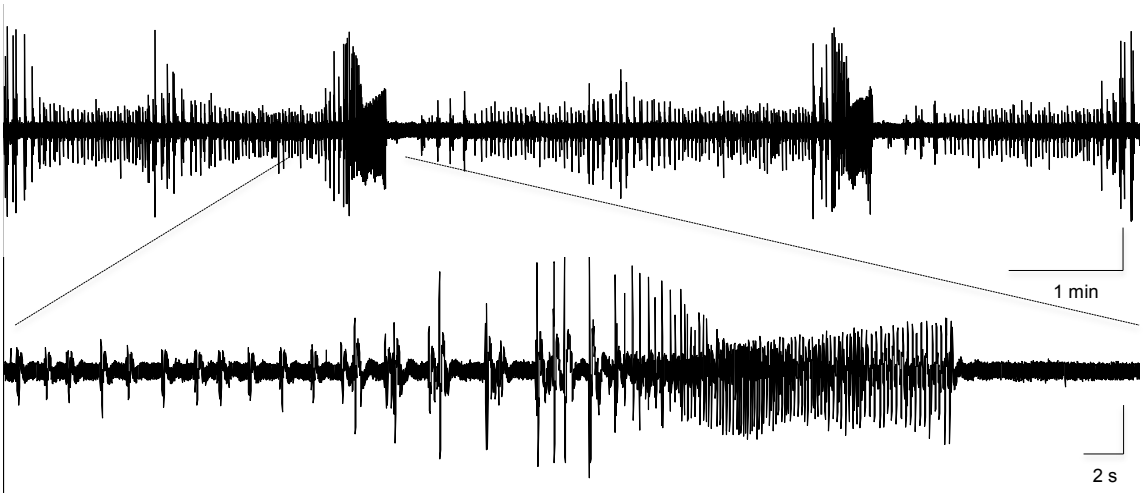

Figure 17| Representative spontaneous epileptiform activity recorded in organotypic slices. A – Interictal-like activity from a slice at 14 days *in vitro* (DIV); **B –** Mixed Interictal and Ictal-like discharges from a slice at 21 DIV. All vertical bars = 1 mV.

As shown in **Figure 18**, at 14 to 17 DIV the majority (57.1%) of recorded slices (n=14) exhibited spontaneous interictal-like discharges, compared to mixed interictal- and ictal-like discharges (35.7%). Inversely, slices at 21 to 29 DIV (n=22) displayed

predominantly mixed interictal- and ictal-like discharges (86.4%), compared to interictal-like discharges alone (13.6%). Interestingly, ictal activity continued to rise with the number of days *in vitro* so that after 3 weeks in culture 90% of the recorded slices exhibited mostly ictal-like activity.

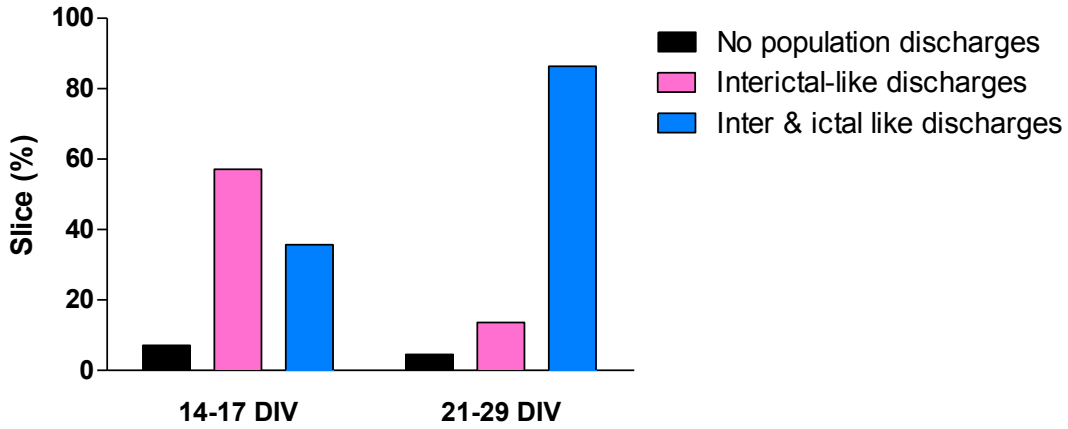

Figure 18| Progression of spontaneous epileptiform activity over the time in culture. The graph shows the absolute percentage of slices developing: no population discharges, interictal-like discharges, and interictal- and ictal discharges. Slices obtained from 4 independent cultures.

4.2.2 Astrocytes and Microglia are Activated

Glial fibrillary acidic protein (GFAP) is a specific marker for differentiated astrocytes in the CNS. GFAP is the principal cytoskeletal protein in astrocytes and is thought to provide structural support for maintenance of cell shape. Therefore, reactive astrocytosis is defined by an increase in GFAP immunostaining plus an increase in the size and/or number of these cells [142]. GFAP staining can result either from dissociation of glial filament bundles due to injury or due to increase in GFAP synthesis [143].

Ionized calcium-binding adapter molecule 1 (Iba1), also known as allograft inflammatory factor 1 (AIF-1), is a microglia-specific calcium-binding protein. Microglia, considered as the tissue macrophages of the CNS, is present with a ramified morphology and low expression levels. Upon a pathological phenomenon, microglia are activated and adopt a reactive phenotype [144].

Astrogliosis and microglia activation were evaluated by two distinct assays: western blot and immunohistochemistry.

4.2.2.1 Astrogliosis

No significant differences (p=0.1718) in GFAP total expression were detected by western blot analysis (**Figure 19**) in 21 DIV slices with respect to the ones at 14 DIV.

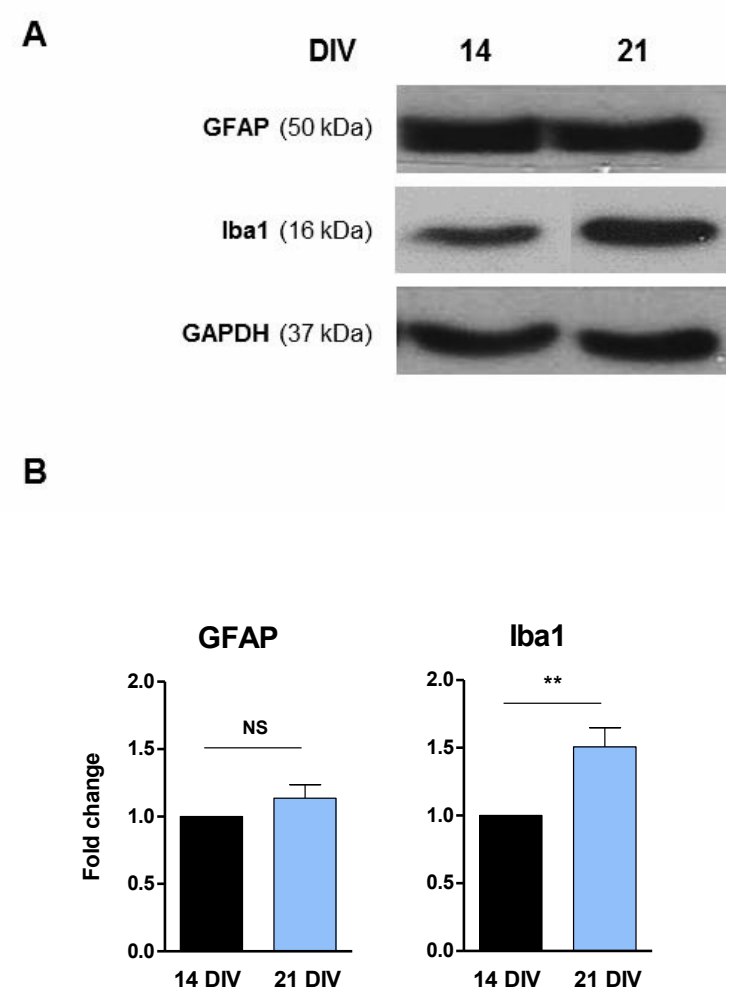

Figure 19| Western blot analysis of GFAP and Iba1. A) Representative immunoblots of GFAP and Iba1. GAPDH was used as the loading control. **B)** Densitometry analysis performed with ImageJ software. All values are mean ± SEM. NS, not statistically significant (p>0.05), **p<0.01, N=6-8 slices, Unpaired t-Test. Statistical tests were performed in comparison with 14 days *in vitro* (DIV) slices. Experiments performed in collaboration with Daniela Magalhães.

However, as observed in all hippocampal areas of 21 DIV slices, depicted in **Figure 20 B**, the intensity of GFAP immunostaining was enhanced in comparison to the obtained in 14 DIV slices, showed in **Figure 20 A**. This suggests that a corresponding

enhancement in GFAP staining is due to the onset of injury and to the dissociation of the glial filament bundles to yield more epitopes available for binding to the GFAP antibody.

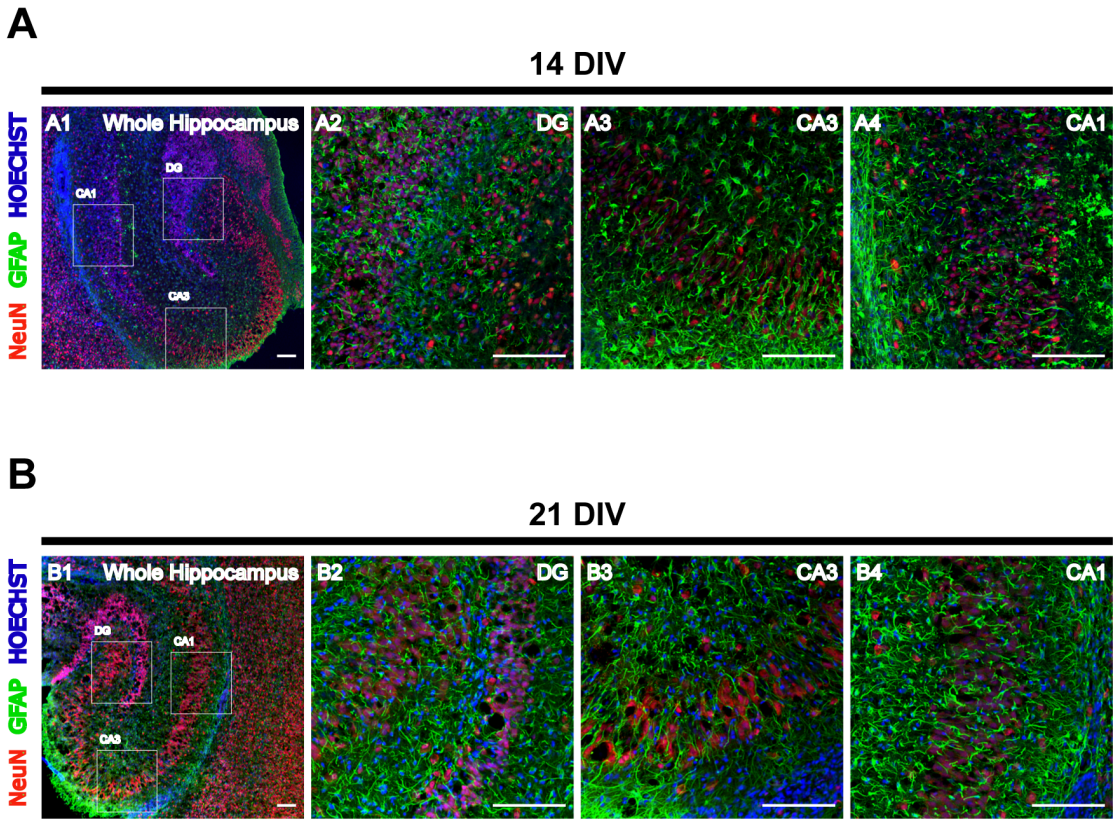

Figure 20| Representative reactive astrocytosis in organotypic slices at 14 and 21 days *in vitro* (DIV). Detection of Hoechst stained nucleus (blue), together with NeuN (red) and GFAP (green), stained neurons and astrocytes, respectively. Confocal images were acquired with a 5x objective (**A1** and **B1**) and 20x objective (**A2-4** and **B2-4**). Scale bar, 200 µm.

4.2.2.2 Microglia activation

Inversely to GFAP, Iba1 overall expression was significantly higher (**p<0.01) in 21 DIV slices, **Figure 19**. These results were corroborated by the immunofluorescence images shown in **Figure 21**. Indeed, slices at 21 DIV, **Figure 21 B,** clearly show a strong enhancement in Iba1 immunoreactivity, in comparison with 14 DIV slices, **Figure 21 A.**

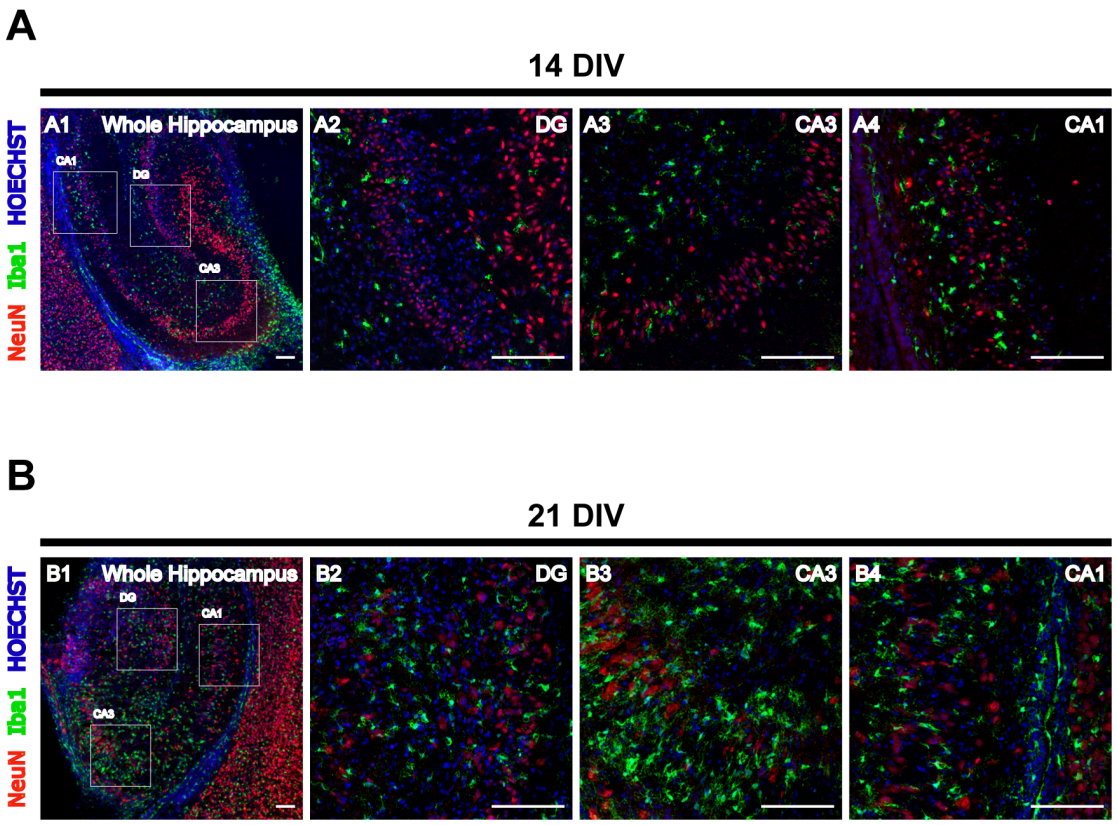

Figure 21| Representative microglia activation in organotypic slices at 14 and 21 days *in vitro* (DIV). Detection of Hoechst stained nucleus (blue), together with NeuN (red) and Iba1 (green), stained neurons and microglia, respectively. Confocal images were acquired with a 5x objective (**A1** and **B1**) and 20x objective (**A2-4** and **B2-4**). Scale bar, 200 µm.

Furthermore, when comparing the amount of astrocytes and microglial cells, astrocytes are by far the most numerous, independently of the age of the explants, which was in accordance with has been already described [105]. The age dependent increase in GFAP staining, as well as the upregulation of Iba1, might be related to the neurodegenerative process inherent to organotypic slices over the time in culture. It should however be noted that this investigation lacks measures of different explant times, in order to precisely look at the progression of astrogliosis and microglial activation.

4.2.3 Inhibitory Neurotransmission Related Receptors are Altered

The next section addresses the two main inhibitory neurotransmission systems in the CNS. Therefore, a transcript expression analysis of the ionotropic $GABA_A$ and glycine receptors was performed. Specifically, mRNA expression of $GABA_AR$ subunits (α1-5, β1-3 and γ2) and GlyR subunits (α1, α2, α3 and β) in the hippocampus of slices at 14-

and 21 DIV was evaluated by RT-qPCR with specific oligonucleotide primers, as detailed in **Table 1 (section 3.4.1.3)**.

4.2.3.1 GABA$_A$ receptor subunits

Most GABA$_A$ receptor subunits transcripts were not altered in 21 DIV slices in respect to 14 DIV slices. GABA$_A$ receptor α1 and β1 subunits mRNA levels exhibited a general trend to increase in 21 DIV (**Figure 22**), although no significance was exhibited (p=1.791 and p=1.706, respectively). However, in 21 DIV slices, GABA receptor γ2 subunit showed a significant decrease (0.4400 ± 0.1877, p<0.05).

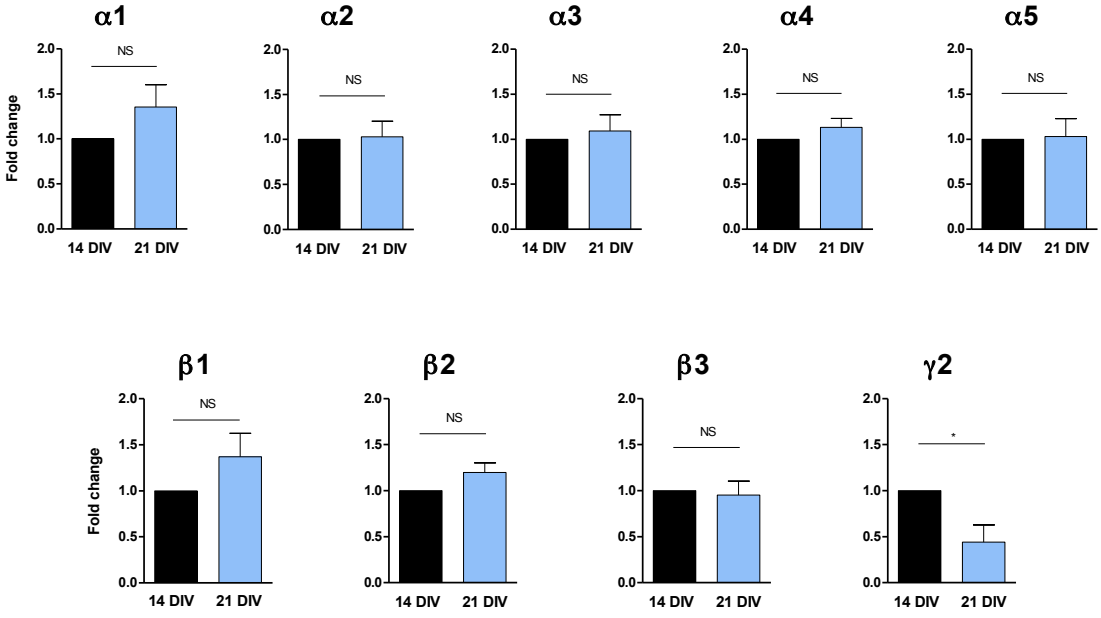

Figure 22| Transcript expression profile of GABA$_A$ receptor (GABA$_A$R) subunits α1-5, β1-3 and γ2. Composition analysis of GABA$_A$R subunit mRNAs in slices at 14 and 21 days *in vitro* (DIV) by relative qPCR. All values are mean ± SEM. NS, not statistically significant (p>0.05), *p<0.05, N=4, Unpaired t-Test. Statistical tests were performed in comparison with 14 DIV slices.

4.2.3.2 Glycine receptor subunits

Regarding mRNA expression levels of GlyR subunits, α1 and β showed a significant increase (p<0.01), 2.975 ± 0.4050 and 1.553 ± 0.1215, respectively, from 14 to 21 DIV slices (**Figure 23**). Inversely, α3 subunit transcript profile revealed a significant decrease

(0.6633 ± 0.0273, p<0.001). Moreover, GlyR α2 subunit transcript level was not altered in 21 DIV slices (p=0.6757).

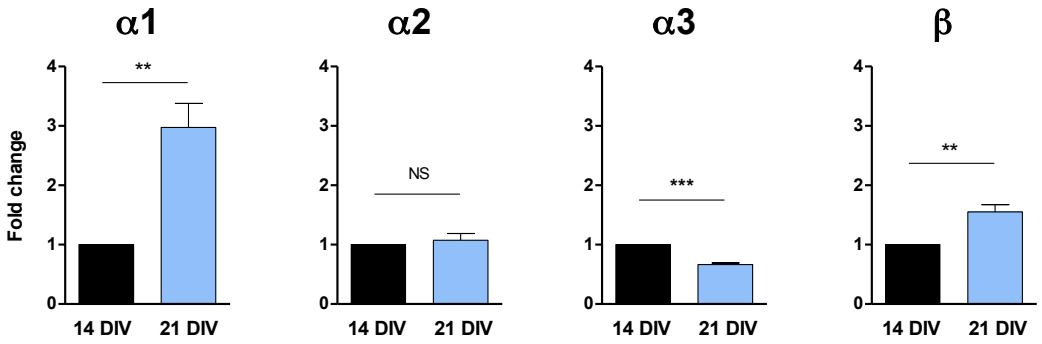

Figure 23| Transcript expression profile of glycine receptor (GlyR) subunits α1-3 and β. Composition analysis of GlyR subunit mRNAs in slices at 14 and 21 days *in vitro* (DIV) by relative qPCR. All values are mean ± SEM. NS, not statistically significant (p>0.05), **p<0.01, ***p<0.001, N=4, Unpaired t-Test. Statistical tests were performed in comparison with 14 DIV slices.

5 DISCUSSION

5.1 Organotypic Hippocampal Slice Cultures

Rat hippocampal slice cultures grown by the interface membrane method were used in all experiments. This *in vitro* system gives a number of advantages over animal models by allowing easy access and precise control of extracellular environment, which makes it suitable to study detailed molecular mechanisms associated with epileptogenesis. To this end, however, it is needed the use of chemically defined culture medium in order to be able to control the cellular environment and avoid variations caused by various batches of serum.

In this study, a method of changing progressively the medium from serum-containing (**SC)** to serum-free (**SF)** medium was developed. Compared with the conventional organotypic slices grown in **SC** culture medium, this **SF** method proved that the slices are kept structurally healthy, without differences in terms of cell death.

Both conditions show preferentially cell lost in CA1 and CA3 areas of the hippocampus, whereas DG cells are more resistant. This pattern of cell loss is remarkably similar to what has been observed in resected human tissue MTLE and animal models of epilepsy [8,145]. The selective vulnerability in MTLE is associated with hyperexcitability of CA1 neurons and has been proposed to result from sprouting of recurrent CA1 axon collaterals [146].

Organotypic hippocampal slices are functionally connected uni-directionally. The EC projects to the DG via the perforant pathway. The DG then projects to the CA3 pyramidal region via the mossy fiber pathway. The CA3 region projects to the CA1 pyramidal region through the Schaffer collaterals. Finally, the CA1 region projects to the subiculum, which in turn, projects back to the EC completing the loop within the hippocampal formation. However, as a consequence of tissue slicing, axonal sprouting and reorganization of excitatory synaptic circuitry occurs during the time in culture [106]. Newly sprouted axons may form synaptic contacts with intrinsically hyperexcitable cells, favoring the occurrence of epileptiform activity. Indeed, suppression of mossy fiber sprouting and reduction of ictal activity decreased cell death in OHSCs [113]. In order to

confirm this hypothesis, spontaneous activity in CA3 pyramidal cells, derived from both growth conditions, was recorded. Both slice cultures developed spikes of epileptiform activity, though this activity was particularly higher in amplitude and frequency in serum-free slices. Probably, **SF** slices have an increased connectivity of the hippocampal network, which increased synchrony and faster propagation of epileptic discharges within the hippocampus.

To address the unanswered issue if serum withdrawal affects the momentary polarization level of the cell membrane and consequently the excitability of the cells, resting membrane potentials were measured. The cells' membrane potential of **SF** slices showed a tendency to become more positive, and thus more likely to fire an action potential. On the other hand, when a neuron discharges from a more depolarized membrane potential, the action potential is proportionally smaller. Such amplitude reduction was posteriorly confirmed by extracellular recordings. **SF** slices showed for the same stimulus intensity a huge reduction in size of the post-synaptic response compared with slices grown in **SC** medium.

Different categories of dendritic spines participate differentially in synaptic function. Dendritic spines provide an anatomic substrate for synaptic transmission, so that they also serve to increase the number of possible contacts between neurons. Abnormalities in dendrites, with a significant decrease in dendritic spine density, are frequently seen in hippocampal pyramidal neurons and dentate granule cells in patients with TLE [147]. These evidences strongly suggest that alterations in dendritic spine structures or function could affect the processing of synaptic inputs and ultimately the excitability of neurons. In OHSCs, serum-withdrawal was reported to cause an increase in the fraction of "immature" thin spines while decreasing the proportion of "mature" stubby spines subtype [100]. Additionally, granule layer cell density decreases over time in **SF** slices compared with cultures grown under **SC** medium [102]. A loss of dendritic spines in organotypic cultures could lead to decreased excitability at the cellular level. However, if loss of excitatory input ultimately had a large effect on inhibitory networks, the net effect on circuit output might be increased excitability and a tendency toward seizures [147]. This suggests that the growth factors of serum could be an important variable for determining spine density of the explants. The change in size of synaptic responses observed can

reflect the lower synapse density in slices growing in **SF** medium. Nonetheless, this hypothesis was not evaluated in this work.

Not only synaptic growth but also modifications of functional synaptic properties can be followed in OHSCs, which can explain why **SF** slices are more prone to develop spontaneous epileptiform activity. On the other hand, given the contribution of astrocytes on cytokine pathways and neurochemical interactions with neighboring neurons, it will be important to consider and evaluate the effect of serum in these glial cells and the role of these cells on neuronal synaptic functionality of the organotypic cultures.

The functional measures used in this work were probably affected by various parameters, including the efficacy of neurotransmitter release, the postsynaptic sensitivity to the released neurotransmitter and the effects of inhibitory synaptic transmission. However, the magnitude of the observed changes and the close correlation found between changes in synaptic response size and the changes in resting membrane potential, as well as changes in synaptic density reported in previous works, highly suggest that these measurements were adequate to address the effects of serum on OHSCs.

The present study indicates that OHSCs can be considered a model of epileptogenesis. Following the trauma of the culturing procedure, sprouting of mossy fibers within CA1 area increase connectivity of the epileptic hippocampal network. The reorganization process of mossy fiber projection of the DG promotes a pattern of cell death, in which CA1 and CA3 are more vulnerable and DG is less affected. Moreover, it increases synchrony and faster propagation of epileptic discharges within the hippocampal structure. This intrinsic mechanism of increased excitability in organotypic cultures appears to be independent of the culture method, so that the use of **SC** or **SF** medium does not change these characteristics. The serum-withdrawal from the slice cultures affect dendritic spine morphology and possibly its function, since it was found that serum removal promote dendritic spine changes [100] and, according with the results of this work, reduces synaptic transmission efficiency. Serum starvation seems to play a significant role underlying persistent cellular hyperexcitability in the circuitry of the hippocampal formation. Nevertheless, future experiments should be performed in order to compare

the properties of synaptic transmission, as well as synaptic density of slices grown in the presence and absence of serum.

It is also important to point out that evoked EPSPs in organotypic slices were quite difficult to obtain, essentially because high frequency stimulation triggers seizures, which abolished synaptic responses and makes analyses of synaptic potentiation quite unreliable. Still, the possibility of functional studies in cultured slices is an important step to validate the use of organotypic culture models.

5.2 OHSC as a Model of Epileptogenesis

As it was described above, OHSCs growing in a chemically defined growth medium, **SF**, spontaneously develop epileptiform activity. Moreover, it was described that the epileptiform activity develop later than 7 DIV, with primarily interictal-like spikes and burst at 14 to 17 DIV and preceding increasingly ictal-like spikes discharges after 21 DIV [111]. This *in vitro* system bears many similarities to *in vivo* epilepsy, including the appearance of spikes before seizures, the progressive increase in seizure-incidence, and the mix of interictal and ictal activity. Early acute cell death occurs as a result of brain slicing, and after 7-10 DIV a second peak of cell death takes place, overlapping the peak of seizure-like activity. Furthermore, suppression of ictal and interictal activity and ictal cell death did not prevent epileptogenesis [112]. However, in order to establish a relationship between spontaneous seizures, neuronal death and epileptogenesis, many questions have to be firstly addressed regarding epileptogenesis hallmarks underlined by this *in vitro* model. For example, it is unknown the role of glial cells and the inhibitory synaptic transmission alterations in the induction and maintenance of seizure activity in this model.

In this work, organotypic hippocampal cultures, progressively depleted of serum in the growth medium, were used as a model of post-traumatic epileptogenesis to monitor the events following brain explant, and to characterize the epileptic correlates concerning astrogliosis and microglia activation, as well as $GABA_A$ and Glycine receptor transcripts expression. Extracellular slice recordings from CA3 region, while bathed in growth medium, were consistent with previous reports in demonstrating predominance of interictal-like spikes and short bursts of population activity between 14 and 17 DIV,

which preceded the increasingly ictal-like discharges after 21 DIV. This result corroborates the development of spontaneous epileptiform activity in this *in vitro* model.
One striking hallmark of the sclerotic hippocampus in MTLE is that while there is a specific pattern of neuronal loss, there is also reactive gliosis with hypertrophic glial cells exhibiting prominent GFAP staining and long, thick processes [26]. Moreover, endogenous glial cells react to the lesion of cultured slice in a manner comparable to their reaction to lesions *in vivo* [148]. Thus, in order to identify epileptic correlates in this *in vitro* model, GFAP- and Iba1-expression was analyzed in 14 and 21 DIV slices using two distinct assays: western blot and immunofluorescence staining. The expression of GFAP was detected in both groups of slices. Although increased GFAP expression was noticed by immunofluorescence assays, no detectable increase in GFAP content was found by western blot. This result suggests that astrocytes proliferation and hypertrophy occur early following injury, and the gradual processes of accumulation of glial intermediate filaments and the formation of glia scars take place around 21 DIV. Probably, chronic astroglial activation resulting from early interictal-like activity increases inflammatory cytokine production, potentiates excessive synaptic activity, and induces activated astrocytes to migrate to the epileptic focus, resulting in sclerosis.
Consistent with this hypothesis, Iba1 detection revealed a significant increase in slices at 21 DIV. Since Iba1 expression is upregulated upon microglia activation allowing the discrimination between surveying and activated microglia, this result indicates the presence of reactive microglia cells at this stage of culture. However, to confirm this hypothesis a most detailed research regarding microglia morphology has to be performed. Taken together, these results strongly suggest that glial cells are altered, which may explain why preventing epileptiform activity, cell death and mossy fiber sprouting is not sufficient to prevent epileptogenesis in this *in vitro* model.

It has been highly postulated that dysfunction of the GABAergic transmission is related to the development of epilepsy, since several animal models of TLE and human studies have revealed considerable changes in the expression of $GABA_A$ receptor subunits in the hippocampus [47,51]. On the other hand, recent evidences suggest that glycine receptors are functionally expressed in adult hippocampal neurons, mediating mostly

tonic currents [60,72,149], and playing a role in epilepsy [80,81]. Moreover, molecular interaction were described to occur between $GABA_A$ and glycine receptors, which provide cross-inhibition in the hippocampus [150]. This interaction may have physiological implications in maintaining the balance between inhibitory and excitatory neurotransmission.

In this work, the levels of $GABA_A$ and glycine receptors subunits were evaluated in this *in vitro* model of epileptogenesis. No significant changes between 14 and 21 DIV slices were found in $GABA_AR$ α and β subunits, but γ2 subunit decreased at 21 DIV. However, a spatial characterization of the $GABA_AR$ subunits is needed, since the expression pattern of the $GABA_AR$ subunits varies regionally and is highly cell type specific, which may be altered by external stimuli [151]. For example, significant decreases in α1-, α3-, β3-, and γ2-subunits were found in the CA1 area of sclerotic hippocampal specimens obtained from surgery of TLE patients, whereas pronounced increases of all three β-subunits were observed in most areas of the hippocampal formation, being especially pronounced in the dentate molecular layer and the subiculum where subunit α3- and γ2- were also elevated [51]. Likewise, changes in subunit composition in this *in vitro* model may occur differently according to hippocampal areas. Nevertheless, the general decrease of γ2-subunit mRNA level may be somehow related with a decrease of synaptic $GABA_ARs$, since γ2 subunit integrates synaptic receptors [152].

Regarding GlyR subunits, α1 and β showed a significant increase at 21 DIV in opposition to α3-subunit, which revealed a significant decline from 14 to 21 DIV slices. Given that in mature hippocampal neurons synaptic GlyR were found to contain α1 subunit [72], these results might indicate an increase of synaptic GlyR α1β in detriment of extrasynaptic GlyRα3. However, further experimental support from immunofluorescence assays is needed.

Although the functional meaning of these results is difficult to comprehend since they lack of a more detailed characterization, the expression pattern changes of subunits may reflect seizure-induced rearrangement of $GABA_A$ and glycine receptors in some subfields of the hippocampal formation. Indeed, it is known that neuronal activity is able to regulate the regional expression *in vitro* [151]. Alternatively, these changes may be

caused by neurodegeneration. Altered subunit composition or modulation in chronically epileptic tissue could conceivably lead to altered pharmacosensitivty of target channels or receptors [11].

Thus, a better knowledge about cellular expression and rearrangement of the inhibitory transmission related receptors during epileptogenesis and during the chronic phase of epilepsy might lead to the development of adequate treatments, and also to the understanding of the pharmacoresistance of AEDs that act upon the GABAergic system.

6 CONCLUSIONS

This study demonstrates that a simple methodological approach, by withdrawing progressively serum from the culture medium, enables cultured hippocampal slices to grow without a permanent support of neurotrophic factors. These slices retain intact synaptic networks, as manifested by a demonstration of evoked excitatory post-synaptic potentials (EPSP) upon stimulation of Schaffer collaterals.

It is important to note, however, that there are also some properties of cultures grown within a progressive serum-free medium that differ from cultures grown in a serum-based medium. In both culture methods, it was found substantial evidence that spontaneous recurrent epileptiform activity, as well as a pattern of neuronal death occurs as a result of the initial trauma of tissue slicing. However, serum-withdrawal induces functional alterations on organotypic hippocampal cells, which seems to greatly increase the vulnerability and incidence of spontaneous epileptogenesis.

Looking in more detail to the development of cultured slices growing in a serum-free medium, it is ascertainable the reproduction of many features of the severe post-traumatic epilepsy, including the progress of epileptiform activity from a pattern of interictal-like activity at early stages to ictal-like activity at late stages of the slice in culture. Moreover, the ongoing reactive gliosis overlaps with the progression pattern of epileptiform activity.

Hence, together with the continual emergence of studies successfully translating results from *in vitro* to *in vivo*, this *in vitro* model of OHSCs can be considered highly suitable to study epileptogenesis and also to screen potential anticonvulsant and antiepileptogenic drugs.

7 REFERENCES

1. Fisher, R. S. *et al.* Epileptic Seizures and Epilepsy: Definitions Proposed by the International League Against Epilepsy (ILAE) and the International Bureau for Epilepsy (IBE). *Epilepsia* **46,** 470–472 (2005).

2. Engel, J. in *Atlas of Epilepsies* (Panayiotopoulos, C. P. et al.) 11–15 (Springer, 2010).

3. Berg, A. T. in *Atlas of Epilepsies* (Panayiotopoulos, C. P. et al.) 5–9 (Springer, 2010).

4. White, S. H., Smith, M. D. & Wilcox, K. S. Mechanisms of Action of Antiepileptic Drugs. *Int. Rev. Neurobiol.* **81,** 85–110 (2007).

5. Schmidt, D. & Löscher, W. Drug resistance in epilepsy: putative neurobiologic and clinical mechanisms. *Epilepsia* **46,** 858–77 (2005).

6. Perry, M. S. & Duchowny, M. Surgical versus medical treatment for refractory epilepsy: outcomes beyond seizure control. *Epilepsia* **54,** 2060–70 (2013).

7. Spencer, S. & Huh, L. Outcomes of epilepsy surgery in adults and children. *Lancet Neurol.* **7,** 525–37 (2008).

8. Sharma, A. K. *et al.* Mesial temporal lobe epilepsy: pathogenesis, induced rodent models and lesions. *Toxicol. Pathol.* **35,** 984–99 (2007).

9. Engel, J. Mesial Temporal Lobe Epilepsy: What Have We Learned? *Neurosci.* **7,** 340–352 (2001).

10. Engel, J. Introduction to temporal lobe epilepsy. *Epilepsy Res.* **26,** 141–150 (1996).

11. Blümcke, I., Beck, H., Lie, a a & Wiestler, O. D. Molecular neuropathology of human mesial temporal lobe epilepsy. *Epilepsy Res.* **36,** 205–23 (1999).

12. Scharfman, H. E. & Pierce, J. P. New insights into the role of hilar ectopic granule cells in the dentate gyrus based on quantitative anatomic analysis and three-dimensional reconstruction. *Epilepsia* **53 Suppl 1,** 109–15 (2012).

13. Scharfman, H., Goodman, J. & McCloskey, D. Ectopic Granule Cells of the Rat Dentate Gyrus. *Dev. Neurosci.* **29,** 14–27 (2006).

14. Sloviter, R. S. The neurobiology of temporal lobe epilepsy: too much information, not enough knowledge. *C. R. Biol.* **328,** 143–153 (2005).

15. Foresti, M. L., Arisi, G. M. & Shapiro, L. A. Role of glia in epilepsy-associated neuropathology, neuroinflammation and neurogenesis. *Brain Res. Rev.* **66,** 115–22 (2011).

16. Lawson, L. J., Perry, V. H., Dri, P. & Gordon, S. Heterogeneity in the distribution and morphology of microglia in the normal adult mouse brain. *Neuroscience* **39,** 151–70 (1990).

17. Araque, A., Parpura, V., Sanzgiri, R. P. & Haydon, P. G. Tripartite synapses: glia, the unacknowledged partner. *Trends Neurosci.* **22,** 208–15 (1999).

18. Perea, G., Navarrete, M. & Araque, A. Tripartite synapses: astrocytes process and control synaptic information. *Trends Neurosci.* **32,** 421–31 (2009).

19. Allaman, I., Bélanger, M. & Magistretti, P. J. Astrocyte-neuron metabolic relationships: for better and for worse. *Trends Neurosci.* **34,** 76–87 (2011).

20. Hamilton, N. B. & Attwell, D. Do astrocytes really exocytose neurotransmitters? *Nat. Rev. Neurosci.* **11,** 227–38 (2010).

21. Clasadonte, J. & Haydon, P. G. in *Jasper's Basic Mech. Epilepsies* (Noebels, J., Avoli, M., Rogawski, M. a, Olsen, R. & Delgado-Escueta, A.) **5,** 1–19 (National Center for Biotechnology Information, 2012).

22. Walter, L. & Neumann, H. Role of microglia in neuronal degeneration and regeneration. *Semin. Immunopathol.* **31,** 513–25 (2009).

23. Devinsky, O., Vezzani, A., Najjar, S., De Lanerolle, N. C. & Rogawski, M. A. Glia and epilepsy: excitability and inflammation. *Trends Neurosci.* **36,** 174–84 (2013).

24. Hüttmann, K. *et al.* Seizures preferentially stimulate proliferation of radial glia-like astrocytes in the adult dentate gyrus: functional and immunocytochemical analysis. *Eur. J. Neurosci.* **18,** 2769–78 (2003).

25. Shapiro, L. A., Perez, Z. D., Foresti, M. L., Arisi, G. M. & Ribak, C. E. Morphological and ultrastructural features of Iba1-immunolabeled microglial cells in the hippocampal dentate gyrus. *Brain Res.* **1266,** 29–36 (2009).

26. Binder, D. K. & Steinhäuser, C. Functional changes in astroglial cells in epilepsy. *Glia* **54,** 358–68 (2006).

27. Dissing-Olesen, L. *et al.* Axonal lesion-induced microglial proliferation and microglial cluster formation in the mouse. *Neuroscience* **149,** 112–22 (2007).

28. Sofroniew, M. V. Molecular dissection of reactive astrogliosis and glial scar formation. *Trends Neurosci.* **32,** 638–47 (2009).

29. Treiman, D. M. GABAergic mechanisms in epilepsy. *Epilepsia* **42 Suppl 3,** 8–12 (2001).

30. Krogsgaard-Larsen, P. Inhibitors of the GABA uptake systems. *Mol. Cell. Biochem.* **31,** 105–121 (1980).

31. Meldrum, B. S. & Rogawski, M. a. Molecular targets for antiepileptic drug development. *Neurotherapeutics* **4,** 18–61 (2007).

32. Bormann, J. Electrophysiology of GABAA and GABAB receptor subtypes. *Trends Neurosci.* **11,** 112–116 (1988).

33. Stafstrom, C. Neurobiological Mechanisms of Developmental Epilepsy: Translating Experimental Findings Into Clinical Application. *Semin. Pediatr. Neurol.* **14,** 164–172 (2007).

34. Ben-Ari, Y. Excitatory actions of GABA during development: the nature of the nurture. *Nat. Rev. Neurosci.* **3,** 728–739 (2002).

35. Jones-Davis, D. & Macdonald, R. GABA receptor function and pharmacology in epilepsy and status epilepticus. *Curr. Opin. Pharmacol.* **3,** 12–18 (2003).

36. Möhler, H. GABA(A) receptor diversity and pharmacology. *Cell Tissue Res.* **326,** 505–16 (2006).

37. Tretter, V. *et al.* Gephyrin, the enigmatic organizer at GABAergic synapses. *Front. Cell. Neurosci.* **6,** 23 (2012).

38. Farrant, M. & Nusser, Z. Variations on an inhibitory theme: phasic and tonic activation of GABA(A) receptors. *Nat. Rev. Neurosci.* **6,** 215–29 (2005).

39. Li, Z.-X., Yu, H.-M. & Jiang, K.-W. Tonic GABA inhibition in hippocampal dentate granule cells: its regulation and function in temporal lobe epilepsies. *Acta Physiol. (Oxf).* **209,** 199–211 (2013).

40. Olsen, R. W. & Avoli, M. GABA and Epileptogenesis. *Epilepsia* **38,** 399–407 (1997).

41. Straessle, A., Loup, F., Arabadzisz, D., Ohning, G. V & Fritschy, J. Rapid and long-term alterations of hippocampal GABAB receptors in a mouse model of temporal lobe epilepsy. **18,** 2213–2226 (2003).

42. Stewart, L. S. *et al.* Severity of atypical absence phenotype in GABAB transgenic mice is subunit specific. *Epilepsy Behav.* **14,** 577–81 (2009).

43. Chan, K. F. Y., Burnham, W. M., Jia, Z., Cortez, M. a & Snead, O. C. GABAB receptor antagonism abolishes the learning impairments in rats with chronic atypical absence seizures. *Eur. J. Pharmacol.* **541,** 64–72 (2006).

44. Swartzwelder, S. H., Bragdon, A. C., Sutch, C. P., Ault, B. & Wilson, W. A. Baclofen Supresses Hippocampal Epileptiform Activity at Low Concentrations Without Suppressing Synaptic Transmission. *J. Pharmacol. Exp. Ther.* **237,** 881–887 (1986).

45. Mott, D. D., Bragdon, A. C., Lewis, D. V. & Wilson, W. A. Baclofen has a Proepileptic Effect in the Rat Dentate Gyrus. *J. Pharmacol. Exp. Ther.* **249,** 721–725 (1989).

46. Park, S.-K. *et al.* Altered GABAB receptor immunoreactivity in the gerbil hippocampus induced by baclofen and phaclofen, not seizure activity. *Neurosci. Res.* **49,** 405–16 (2004).

47. Loup, F., Wieser, H., Yonekawa, Y., Aguzzi, A. & Fritschy, J. Selective Alterations in GABAA Receptor Subtypes in Human Temporal Lobe Epilepsy. *J. …* **20,** 5401–5419 (2000).

48. Nusser, Z., Hájos, N., Somogyi, P. & Mody, I. Increased number of synaptic GABA(A) receptors underlies potentiation at hippocampal inhibitory synapses. *Lett. to Nat.* **395,** 172–177 (1998).

49. Brooks-Kayal, A., Shumate, M., Jin, H., Rikhter, T. & Coulter, D. Selective changes in single cell GABAA receptor subunit expression and function in temporal lobe epilepsy. *Nat. Med.* **4,** 1166–1172 (1998).

50. Drexel, M., Kirchmair, E. & Sperk, G. Changes in the expression of GABAA receptor subunit mRNAs in parahippocampal areas after kainic acid induced seizures. *Front. Neural Circuits* **7,** 142 (2013).

51. Pirker, S. *et al.* Increased Expression of GABAA Receptor beta-Subunits in the Hippocampus of Patients with Temporal Lobe Epilepsy. *J. Neuropathol. Exp. Neurol.* **62,** 820–34 (2003).

52. Semyanov, A., Walker, M., Kullmann, D. & Silver, R. Tonically active GABAA receptors: modulating gain and maintaining the tone. *Trends Neurosci.* **27,** 262–269 (2004).

53. Schwarzer, C. *et al.* GABAA Receptor Subunits in the Rat Hippocampus II: Altered Distribution in Kainic Acid-Induced Temporal Lobe Epilepsy. **80,** 1001–1017 (1997).

54. Macdonald, R. L., Gallagher, M. J., Feng, H.-J. & Kang, J. GABA(A) receptor epilepsy mutations. *Biochem. Pharmacol.* **68,** 1497–506 (2004).

55. Aprison, M. & Werman, R. The distribution of glycine in cat spinal cord and roots. *Life Sci.* **4,** 2075–2083 (1965).

56. Malosio, M., Marqueze-Pouey, B., Kuhse, J. & Betz, H. Widespread expression of glycine receptor subunit mRNAs in the adult and developing rat brain. *EMBO J.* **10,** 2401–2409 (1991).

57. Bowery, N. G. & Smart, T. G. GABA and glycine as neurotransmitters: a brief history. *Br. J. Pharmacol.* **147 Suppl ,** S109–19 (2006).

58. Danglot, L., Rostaing, P., Triller, A. & Bessis, A. Morphologically identified glycinergic synapses in the hippocampus. *Mol. Cell. Neurosci.* **27,** 394–403 (2004).

59. Song, W., Chattipakorn, S. C. & McMahon, L. L. Glycine-gated chloride channels depress synaptic transmission in rat hippocampus. *J. Neurophysiol.* **95,** 2366–79 (2006).

60. Zhang, L.-H., Gong, N., Fei, D., Xu, L. & Xu, T.-L. Glycine uptake regulates hippocampal network activity via glycine receptor-mediated tonic inhibition. *Neuropsychopharmacology* **33,** 701–11 (2008).

61. Zafra, F., Aragón, C. & Giménez, C. Molecular biology of glycinergic neurotransmission. *Mol. Neurobiol.* **14,** 117–42 (1997).

62. Legendre, P. The glycinergic inhibitory synapse. *Cell. Mol. Life Sci. C.* **58,** 760–793 (2001).

63. Dumoulin, a *et al.* Presence of the vesicular inhibitory amino acid transporter in GABAergic and glycinergic synaptic terminal boutons. *J. Cell Sci.* **112 (Pt 6,** 811–23 (1999).

64. Burger, P. M. *et al.* GABA and Clycine in Synaptic Vesicles: Storage and Transport Characteristics. *Neuron* **7,** 287–293 (1991).

65. Xu, T.-L. & Gong, N. Glycine and glycine receptor signaling in hippocampal neurons: diversity, function and regulation. *Prog. Neurobiol.* **91,** 349–61 (2010).

66. Eulenburg, V., Armsen, W., Betz, H. & Gomeza, J. Glycine transporters: Essential regulators of neurotransmission. *Trends Biochem. Sci.* **30,** 325–333 (2005).

67. Aroeira, R. I., Sebastião, A. M. & Valente, C. a. GlyT1 and GlyT2 in brain astrocytes: expression, distribution and function. *Brain Struct. Funct.* **219,** 817–30 (2014).

68. Verleysdonk, S., Martin, H., Willker, W., Leibfritz, D. & Hamprecht, B. Rapid Uptake and Degradation of Glycine by Astroglial Cells in Culture: Synthesis and Release of Serine and Lactate. *Glia* **27,** 239–248 (1999).

69. Baer, K. *et al.* Association of Gephyrin and Glycine Receptors in the Human Brainstem and Spinal Cord: an Immunohistochemical Analysis. *Neuroscience* **122,** 773–784 (2003).

70. Moss, S. J. & Smart, T. G. Constructing inhibitory synapses. *Nat. Rev. Neurosci.* **2,** 240–50 (2001).

71. Muller, E., Le-Corronc, H. & Legendre, P. Extrasynaptic and postsynaptic receptors in glycinergic and GABAergic neurotransmission: a division of labor? *Front. Mol. Neurosci.* **1,** 3 (2008).

72. Aroeira, R. I., Ribeiro, J. A., Sebastia, A. M. & Valente, C. Age-related changes of glycine receptor at the rat hippocampus: from the embryo to the adult. *J. Neurochem.* 339–53 (2011).

73. Mori, M., Gähwiler, B. H. & Gerber, U. b-Alanine and taurine as endogenous agonists at glycine receptors in rat hippocampus in vitro. *J. Physiol.* **539,** 191–200 (2002).

74. Rivera, C. *et al.* The K+/Cl- co-transporter KCC2 renders GABA hyperpolarizing during neuronal maturation. *Nature* 251–255 (1999).

75. Cherubini, E., Bernardi, G., Stanzione, P., Marciani, M. G. & Mercuri, N. The action of glycine on rat epileptic foci. *Neurosci. Lett.* **21,** 93–7 (1981).

76. Seiler, N. & Sarhan, S. v. *Naunyn. Schmiedebergs. Arch. Pharmacol.* 49–57 (1984). at <http://link.springer.com/article/10.1007/BF00518778>

77. Chattipakorn, S. C. & McMahon, L. L. Strychnine-sensitive glycine receptors depress hyperexcitability in rat dentate gyrus. *J. Neurophysiol.* **89,** 1339–42 (2003).

78. Kirchner, A., Breustedt, J., Rosche, B., Heinemann, U. F. & Schmieden, V. Effects of Taurine and Glycine on Epileptiform Activity Induced by Removal of Mg2+ in Combined Rat Entorhinal Cortex – Hippocampal Slices. *Epilepsia* **44,** 1145–1152 (2003).

79. Song, W., Chattipakorn, S. C. & Mcmahon, L. L. Glycine-Gated Chloride Channels Depress Synaptic Transmission in Rat Hippocampus. *J. Neurophysiol.* **95,** 2366–2379 (2006).

80. Eichler, S. *et al.* Glycinergic tonic inhibition of hippocampal neurons with depolarizing GABAergic transmission elicits histopathological signs of temporal lobe epilepsy. *J. Cell. Mol. Med.* **12,** 2848–2866 (2008).

81. Eichler, S. *et al.* Splice-specific roles of glycine receptor a 3 in the hippocampus. *Eur. J. Neurosci.* **30,** 1077–1091 (2009).

82. Engel, J. & Schwartzkroin, P. in *Model. Seizures Epilepsy* (Pitkanen, A., Schwartzkroin, P. & Moshé, S.) 1–14 (Elsevier Academic Press, 2006).

83. Raol, Y. H. & Brooks-Kayal, A. R. Experimental Models of Seizures and epilepsies. *Prog. Mol. Biol. Transl. Sci.* **105,** 57–82 (2012).

84. Löscher, W. Animal models of epilepsy for the development of antiepileptogenic and disease-modifying drugs. A comparison of the pharmacology of kindling and post-status epilepticus models of temporal lobe epilepsy. *Epilepsy Res.* **50,** 105–23 (2002).

85. Bausch, S. in *Anim. Model. Epilepsy Methods Innov.* (Baraban, S. C.) 183–201 (Humana Press, 2009).

86. Wong, M. Epilepsy in a dish: an in vitro model of epileptogenesis. *Epilepsy Curr.* **11,** 153–4 (2011).

87. Khalilov, I. *et al.* A Novel In Vitro Preparation: the Intact Hippocampal Formation Neurotechnique. *Neuron* **19,** 743–749 (1997).

88. Gähwiler, B. H., Capogna, M., Debanne, D., McKinney, R. a & Thompson, S. M. Organotypic slice cultures: a technique has come of age. *Trends Neurosci.* **20,** 471–7 (1997).

89. Schwartzkroin, P. Hippocampal slices in experimental and human epilepsy. *Adv. Neurol.* **44,** 991–1010 (1986).

90. Heinemann, U., Kann, O. & Schuchmann, S. in *Model. Seizures Epilepsy* (Pitkanen, A., Schwartzkroin, P. A. & Moshé, S. L.) 35–44 (Elsevier Academic Press, 2006).

91. Morrison, B., Elkin, B. S., Dollé, J.-P. & Yarmush, M. L. In Vitro Models of Traumatic Brain Injury. *Annu. Rev. Biomed. Eng.* **13,** 91–126 (2011).

92. Gähwiler, B. H. Organotypic monolayer cultures of nervous tissue. *J. Neurosci. Methods* **4,** 329–42 (1981).

93. Stoppini, L., Buchs, P. & Muller, B. A simple method for organotypic cultures of nervous tissue. *J. Neurosci. Methods* **37,** 173–182 (1991).

94. Noraberg, J., Kristensen, B. W. & Zimmer, J. Markers for neuronal degeneration in organotypic slice cultures. *Brain Res. Protoc.* **3,** 278–290 (1999).

95. Van der Valk, J. *et al.* Optimization of chemically defined cell culture media--replacing fetal bovine serum in mammalian in vitro methods. *Toxicol. In Vitro* **24,** 1053–63 (2010).

96. Wallace, T. L. & Johnson, E. M. Cytosine arabinoside kills postmitotic neurons: evidence that deoxycytidine may have a role in neuronal survival that is independent of DNA synthesis. *J. Neurosci.* **9,** 115–24 (1989).

97. Annis, C. M., Edmond, J. & Robertson, R. T. A chemically-defined medium for organotypic slice cultures. *J. Neurosci. Methods* **32,** 63–70 (1990).

98. Brewer, G. J., Torricelli, J. R., Evege, E. K. & Price, P. J. Optimized survival of hippocampal neurons in B27-supplemented Neurobasal, a new serum-free medium combination. *J. Neurosci. Res.* **35,** 567–76 (1993).

99. Cressey, D. Neuroscientists claim growing pains. *Nature* **459,** 19 (2009).

100. Chapleau, C. A., Carlo, M. E., Larimore, J. L. & Pozzo-Miller, L. The actions of BDNF on dendritic spine density and morphology in organotypic slice cultures depend on the presence of serum in culture media. *J. Neurosci. Methods* **169,** 182–90 (2008).

101. Martinez, R., Eraso, D., Geffin, R. & McCarthy, M. A two-culture method for exposure of human brain organotypic slice cultures to replicating human immunodeficiency virus type 1. *J. Neurosci. Methods* **200,** 74–9 (2011).

102. Sadgrove, M. P., Laskowski, A. & Gray, W. P. Examination of granule layer cell count, cell density, and single-pulse BrdU incorporation in rat organotypic hippocampal slice cultures with respect to culture medium, septotemporal position, and time in vitro. *J. Comp. Neurol.* **497,** 397–415 (2006).

103. Caeser, M. & Aertsen, A. Morphological Organization of Rat Hippocampal Slice Cultures. *J. Comp. Neurol.* **307,** 87–106 (1991).

104. Dailey, M. E., Buchanan, J., Bergles, D. E. & Smith, S. J. Mossy Fiber Growth and Synaptogenesis in Rat Hippocampal Slices in vitro. *Jounal Neurosci.* **14,** 1060–1078 (1994).

105. Muller, D., Buchs, P.-A. & Stoppini, L. Time course of synaptic development in hippocampal organotypic cultures. *Dev. Brain Res.* **71,** 93–100 (1993).

106. Gutiérrez, R. & Heinemann, U. Synaptic reorganization in explanted cultures of rat hippocampus. *Brain Res.* **815,** 304–316 (1999).

107. Zimmer, J. & Gähwiler, B. H. Cellular and Connective Organization of Slice Cultures of the Rat Hippocampus and Fascia Dentata. *J. Comp. Neurol.* **228,** 432–446 (1984).

108. Zimmer, J. & Gähwiler, B. H. Growth of Hippocampal Mossy Fibers: A Lesion and Coculture Study of Organotypic Slice Cultures. *J. Comp. Neurol.* **264,** 1–13 (1987).

109. Thompson, S. M., Cai, X., Dinocourt, C. & Nestor, M. W. in *Model. Seizures Epilepsy* (Pitkanen, A., Schwartzkroin, P. & Moshé, S. L.) 45–58 (Elsevier Academic Press, 2006).

110. McBain, C. J., Boden, P. & Hill, R. G. Rat hippocampal slices “in vitro” display spontaneous epileptiform activity following long-term organotypic culture. *J. Neurosci. Methods* **27,** 35–49 (1989).

111. Dyhrfjeld-Johnsen, J., Berdichevsky, Y., Swiercz, W., Sabolek, H. & Staley, K. J. Interictal Spikes Precede Ictal Discharges in an Organotypic Hippocampal Slice Culture Model of Epileptogenesis. *J. Clin. Neurophysiol.* **27,** 418–424 (2010).

112. Berdichevsky, Y., Dzhala, V., Mail, M. & Staley, K. J. Interictal spikes, seizures and ictal cell death are not necessary for post-traumatic epileptogenesis in vitro. *Neurobiol. Dis.* **45,** 774–785 (2012).

113. Berdichevsky, Y. *et al.* PI3K-Akt Signaling Activates mTOR-Mediated Epileptogenesis in Organotypic Hippocampal Culture Model of Post-Traumatic Epilepsy. *Jounal Neurosci.* **33,** 9056–67 (2013).

114. Johnston, D. & Brown, T. The synaptic nature of the paroxysmal depolarizing shift in hippocampal neurons. *Ann. Neurol.* **16 Suppl,** S65–71 (1984).

115. Bristol University | Centre for Synaptic Plasticity | Neural pathways. at <http://www.bristol.ac.uk/synaptic/pathways/>

116. Sweatt, D. J. *Mechanisms of Memory*. 450 (Academic Press, 2009).

117. Andersen, P., Bliss, T. & Skrede, K. Unit Analysis of Hippocampal Population Spikes. *Exp. Brain Res.* **221,** 208–221 (1971).

118. Johnston, D. & Wu, S. M.-S. in *Found. Cell. Neurophysiol.* 676 (MIT Press, 1995).

119. Prince, D. a & Connors, B. W. Mechanisms of epileptogenesis in cortical structures. *Ann. Neurol.* **16 Suppl,** S59–64 (1984).

120. Anderson, W. W. & Collingridge, G. L. Capabilities of the WinLTP data acquisition program extending beyond basic LTP experimental functions. *J. Neurosci. Methods* **162,** 346–56 (2007).

121. Daw, M. & Isaac, J. Electrophysiological Recordings from Neonatal Neocortical Brain Slices. *Curr. Protoc. Neurosci.* 6.23.1–6.23.12 (2007).

122. Pelt-Verkuil, E. van, Belkum, A. van & Hays, J. P. *Principles and Technical Aspects of PCR Amplification*. 342 (Springer, 2008).

123. Bustin, S. A. Absolute quantification of mRNA using real-time reverse transcription polymerase chain reaction assays. *J. Mol. Endocrinol.* **25,** 169–193 (2000).

124. Nolan, T., Hands, R. E. & Bustin, S. a. Quantification of mRNA using real-time RT-PCR. *Nat. Protoc.* **1,** 1559–82 (2006).

125. Thellin, O., Zorzi, W., Lakaye, B., Borman, B. De & Coumans, B. Housekeeping genes as internal standards : use and limits. *J. Biotechnol.* **75,** 291–295 (1999).

126. Heid, C. a, Stevens, J., Livak, K. J. & Williams, P. M. Real time quantitative PCR. *Genome Res.* **6,** 986–994 (1996).

127. Corley, B. A Guide to Methods in the Biomedical Sciences. *Springer* **6,** 125 (2005).

128. Wilson, K. & Walker, J. *Principles and Techniques of Biochemistry and Molecular Biology*. *Vasa* (Cambrige University Press, 2010).

129. Cikos, S., Bukovská, A. & Koppel, J. Relative quantification of mRNA: comparison of methods currently used for real-time PCR data analysis. *BMC Mol. Biol.* **8,** 113 (2007).

130. Pfaffl, M. W. A new mathematical model for relative quantification in real-time RT-PCR. *Nucleic Acids Res.* **29,** e45 (2001).

131. Coons, A. H., Creech, H. J. & Jones, R. N. Immunological Properties of an Antibody Containing a Fluorescent Group. *Exp. Biol. Med.* **47,** 200–202 (1941).

132. Langley, O., Ghandour, M. & Gombos, G. in *Handb. Neurochem.* (Lajtha, A.) **7,** 545–597 (Plenum Press, 1984).

133. Fritschy, J.-M. Is my antibody-staining specific? How to deal with pitfalls of immunohistochemistry. *Eur. J. Neurosci.* **28,** 2365–70 (2008).

134. Robinson, J. P., Bs, J. S. & Kumar, G. L. in *Educ. Guid. Immunohistochem. Stain. Methods* 61–65 (Dako, 2013).

135. Ramos-Vara, J. a. Technical aspects of immunohistochemistry. *Vet. Pathol.* **42,** 405–26 (2005).

136. Buchwalow, I. & Böcker, W. *Immunohistochemistry: basics and methods*. *Vasa* (Springer, 2010).

137. Pawley, J. *Handbook of biological confocal microscopy*. 80–118 (Springer, 2010).

138. Macklis, J. D. & Madison, R. D. Progressive incorporation of propidium iodide in cultured mouse neurons correlates with declining electrophysiological status: a fluorescence scale of membrane integrity. *J. Neurosci. Methods* **31,** 43–6 (1990).

139. Mahmood, T. & Yang, P.-C. Western Blot: Technique, Theory, and Trouble Shooting. *N. Am. J. Med. Sci.* **4,** 429–434 (2012).

140. Kurien, B. T. & Scofield, R. H. Western blotting. *Methods* **38,** 283–93 (2006).

141. Avoli, M., Biagini, G. & de Curtis, M. Do interictal spikes sustain seizures and epileptogenesis? *Epilepsy Curr.* **6,** 203–7 (2006).

142. Petito, C. K., Morgello, S., Felix, J. C. & Lesser, M. L. The two patterns of reactive astrocytosis in postischemic rat brain. *J. Cereb. Blood Flow Metab.* **10,** 850–9 (1990).

143. Eng, L. F. & Ghirnikar, R. S. GFAP and astrogliosis. *Brain Pathol.* **4,** 229–37 (1994).

144. Eggen, B. J. L., Raj, D., Hanisch, U.-K. & Boddeke, H. W. G. M. Microglial phenotype and adaptation. *J. Neuroimmune Pharmacol.* **8,** 807–23 (2013).

145. O'Dell, C. M., Das, A., Wallace, G., Ray, S. K. & Banik, N. L. Understanding the basic mechanisms underlying seizures in mesial temporal lobe epilepsy and possible therapeutic targets: a review. *J. Neurosci. Res.* **90,** 913–24 (2012).

146. Cavazos, J. E. & Cross, D. J. The role of synaptic reorganization in mesial temporal lobe epilepsy. *Epilepsy Behav.* **8,** 483–93 (2006).

147. Wong, M. & Guo, D. Dendritic spine pathology in epilepsy: cause or consequence? *Neuroscience* **251,** 141–50 (2013).

148. Noraberg, J. *et al.* Organotypic hippocampal slice cultures for studies of brain damage, neuroprotection and neurorepair. *Curr. Drug Targets. CNS Neurol. Disord.* **4,** 435–52 (2005).

149. Danglot, L., Rostaing, P., Triller, A. & Bessis, A. Morphologically identified glycinergic synapses in the hippocampus. *Mol. Cell. Neurosci.* **27,** 394–403 (2004).

150. Li, Y. & Xu, T.-L. State-dependent cross-inhibition between anionic GABA(A) and glycine ionotropic receptors in rat hippocampal CA1 neurons. *Neuroreport* **13,** 223–6 (2002).

151. Holopainen, I. & Lauren, H. Neuronal Activity Regulates GABAA Receptor Subunit Expression in Organotypic Hippocampal Slice Cultures. *Neuroscience* **118,** 967–974 (2003).

152. Schweizer, C. *et al.* The gamma 2 subunit of GABA(A) receptors is required for maintenance of receptors at mature synapses. *Mol. Cell. Neurosci.* **24,** 442–50 (2003).

8 APPENDIX

8.1 qPCR standard and melting curve analysis

For the analysis of the transcript expression, 5-fold serial dilutions of the cDNA net solutions were used to create a standard curve for each gene. As explained in **section 3.4.1**, the Pfaffl relative quantification method requires the crossing point (CP) determination indicated by the threshold (red line) in the normalized fluorescence *vs* cycle plot (**panels A** in each figure). The standard curves were created by ploting CP vs the log concentration of cDNA (ng/uL) (**panels B**). The parameters calculated using the standard curve are efficiency (**E**), relative expression rate (**R**) and slope value (**M**). Slope value is required in order to calculate the amplification efficiency [E=10^(-1/slope)] for the Pfaffl relative quantification method and should be included in the [3.1; 3.7] interval. E(Corbett) is a parameter determined by the software which is a measure of the overall efficiency of the reaction and should be included in the [0.85; 1.10] interval. R^2 gives a measure of the fitting of the linear regression and the linearity of the PCR assay. The assessment of the reaction specificity was also evaluated by melting curve analysis (**panels C**). The visualization of one single peak in the Derivate (dF/dt) *vs* Temperature plot indicates a specific amplification of the targeted gene. All plots were created using Corbett software (Corbett Life Science). The following figures illustrate qPCR standards and melting curves analysis for each analyzes gene.

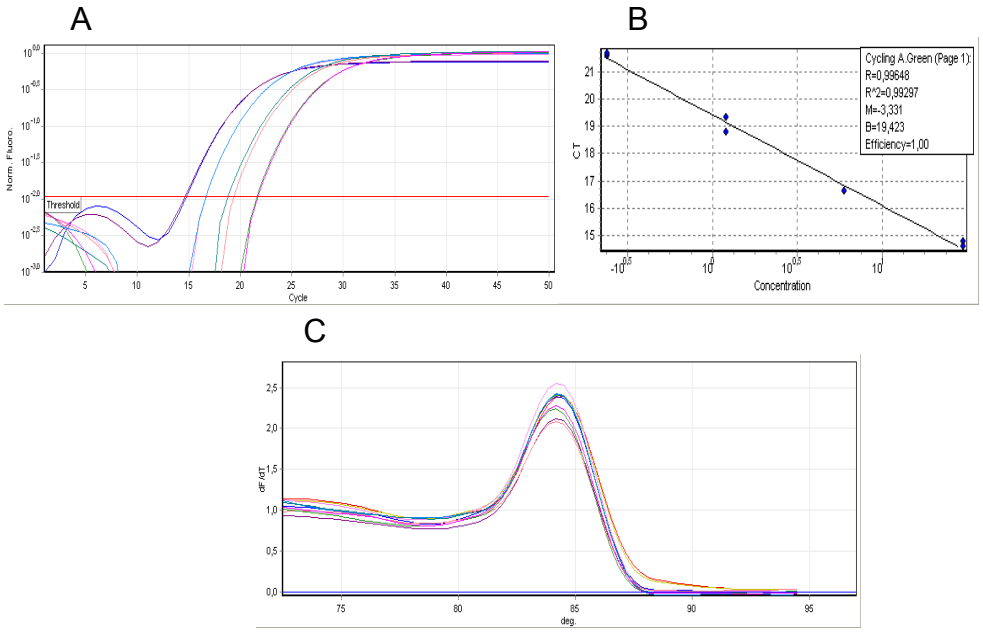

Figure 24| qPCR Standard and melting curves analysis for the GAPDH gene - endogenous control. (A) PCR amplification plot for the GAPDH gene. **(B)** Parameters calculated using standard curve created by plotting CP vs. the log concentration of cDNA (ng/uL). **(C)** Assessment of the reaction specificity by melting curve analysis.

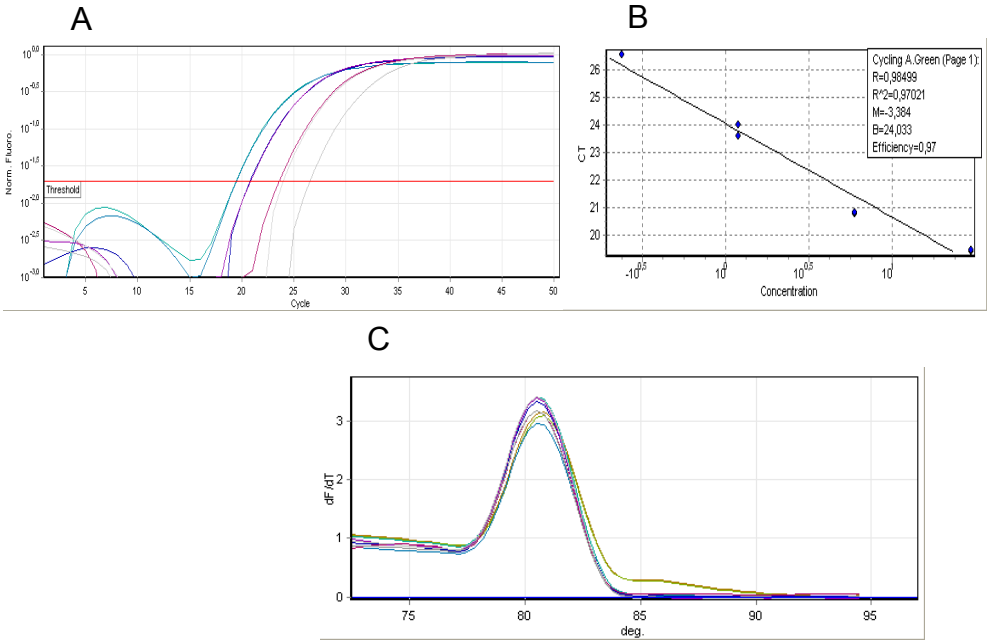

Figure 25| qPCR Standard and melting curves analysis for the GABAARα1. (A) PCR amplification plot for the $GABA_AR\alpha1$ gene. **(B)** Parameters calculated using standard curve created by plotting CP vs. the log concentration of cDNA (ng/uL). **(C)** Assessment of the reaction specificity by melting curve analysis.

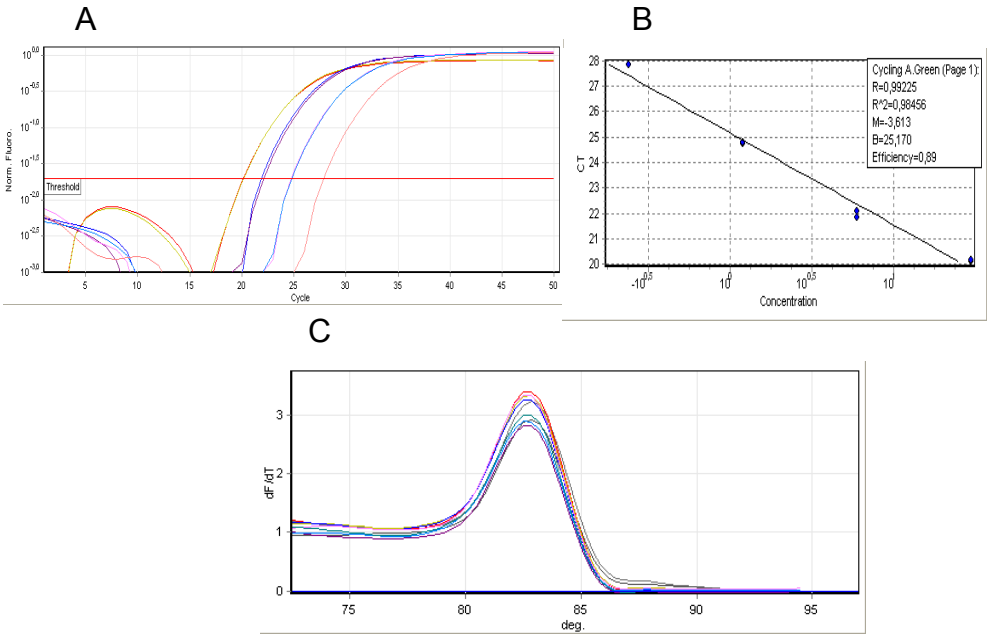

Figure 26| qPCR Standard and melting curves analysis for the GABAARα2. (A) PCR amplification plot for the $GABA_AR\alpha2$ gene. **(B)** Parameters calculated using standard curve created by plotting CP vs. the log concentration of cDNA (ng/uL). **(C)** Assessment of the reaction specificity by melting curve analysis.

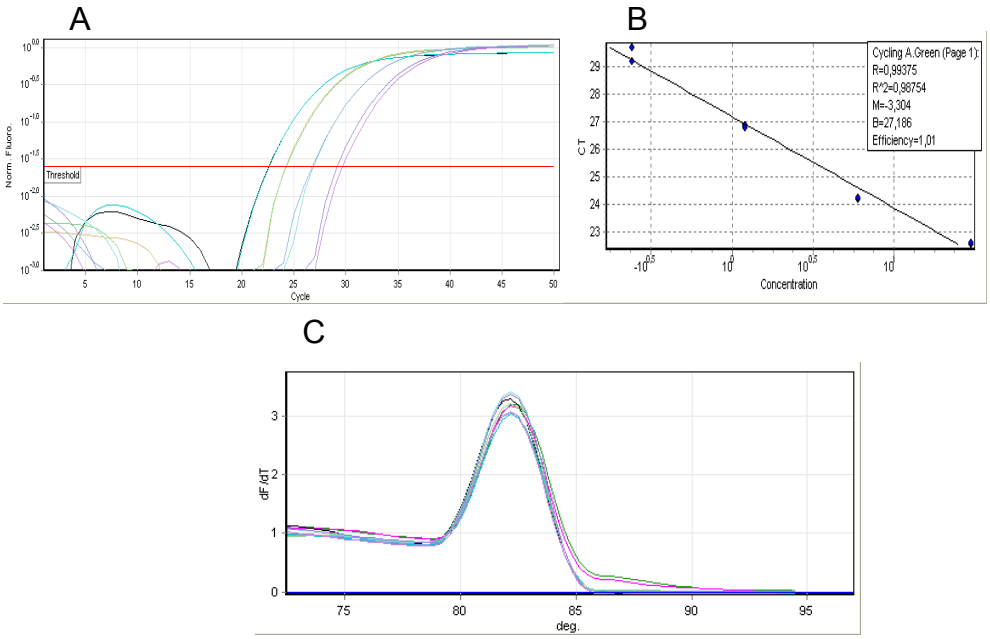

Figure 27| qPCR Standard and melting curves analysis for the GABAARα3. (A) PCR amplification plot for the $GABA_AR\alpha3$ gene. **(B)** Parameters calculated using standard curve created by plotting CP vs. the log concentration of cDNA (ng/uL). **(C)** Assessment of the reaction specificity by melting curve analysis.

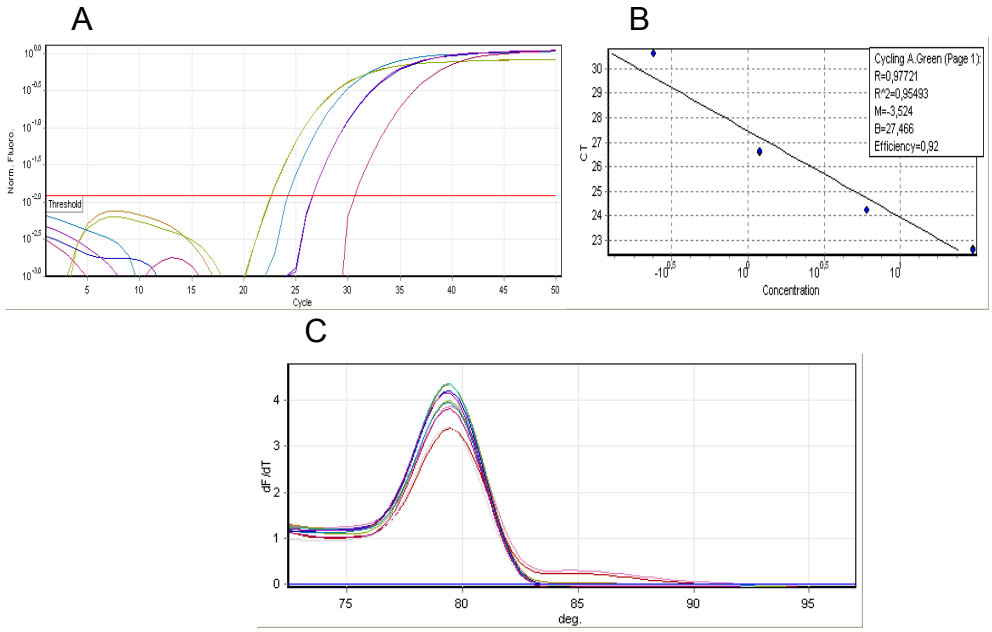

Figure 28| qPCR Standard and melting curves analysis for the GABAARα4. (A) PCR amplification plot for the $GABA_AR\alpha4$ gene. **(B)** Parameters calculated using standard curve created by plotting CP vs. the log concentration of cDNA (ng/uL). **(C)** Assessment of the reaction specificity by melting curve analysis.

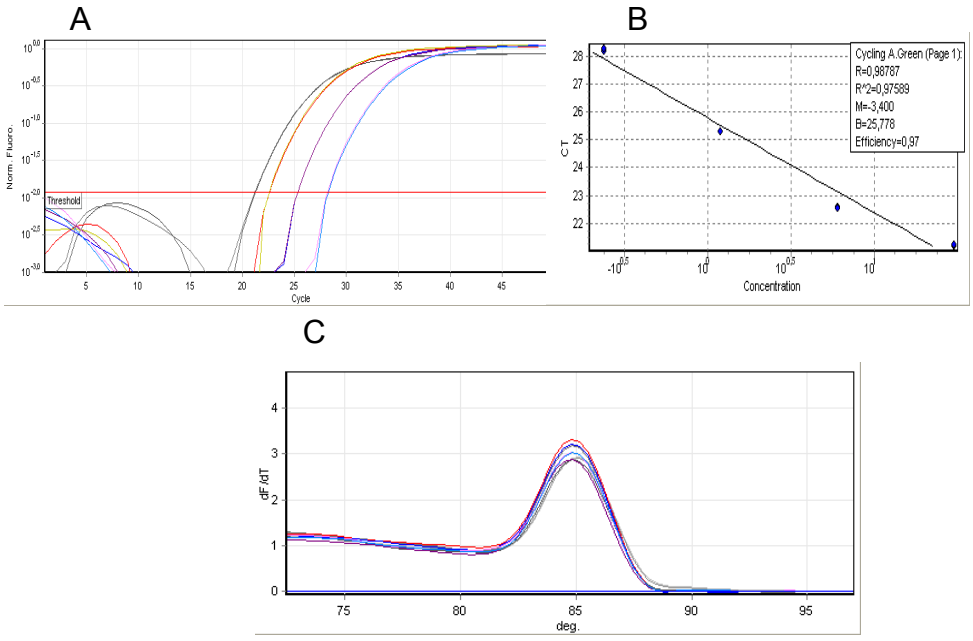

Figure 29| qPCR Standard and melting curves analysis for the GABAARα5. (A) PCR amplification plot for the $GABA_AR\alpha5$ gene. **(B)** Parameters calculated using standard curve created by plotting CP vs. the log concentration of cDNA (ng/uL). **(C)** Assessment of the reaction specificity by melting curve analysis.

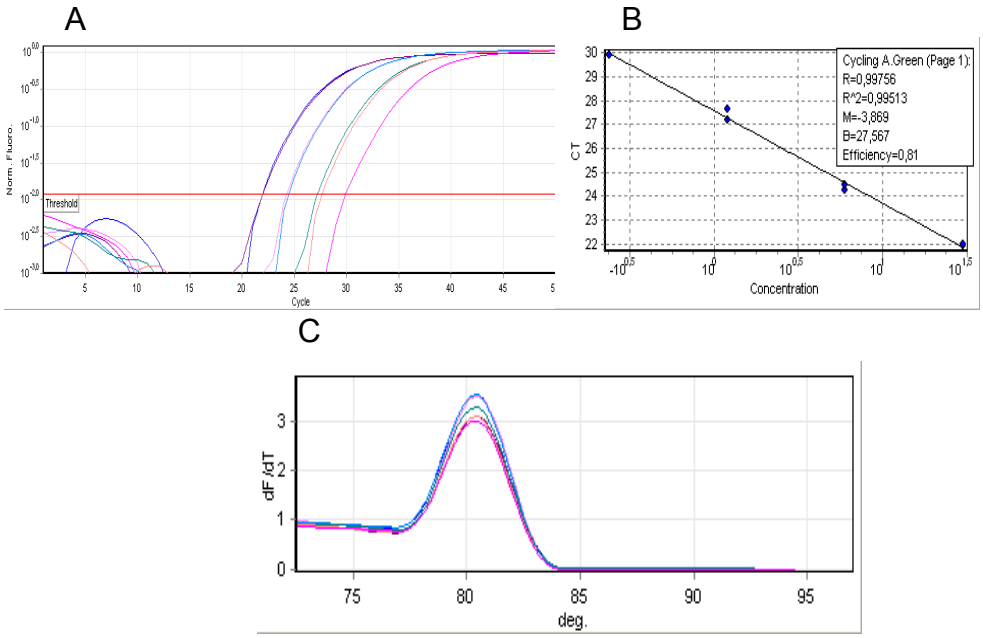

Figure 30| qPCR Standard and melting curves analysis for the GABAARβ1. (A) PCR amplification plot for the $GABA_AR\beta1$ gene. **(B)** Parameters calculated using standard curve created by plotting CP vs. the log concentration of cDNA (ng/uL). **(C)** Assessment of the reaction specificity by melting curve analysis.

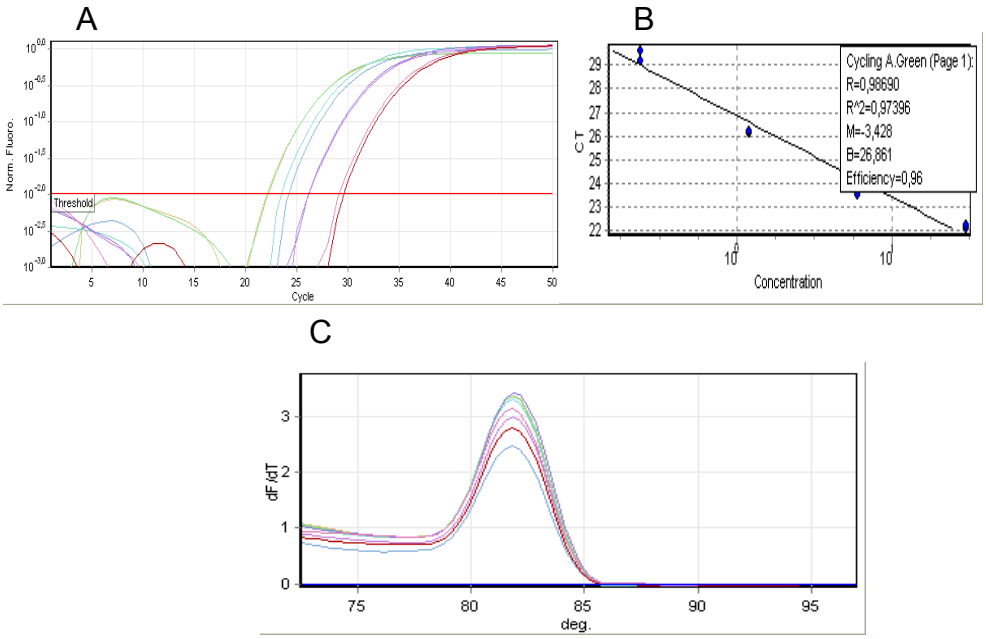

Figure 31| qPCR Standard and melting curves analysis for the GABAARβ2. (A) PCR amplification plot for the $GABA_AR\beta2$ gene. **(B)** Parameters calculated using standard curve created by plotting CP vs. the log concentration of cDNA (ng/uL). **(C)** Assessment of the reaction specificity by melting curve analysis.

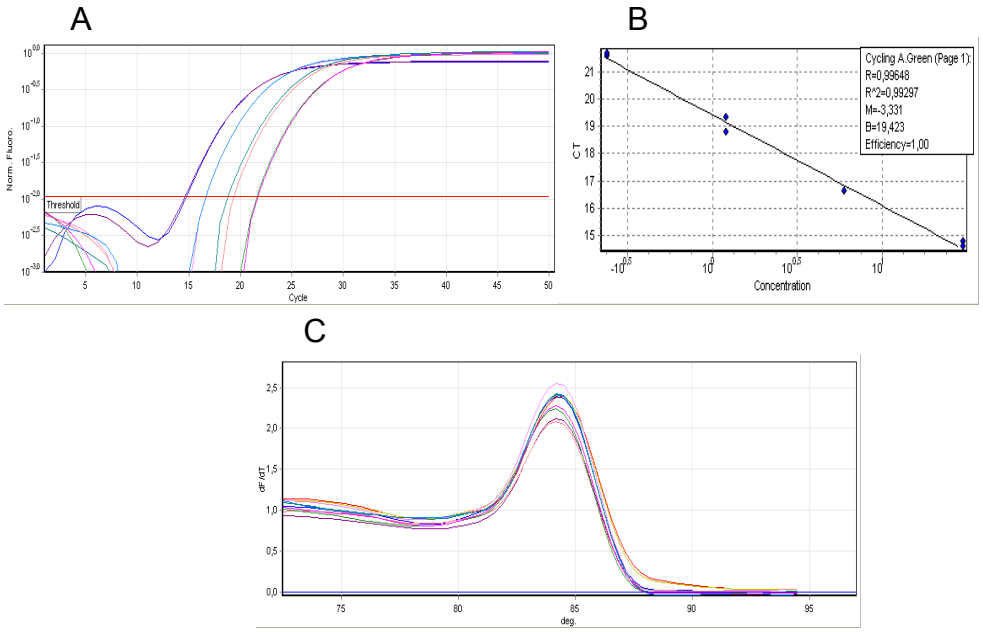

Figure 32| qPCR Standard and melting curves analysis for the GABAARβ3. (A) PCR amplification plot for the $GABA_AR\beta3$ gene. **(B)** Parameters calculated using standard curve created by plotting CP vs. the log concentration of cDNA (ng/uL). **(C)** Assessment of the reaction specificity by melting curve analysis.

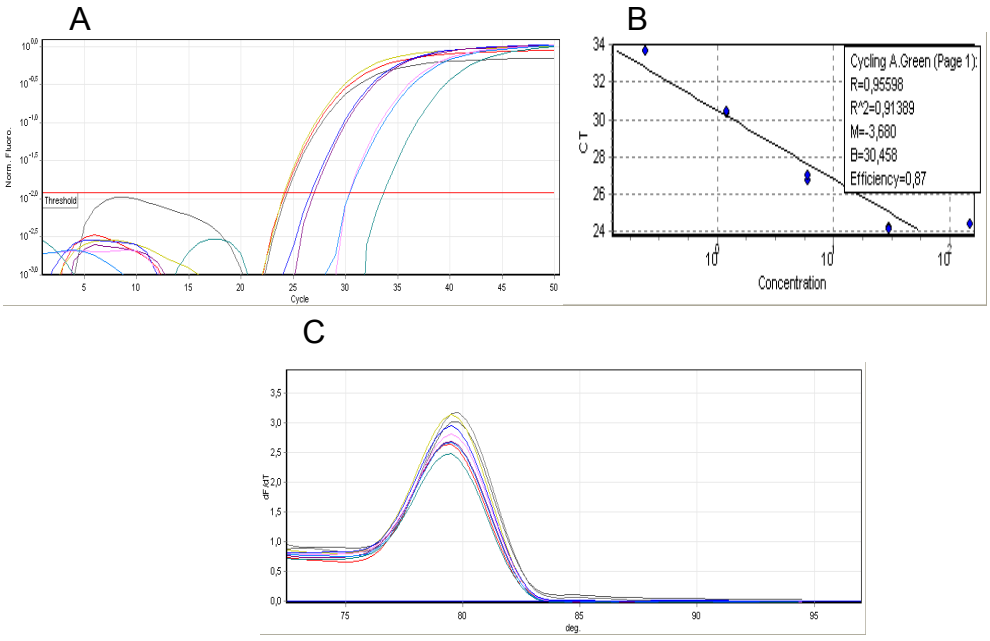

Figure 33| qPCR Standard and melting curves analysis for the GABAARγ2. (A) PCR amplification plot for the $GABA_AR\gamma2$ gene. **(B)** Parameters calculated using standard curve created by plotting CP vs. the log concentration of cDNA (ng/uL). **(C)** Assessment of the reaction specificity by melting curve analysis.

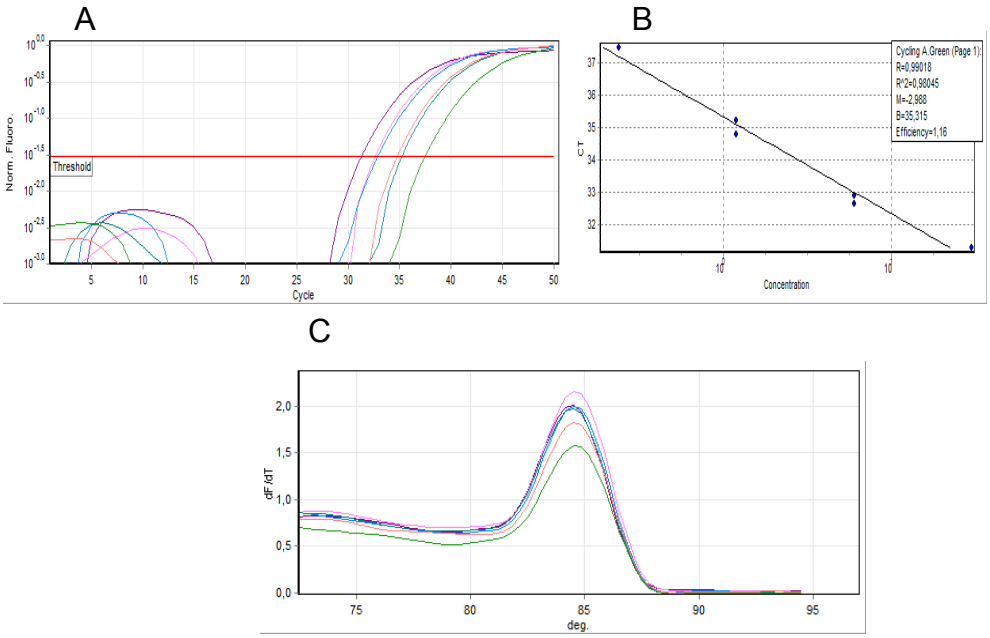

Figure 34| qPCR Standard and melting curves analysis for the GlyRα1. (A) PCR amplification plot for the GlyRα1 gene. **(B)** Parameters calculated using standard curve created by plotting CP vs. the log concentration of cDNA (ng/uL). **(C)** Assessment of the reaction specificity by melting curve analysis.

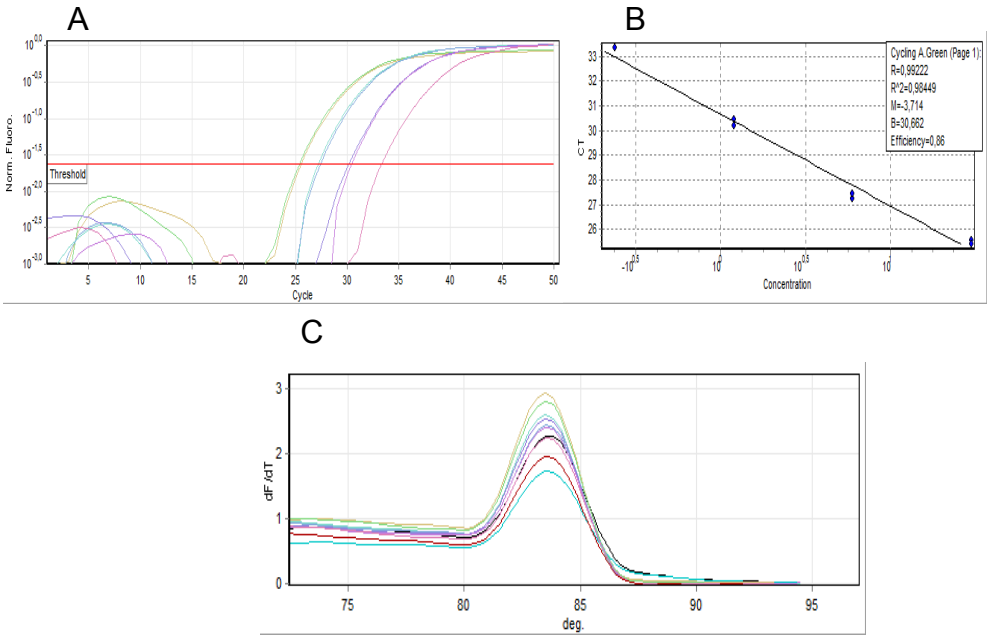

Figure 35| qPCR Standard and melting curves analysis for the GlyRα2. (A) PCR amplification plot for the GlyRα2 gene. **(B)** Parameters calculated using standard curve created by plotting CP vs. the log concentration of cDNA (ng/uL). **(C)** Assessment of the reaction specificity by melting curve analysis.

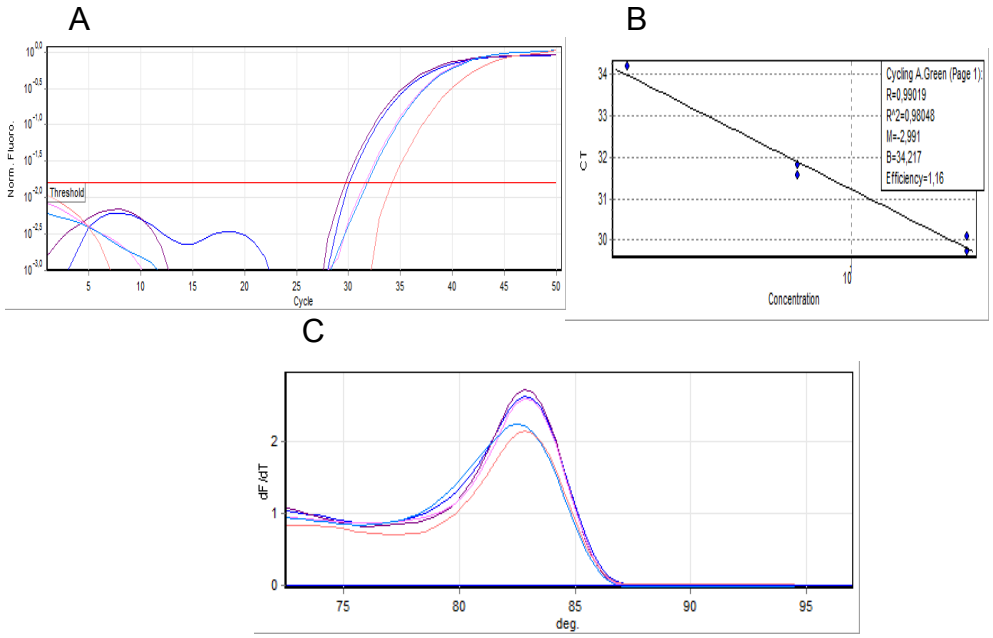

Figure 36| qPCR Standard and melting curves analysis for the GlyRα3. (A) PCR amplification plot for the GlyRα3 gene. **(B)** Parameters calculated using standard curve created by plotting CP vs. the log concentration of cDNA (ng/uL). **(C)** Assessment of the reaction specificity by melting curve analysis.

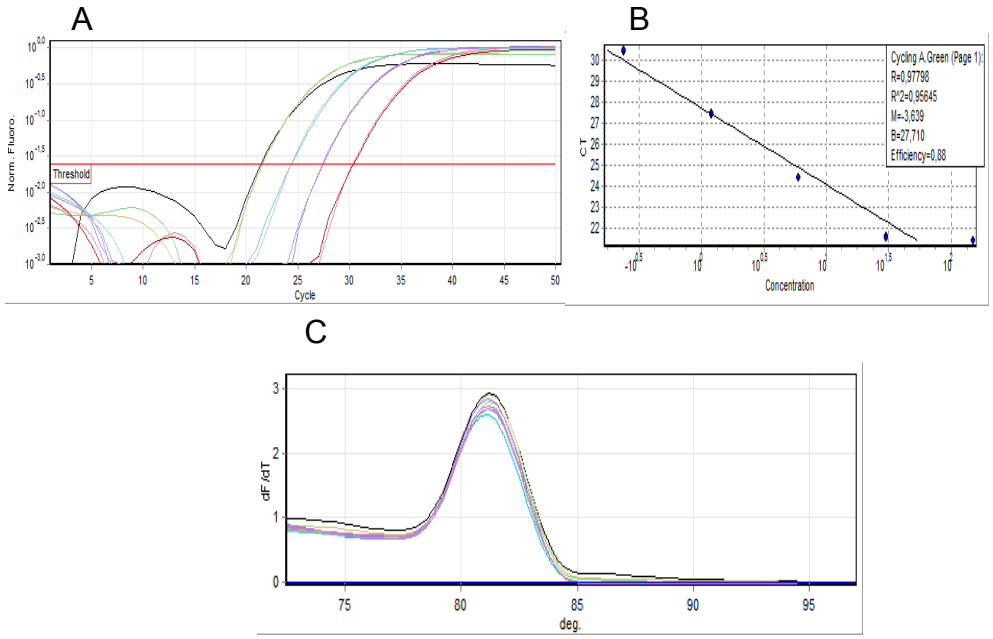

Figure 37| qPCR Standard and melting curves analysis for the GlyRβ. (A) PCR amplification plot for the GlyRβ gene. **(B)** Parameters calculated using standard curve created by plotting CP vs. the log concentration of cDNA (ng/uL). **(C)** Assessment of the reaction specificity by melting curve analysis.